

Final Report

**Application of Next Generation Air Monitoring
Methods in the South Coast Air Basin.**

Prepared for

South Coast Air Quality Management District (SCAQMD)

Tara I. Yacovitch, Scott C. Herndon, Ed Fortner, Conner Daube, Rob Roscioli
Aerodyne Research, Inc.

In association with:

W. Berk Knighton
Montana State University

And

Andrey Khystov, Dave Campbell
Desert Research Institute

January 2019

Executive Summary

Between Thursday March 1st and Wednesday April 5th, 2018, measurements were conducted in the greater Los Angeles area, focusing on Paramount, Compton, Gardena and the City of Industry. The Aerodyne Mobile Laboratory was equipped with state-of-the-art instrumentation to measure a broad range of atmospheric tracers, including volatile organic hydrocarbons (e.g. benzene, a carcinogen, and styrene, an odor concern), combustion species (e.g. CO₂ and CO from vehicle exhaust), particulate matter size, composition and mass, particulate matter hexavalent chromium and others.

This campaign has demonstrated that the **use of a well-equipped mobile laboratory is valuable for emission studies in complex urban environments** (Figure 1).

- Mobile surveys of a neighborhood produce concentration maps which can quickly **identify emissions hotspots**.
- Mobile laboratory measurements that include instrumentation to measure combustion markers, speciated volatile organic hydrocarbons, particulate matter, and other compounds of interest (like hexavalent chromium, in this project) are ideal for urban or industrial areas with **numerous, varied and sometimes uncharacterized emission types**.
- **Unexpected emission sources** were encountered numerous times during neighborhood surveys or during drives focused on other potential sources. This type of “by-catch” increases the productivity and value of mobile laboratory studies.
- Mobile measurements under **different wind conditions** help narrow down source locations in congested areas.
- The **live data display and mapping** in the Aerodyne Mobile Laboratory allowed scientists to regularly brief project management on the latest observations during the field campaign and maximize the time spent on project priorities.
- The rapid preliminary data allowed for the campaign goals to be flexible and adaptable.

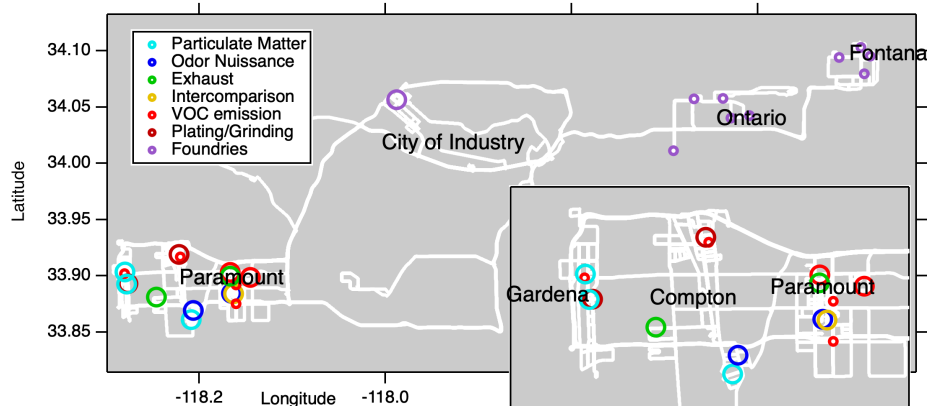


Figure 1. Overview showing a subset of the mobile laboratory path (white) and approximate case study locations (circles) colored by category. The inset zooms in on the cities of Gardena, Compton and Paramount, where the majority of measurement time was focused. Large markers are described in detail in the report.

The types of emissions measured during this campaign were diverse. In some cases, the emissions could be traced back to a source located within one or two blocks. In other cases, specific source facilities were identified. Examples include:

- An odor plume in downtown Paramount, characterized by the presence of particulate matter organics,
- Styrene emissions, which also have a strong odor, from facilities that use solvents,
- Particulate matter cadmium emissions in one small area of Compton (Figure 2).

Example data in Figure 2 shows seconds-long enhancements in particulate matter containing cadmium. This data was collected on the soot particle aerosol mass spectrometer (SP-AMS), which had a particle size cutoff of $<1\ \mu\text{m}$ (first half of campaign) or $<2.5\ \mu\text{m}$ (second half of campaign). This implies that the cadmium-containing particles are small in size, in stark contrast to the other metals sampled by the SP-AMS in this study. Additional details on these cadmium measurements are described starting on page 41.

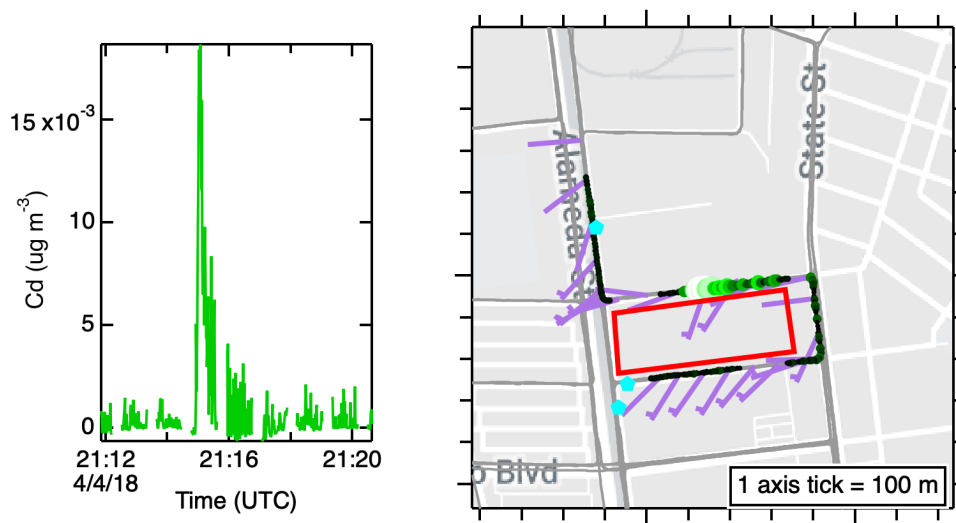


Figure 2. Example particulate matter cadmium (Cd) plume in North Compton. Particulate matter concentrations (left) are expressed in micrograms per meter cubed, $\mu\text{g m}^{-3}$. The map (right) shows Cd intensity (green). The suspected source is located in the city block outlined in red. Wind barbs (violet) point into the wind, and the location of some of SCAQMD's portable samplers are shown as blue dots.

A small handful of hexavalent chromium enhancements were measured and analyzed. Evidence from this study suggests that the **hexavalent chromium measured is primarily present in coarse-mode particulate matter (1-100 μm).**

The typical example of coarse-mode particulate matter is wind-generated dust. In the measurements done here, we hypothesize that industrial activities related to metal grinding or cement manufacturing create coarse-mode particles containing hexavalent chromium. Even chrome plating is expected to yield relatively large particulate emissions in the $0.75 - 6.4\ \mu\text{m}$ range (see Table 1). Such large particles settle quickly out of the air, but may be resuspended by wind, road traffic, street sweeping, etc. In this study, the

coarse-mode evidence includes: 1) no sustained multi-second long particulate matter chromium emissions detected with the SP-AMS; 2) sustained plumes of metals are observable with the AMS, as demonstrated for cadmium; 3) increased chromium detection when SP-AMS lens was changed from 1 to 2.5 μm cutoff; 4) increased chromium concentrations noted when following street-sweepers; 5) hexavalent chromium enhancements were short in duration and did not persist; 6) hexavalent chromium detected near cement ready-mix facility, and hard chrome plating/grinding facility. Questions remain as to the particle size distribution and typical emission vectors in the studied areas.

Particulate matter concentrations for hexavalent chromium, Cr(VI), are shown in Figure 3, binned and normalized, for the duration of the campaign. This data was collected by the steam-jet aerosol collector long pathlength absorbance spectrometer (SJAC-LPAS). The cities of Gardena/West Rancho Dominguez (left), Compton (center) and Paramount (right) are shown. Enhancements measured on highways were smeared out due to the response time of this instrument coupled with the speed of the mobile laboratory, and so were not attributable to specific source areas. On the other hand, enhancements in West Rancho Dominguez (left center) occur in an industrial area that included both cement ready-mix and hard chrome plating facilities. Both of these industries are potential hexavalent chromium sources. Analysis of the hexavalent chromium enhancements noted in this area are described in greater detail starting on page 38.

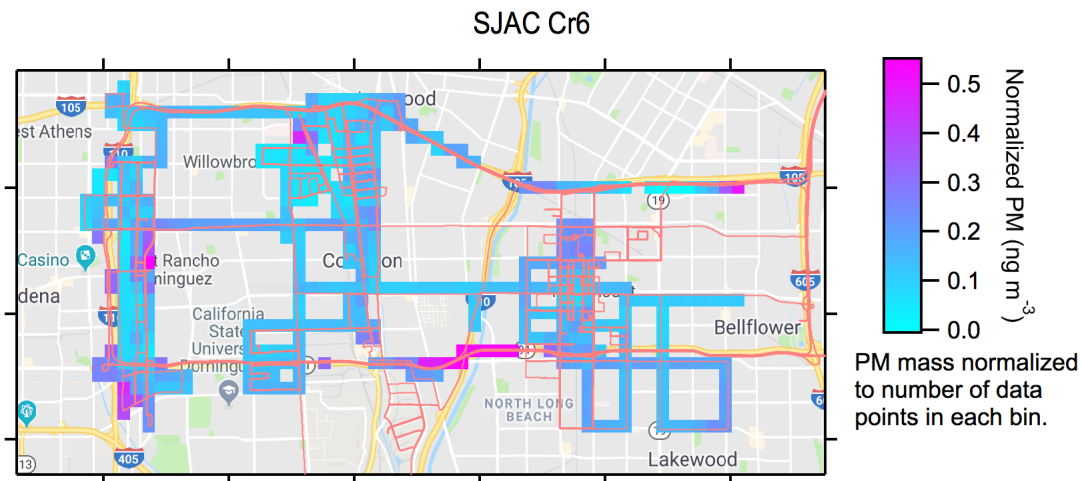


Figure 3. Particulate matter hexavalent chromium mass concentration in the study region (Cr(VI) or Cr6 for short, in nanograms per meter cubed, ng m^{-3}). Data is binned in 300m x 300m boxes and normalized by the number of data points per bin. No data is shown for speeds ≥ 50 km/hr or when the instrument was off. The light red trace shows the AML route for the entire campaign. See Figure 9 and surrounding text for additional details.

These and other results within suggest that **additional hexavalent chromium monitoring be undertaken in Gardena, West Rancho Dominguez, and any other area where there is a high density of concrete and metal grinding operations.**

Table of Contents

Executive Summary	2
Introduction	6
Industrial Sources of Hexavalent Chromium	7
Cement.....	7
Painting.....	8
Metal-Working.....	8
Electroplating	9
Expected Particle Sizes	9
Experimental	10
AMS Detection of Cr	12
Data Access	15
Results	15
Overview of Particulate Matter Cr(VI) and Cr in the Study Area	15
Street Sweeping	19
Paramount Odor Plume	20
Stationary Measurements at Promise Hospital	25
PM Metal Intercomparisons.....	26
Hexavalent Chromium at the Promise Hospital Site.....	28
VOC Emissions	29
Paramount Petroleum.....	29
Paramount Styrene Plume.....	30
HCHO and Ethane in Paramount	32
Ambient Air Comparison	33
Exhaust Emissions	34
Vehicle Exhaust Comparison	34
Truck Depots and Grocery Outlets	36
Chrome Plating/Grinding Facilities, and Cement Ready-Mix Facilities	38
Cr(VI) in West Rancho Dominguez.....	38
Cadmium Plumes in the North Compton Area.....	41
Robertson’s Ready Mix, Gardena and A&A Ready Mixed.....	43
Foundries	45
Custom Alloy Light Metals, City of Industry	46
Discussion	49
Conclusions	51
Recommendations for Future Studies	52
List of Appendices	54
References	54

Introduction

Since 2013 the South Coast Air Quality Management District (SCAQMD) has been conducting monitoring for air toxic metals, including hexavalent chromium, Cr(VI), in the community of Paramount, which has a large number of metal forging, grinding and plating facilities. For this purpose, SCAQMD has deployed portable filter samplers at nearly 30 different locations in the City of Paramount. These numbers are expected to increase substantially in the near future as SCAQMD has been receiving requests for further monitoring from other communities in the South Coast Air Basin (SCAB) that are adjacent to metal forging and grinding operations (e.g. cities of Compton, Anaheim, and Long Beach).

Conducting surveys using filter sampling is labor-intensive and time-consuming, and does not allow for continuous monitoring, dense spatial coverage, or effective screening. Therefore, SCAQMD has a pressing need to implement an alternative approach to screening for Cr(VI) and other air toxics. Recent advancements in real-time analytical techniques offer such promise. This study is therefore targeted at making significant advancements in monitoring Cr(VI) and other toxic metals in communities located near metal process facilities. A Cr(VI) monitor and other instrumentation mounted in a mobile platform has the potential to:

1. Provide real-time detection and quantification of Cr(VI) and other toxic metals for assessing levels of these air toxics on a community-scale.
2. Use mobile Cr(VI) monitoring to guide placement of longer-term monitoring sites that use the conventional method to assess the long-term impact of emissions on surrounding communities and to measure pollution reduction efforts of facilities.

In order to fulfill these objectives, Aerodyne Research, Inc. and Desert Research Institute (DRI) were selected to conduct a comprehensive study to locate emission sources of hexavalent chromium, Cr(VI) in several areas of the SCAB using a suite of near-real-time next generation analytical equipment on board the Aerodyne Mobile Laboratory (AML). Characterization the surrounding neighborhoods to evaluate potential exposure levels was conducted. Detailed maps of ambient Cr(VI) concentrations and other air toxics were generated for the cities Paramount, Compton, Gardena, and other areas of the SCAB. A Cr(VI) monitor developed by Khystov, and 15 other air sensors were integrated onto the Aerodyne Mobile Laboratory to afford mobile Cr(VI) monitoring capability. Applying a suite of instrumentation enables evaluation of not only the target species but the presence of other components that are co-emitted or collocated to be identified. thus establishing, a comprehensive chemical profile of the air in the measurement areas. As will be seen below, this chemical context provides important details about pollution sources, and allows for identification of other (non-Cr(VI)) pollutants in the area.

The Aerodyne mobile laboratory was deployed between Thursday March 1st and Wednesday April 5th, 2018. Measurements were taken in the greater Los Angeles area, focusing on Paramount, Compton, Gardena and the City of Industry. Throughout this

report, individual facilities are named or drawn on a map. It is important to note that this does not indicate that they are the source of a given emission unless specifically described as such.



Figure 4. The Aerodyne Mobile Laboratory (AML) parked at SCAQMD location Diamond Bar.

Industrial Sources of Hexavalent Chromium

Cement

Most cements are composed primarily of calcium silicate nodules, known as “clinker”, which are blended with varying amounts of gypsum, “slag” (a by-product of iron manufacturing), or other material. Cement, including the most common formulation, Portland cement, contains Cr(VI). The Cr(VI) contaminant comes from several possible vectors during the production, such as initial Cr content of the raw material, introduction from kiln lining, and abrasion of steel during grinding (CSTEE, 2002). Studies at a California cement plant (Klemm, 1994) showed that more than half of the hexavalent chromium in the cement was contributed by the grinding media in the finish mill. Importantly, during heating in the kiln to create calcium silicate nodules (a process called “sintering”), the kiln temperature reaches 1450 °C, which is also the oxidation temperature range (1400-1500 °C) that converts the less-harmful Cr(III) to hazardous Cr(VI).

According to OSHA, typical Cr(VI) concentrations in Portland cement are 20 parts per million (ppm) by mass (Foulke, 2007). Analysis of samples of Portland cement from by Slovakian producers (Eštoková et al., 2012) showed that the average concentrations of the total chromium (all oxidation states) in cements vary from 178.5 to 257.3 mg per kg of cement (179-257 ppm by mass). The concentration of Cr(VI) in cement depends on the number of nodules produced during sintering (also known as “clinkers”). Eštoková et al.

(2012) found that only the clinker contained Cr(VI), so cements with higher clinker content have more soluble Cr(VI). The average concentrations of Cr(VI) in these Slovakian samples was in the range of 0.5 to 2.46 mg/kg (0.5-2.5 ppm by mass). Similarly, determination of the water-soluble fraction of Cr(VI) measured in Swedish (Wahlberg et al., 1977) and Australian (Tandos and Aarts, 1993) cements are reported to be ranging from 0.2 to 20 mg/kg (0.2-20 ppm by mass), and from Spanish cements (Frias and Sánchez de Rojas, 2002) in the range of 0.1-7.5 mg/kg (0.1-7.5 ppm by mass). There is always the possibility that some fraction to that soluble Cr(VI) is leached into water during production. However, the Slovakian study found only a small fraction of total chromium in the leachate. Of that, only 0.19 to 1.38% of Cr(VI) was found to enter the water.

There have been efforts to mitigate the Cr(VI) in cement and its impacts. One solution is to chemically reduce the Cr(VI) using iron, tin, and antimony salts (C-ADD Mapei), then chemical conversion to a highly insoluble compound, which will minimize environmental impact. A very recent study (Bae et al., 2018) found that ground granulated blast furnace slag (an iron manufacturing by-product) can be incorporated into concrete to reduce Cr(VI) to Cr(III).

Painting

Chromates are common additives to paint to and other surface applications to improve anticorrosion. As such its aerosolization at industrial painting facilities can result in airborne hexavalent chromium unless mitigation measures take place. Such mitigation schemes include exhaust filtering and operation in a spray booth. In addition to application, removal and/or cleaning of these surfaces can also result in Cr(VI) emissions, where the Cr can be volatilized in the form of paint chips and dust. Again in these cases the mitigation strategy is to use HEPA-style particle filtering, as well as spray mists to remove particulates.

Metal-Working

Because chromium is a major component of steel, many metal-working facilities will create airborne Cr. Such activities include welding, thermal cutting, and steel mill operation. Of central importance is that many of the processes that manipulate steel do so at very high temperatures, where Cr(III) and metallic Cr can be oxidized to Cr(VI). Welding itself not only creates temperatures above the melting point of steel, but also vaporizes it. According to Seragaldin (2009), 0.4-0.6% of electrode mass is converted to fumes during shielded metal arc welding (SMAW) and gas metal arc welding (GMAW). This creates the potential for condensation of Cr onto existing particles (e.g. dust and aerosols), or the formation of vapor particles. According to NIOSH (2013), “Any vaporized metal that escapes the welding-arc area quickly condenses and oxidizes into welding fume, and an appreciable fraction of the chromium in this fume is in the form of Cr(VI).”

The EPA emission factor for Cr(VI) from steel welding is in the range of 0.01-0.33 g Cr(VI) per g of welding electrode ("Metallurgical Industry", 1994). Heung et al. (2007) found similar results (0.015-0.257 g/kg), but also found that the Cr(VI) emission factor

could be reduced by a factor of 10 by using a sufficient shielding gas flow rate (>20 cu ft/hr).

Electroplating

Two different types of chromium electroplating are used depending on the application. Hard chrome plating involves deposition of a thick chromium coating onto a part to enhance material properties like hardness, coefficient of friction and wear- or corrosion-resistance. This type of plating is used for high-friction parts like machine rollers. Hard chrome plating typically requires the use of hexavalent chromium (from chromic acid, CrO₃) in a highly acidic bath, often heated to 120-150 Fahrenheit (NEWMOA, 2010). The presence of an excess of trivalent chromium Cr(III) can impede the process. Though it is not an electroplating process, aluminum alloy anodization may also use chromic acid. Anodization is a process that harden a material's surface and increases its corrosion resistance by through the creation of a surface oxide layer.

Decorative chrome plating (or bright chrome plating), involves only a thin layer of chromium deposited directly onto the material or as a final coating on top of another electrodeposited metal like nickel. It is used for decoration and corrosion-resistance in applications like wheels and plumbing fixtures. Though decorative chrome plating traditionally used hexavalent chromium baths, trivalent solutions coupled with changes to the process and additives to correct for color can yield acceptable decorative coatings (NEWMOA, 2010).

Exposure in electroplating and anodizing operations typically occurs via mist from the chromic acid baths. OSHA states that the risk of exposure is greatest for hard chrome applications (OSHA). Other work practices may also increase exposure, including inserting or removal of parts from baths, spills, and open containers. EPA emission factors for electroplating are based on the energy input, and are estimated at 0.0078 and 0.0021 grams per Ampere-hour for hard and decorative chrome plating, respectively ("Metallurgical Industry", 1994).

Expected Particle Sizes

Typical Cr(VI)-containing particulate sizes can differ by process. The table below is reproduced from a white paper from Donaldson Filtration Solutions (Abelson, 2008), a filter systems provider. According to the author, the data is based on internal company information (private communication).

Table 1. Typical particle sizes produced from material containing hexavalent chromium (Abelson, 2008)

Type of Fume	Size Range of Fume Particles
Wet paints with chromates	0.7 - 34 microns
Chrome plating	0.75 - 6.4 microns
Welding	0.05 - 2.0 microns*
Thermal Spraying	0.05 - 2.0 microns*

* 80% of total fume is in this very small size range.

Of particular note here are the large particle sizes produced by chrome plating (0.75-6.4 μm or 750- 6,400 nm) compared to heat-based processes like welding and thermal spraying. Indeed, most of the chrome plating particles fall in the coarse-mode (1-100 μm) size range, where particles settle out of the atmosphere quickly, while welding and thermal spraying are shifted towards fine particles that are more likely to result in “plumes”. The EPA also states that most electroplating emissions will be in the PM10 range (“Metallurgical Industry”, 1994). Metal grinding and concrete, two other potential sources, are not included in this table.

The Donaldson white paper also suggests another reason why direct emissions of hexavalent chromium particles from the processes in Table 1 may be difficult to measure outside of facilities: they may already be mitigated by dedicated filtration systems. An example of such a system is shown in the Donaldson document (Abelson, 2008). Suspended particulate matter from chrome plating would be even easier to remove with filters due to its larger size. In fact, Bonin et al. (1995) studied a commercial chrome plating facility, and measured particle sizes of 0.3-25 μm at the plating bath; decreasing to a maximum size of 5 μm downstream of a first particle removal cyclone; and a 0.7 μm maximum downstream of a final mesh pad filter. They also calculated a collection efficiency of 99.997% for the combined particle abatement system. Pilat et al. (2006) further studied the details of bath particle sizes and formation.

Experimental

The 2016 Aerodyne Mobile Laboratory is an instrumented box truck (Figure 4) designed to support a flexible deployment of research-grade air monitoring equipment. A schematic in Figure 5 shows the instrumentation used during this field campaign.

Ambient air is continuously drawn through the inlets at the front of the vehicle, which extend out on booms mounted to the roof. Every 15 minutes, clean air was delivered in excess of the intake flow for two of the inlets: the trace-gas inlet (blue, Figure 5) and the VOC inlet (purple, Figure 5). The air was either dry ultra-zero air or humidity-matched air from an Aadco ZA30 zero-air generator, respectively. These gas additions served to spectroscopically background select laser-based instruments, and to check zero values for the other instruments. The other two inlets were dedicated to particulate matter measurements (red, Figure 5) and hexavalent chromium (green, Figure 5), and were manually checked for zero levels using a removable filter on the inlet tip.

Meteorological conditions and GPS-based positioning were measured on the rooftop. A Hemisphere (V103) GPS Compass was operated in conjunction with an RMYoung 2D anemometer to determine wind speed and direction and to map vehicle location, speed and bearing during measurements. True wind was determined by vector subtraction of the mobile laboratory speed from the raw measured wind speed.

Inside the AML, air in the trace-gas inlet is sampled by a LiCOR 7000 for CO₂, a Thermo Scientific 42i chemiluminescence sensor for NO, an Aerodyne cavity attenuated phase shift (CAPS) sensor for nitrogen dioxide (NO₂), and a 2BTech Model 205 ozone (O₃) monitor. Four Tunable Infrared Laser Direct Absorption Spectroscopy (TILDAS) trace-gas monitors from Aerodyne Research, Inc. performed gas phase measurements of the ambient air (McManus et al., 2015). Three single laser “mini” instruments and one

dual-laser instrument measured 1) formaldehyde and water (HCHO, H₂O), 2) nitrous oxide, carbon monoxide and water (N₂O, CO, and H₂O); 3) ethane and methane (C₂H₆ and CH₄); and 4) nitrogen oxide and nitrogen dioxide (NO, NO₂). The TILDAS instruments were operated in series at pressures between 30-50 Torr, with an upstream pressure controller managing flow from a downstream scroll pump (Agilent TriScroll TM 600). All TILDAS instruments were spectroscopically zeroed, except for the N₂O-CO monitor, due to residual CO present in ultra-zero air.

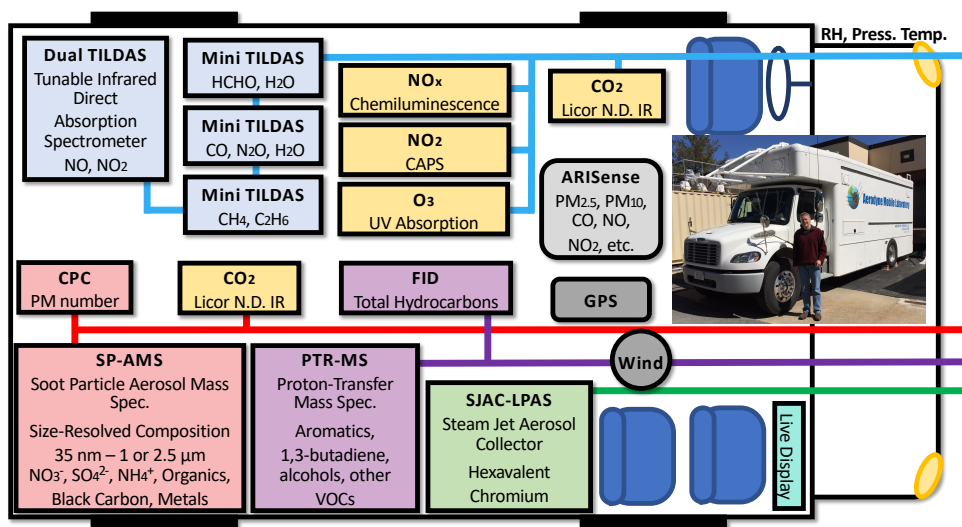


Figure 5. Schematic of the Aerodyne Mobile Laboratory during the 2018 SCAQMD field campaign. Particulate matter instrumentation (red, green) include condensation particle counter (CPC), soot particle aerosol mass spectrometer (SP-AMS), proton transfer mass spectrometer (PTR-MS), and the steam-jet aerosol collector long pathlength absorbance spectrometer (SJAC-LPAS). Trace gas and VOC instrumentation (blue) includes mini or dual tunable infrared direct absorption spectrometers (TILDAS) as well as a number of other commercial instruments (yellow). Roof-mounted sensors include global positioning system (GPS), wind, and the ARISense small sensor.

A CAI flame ionization detector (FID) measured total hydrocarbons and sampled from the VOC inlet along with a proton-transfer reaction mass spectrometer (PTR-MS) with quadrupole MS, operated in NO⁺ mode. In this mode, the instrument is also called NOMS. It measured ethanol, the sum of isopropanol and *n*-propanol (C₃ alcohols), 1,3-butadiene, benzene, toluene, the sum of xylenes and ethylbenzene (C₂ benzenes), C₃ benzenes, acetone, methyl ethyl ketone (MEK), styrene, and isoalkanes with the formula C₆H₁₄. Instrument calibrations for gas-phase species were performed by overblow of the inlet with a quantitatively blended mix of ppm-level calibration standards with a diluent (ultra-zero air or ZAG air).

A steam-jet aerosol collector (Khlystov et al., 1995) with long pathlength absorbance spectroscopy (SJAC-LPAS) measured particulate matter hexavalent chromium (Cr(VI)). Particulate matter (PM) is collected with the SJAC and the resulting liquid, containing dissolved aerosol species, is mixed with diphenylcarbazide (DPC) reagent for subsequent colorimetric detection. The SJAC-LPAS system was backgrounded with ultrapure water

and calibrated with deliveries of standard solutions of Cr(VI). Additional SJAC-LPAS instrument details are described in Appendix C.

An Aerodyne soot particle aerosol mass spectrometer (SP-AMS) measured particulate matter mass (PM_m in $\mu m m^{-3}$) and composition. It was equipped with a high-resolution time-of-flight mass spectrometer (HR-ToF). Particulate matter sulfate (SO_4^{2-}), nitrate (NO_3^-), ammonium (NH_4^+), chloride (Cl^-) and organic carbon (org) were measured with this instrument. The addition of the SP laser allowed for measuring both black carbon (BC) and metals. The metals monitored with this instrument include: chromium (Cr), cadmium (Cd), aluminum (Al), Tin (Sn), and many others. The full list of output species is available in Appendix B. This instrument has an internal size cutoff ($< 1 \mu m$ initially; $< 2.5 \mu m$ partway through the campaign) and the inlet sampled from a $< 2.5 \mu m$ cyclone. A condensation particle counter (CPC) measured particulate matter number (PM_n , in $\# cm^{-3}$).

An ARISense mounted to the vehicle rooftop measured particulate matter number in 16 size bins between $0.4 - 16 \mu m$ with an optical particle counter (Alphasense model OPC-N2). Subsequent analysis provided measures of integrated size-dependent particulate matter mass, like PM_2 and PM_{10} (see Appendix B). Other measured quantities include solar insolation, wind, RH, and duplicate measurements of CO, NO and NO_2 . The unit was mounted flat against the roofline (“up” points forward) to prevent exceeding vehicle height restrictions, and so this unit’s wind measurements were not used and the solar insolation used only qualitatively.

Real-time data was logged and displayed on monitors in the AML, allowing scientists to rapidly detect and follow plumes of interest. Custom software was used to download, display and update maps of the area, which were overlaid on live data graphs. Notes were recorded on the same computer and the observer defined periods of trace-gas data showing enhancements above background (plumes) while in the field.

AMS Detection of Cr

The Aerosol Mass Spectrometer was equipped with a high-resolution time-of-flight mass spectrometer (AMS-HR-ToF). This instrument does speciation of small particulate matter and, equipped with a laser vaporizer, can detect selected metals. In the initial parts of the campaign, a standard aerodynamic lens (Liu et al., 2007) was used, with a particle cut-off size around $1 \mu m$. Data after 3/18/2018 uses a $2.5 \mu m$ lens, which was installed in the field in order to enhance detection of larger particle sizes. The particle size cutoff for this instrument, however, precludes the detection of coarse-mode particulate matter (e.g. large dust particles), as might be expected from some sources. Furthermore, since detection is based on atomic mass, this instrument is not able to identify the oxidation state of a metal. For hexavalent chromium measurements, the SJAC-LPAS instrument operated by the Desert Research Institute is used.

High-resolution analysis of AMS-HR-ToF data was done (see, for example Figure 6), identifying very brief PM encounters with chromium (Cr) (see mass spectrum figure). This result demonstrates our ability to resolve atomic chromium from the neighboring organic PM mass (C_4H_4).

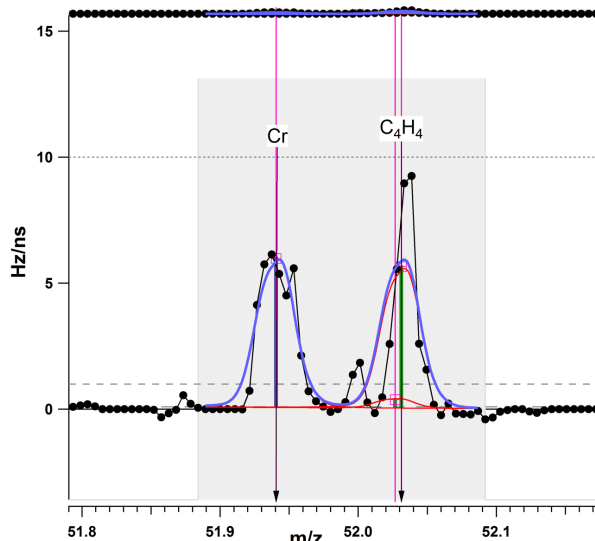


Figure 6. High-resolution fit of Cr (left) and neighboring organic fragment C₄H₄ (right)

The reference Cr isotope pattern was checked to verify that it matched with measured Chromium intensities and found to match up well (see Figure 7).

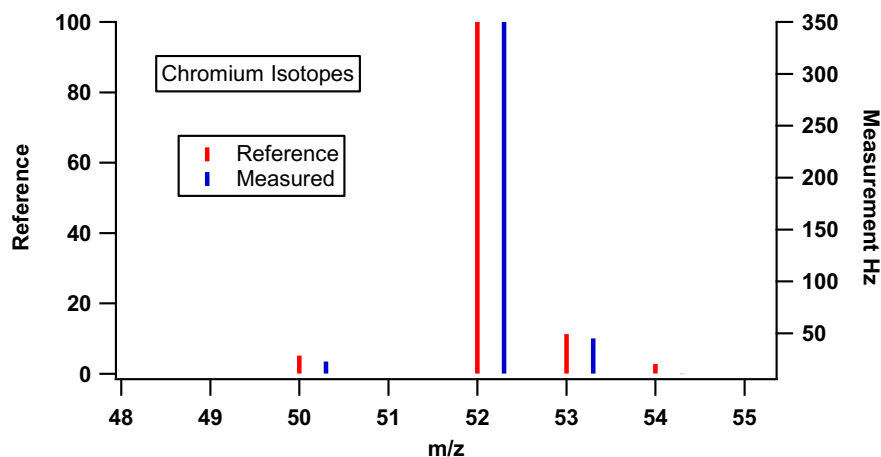


Figure 7. Measured (blue) and reference (red) isotope pattern for chromium isotopes. The measured signal is offset for clarity by 0.2 atomic mass units.

These Cr peaks detected by the AMS were single-second enhancements and were not sustained, multi-second-long enhancements. Indeed, during the campaign, no sustained multiple-seconds-long plumes of Cr and most other metals (with the exception of cadmium) were observed with the AMS. This observation, in combination with the <1 or <2.5 μm size range of the AMS, and the types of facilities where hexavalent chromium was detected, leads us to hypothesize that the hexavalent chromium measured in this study exists in coarse-mode particulate matter. Coarse mode particles consist of 1-100 μm particles generated through mechanical processes like sea spray, dust lifted by the wind, or mining activities (Hinds, 1999). Their size means that they settle quickly out of the air.

The coarse mode particle hypothesis is further supported by measurements with the AMS with two lenses with different size cutoffs. Initially, the instrument was operated with an internal PM1.0 lens. Partway through the campaign, on 3/18, a PM2.5 inlet lens was installed in the AMS. This lens enhances the collection efficiency of the AMS for particles in the size range of 600 – 2500 nm. This size range is generally not emphasized in AMS measurements because the accumulation size mode for aerosol particles is typically around 300 nm and the size mode for primary particles is typically around 90 nm. Installation of the PM2.5 inlet gave us the ability to compare chromium signals before and after the installation with the theory that if most of these particles were in the primary or accumulation mode it would have little effect on the magnitude of chromium signals seen, while if these particles were primarily larger and crustal in nature we would see an increase with the installation of the PM 2.5 lens. Figure 8 shows that we do see a considerable increase in the frequency of these 1-second chromium spikes with AMS. PM10 (PM mass of particles with sizes between 0 and 10 μm) as measured by ARISense is also depicted, and confirms that we seeing similar magnitudes of PM10 before and after the lens change.

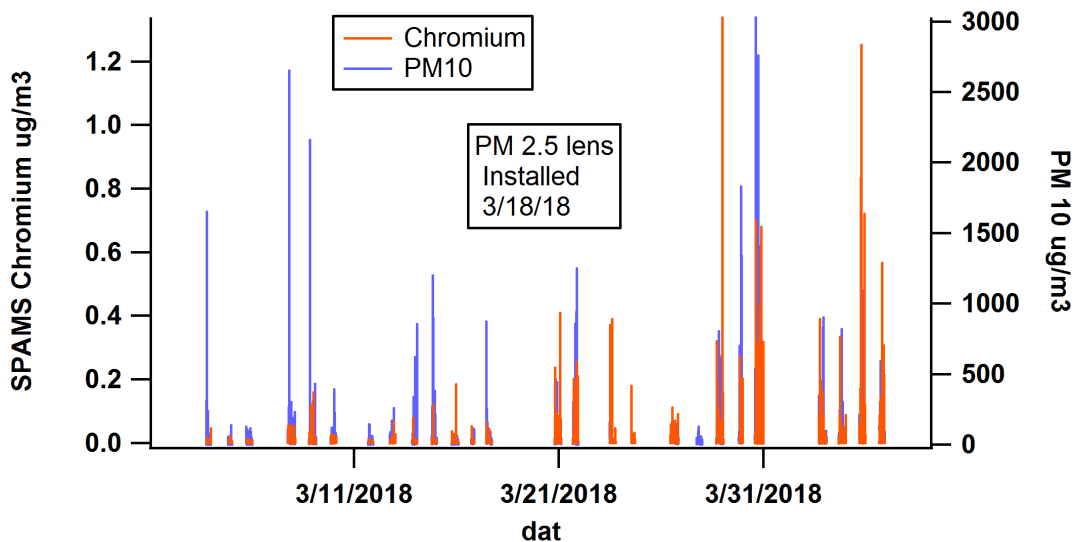


Figure 8. Comparison of particulate matter chromium (red) measured with the AMS before and after an internal lens change. PM10 (blue) measured with the ARISense is shown for comparison.

There are occasions where the SJAC-LPAS instrument does see a Cr(VI) signal while the SPAMS does not see any corresponding signal enhancement with its Cr^+ ion signal. We have done laboratory tests prior to the field deployment examining the mass spectrum of elemental Cr and Cr_2O_3 samples (Cr(III) oxidation state) but we did not examine any CrO_3 samples (Cr(VI) oxidation state) due to the hazards associated with Cr(VI) handling and sampling. Cr(VI) does have a relatively low boiling point at 250°C so that both vaporizers present in the SP-AMS should be able to convert the CrO_3 into the gas phase if present. In future work, it would be beneficial to do these difficult laboratory measurements to gain confidence in the instruments ability to detect CrO_3 .

We have investigated other ions associated with CrO_3 including CrO^+ , CrO_2^+ , Cr_2^+ , Cr_2O^+ , Cr_2O_2^+ and Cr_2O_3^+ . In general all of these species have smaller peak signals than the Cr^+ and most of them do have occasional 1 second enhancements but without any

coincident signal enhancement between the Cr(VI) signal from the SJAC-LPAS and these ions.

Data Access

Campaign data is stored on a shared cloud drive.

<https://herndon.homeunix.net/owncloud/index.php/f/211027>

Project collaborators have been given a campaign-specific password and user name.

A single time base is used throughout, covering the entire campaign. A quality assurance document accompanies the data and describes each produced data series. When appropriate, instrument details, calibration factors, and representative plots are shown.

Data reported includes only mobile data taken 30 meters or more away from the overnight parking location at SCAQMD headquarters. There are two reasons for paring down the data in this way:

1. Some instruments were not collecting data overnight, including particulate matter speciation data from the Aerosol Mass Spectrometer (AMS), volatile organic hydrocarbon data (VOC) from the proton-transfer mass spectrometer (PTR-MS) and hexavalent chromium data from collaborators at the Desert Research Institute.
2. Excluding overnight data allows for the creation of comma-separated-value (csv) files that have few enough columns to be opened in Microsoft Excel. This makes these data files easily accessible to future researchers and collaborators.

This data includes 26 driving days between Sunday March 3rd and Wednesday April 5th, 2018.

A subset of instruments collected stationary data at the SCAQMD parking lot between drives, for the period spanning Thursday March 1st to Wednesday April 5th, 2018. This data is not reported here for the reasons above, but is archived and backed up at Aerodyne Research, Inc.

Results

In this section, we outline a number of different emissions case studies.

Overview of Particulate Matter Cr(VI) and Cr in the Study Area

Summary heat maps of metal-containing particulate matter have been produced for the studied neighborhoods. Cr(VI) (Figure 9, data from the SJAC-LPAS) and Cr (Figure 10, data from SP-AMS) are discussed here, but maps of additional species are shown in Appendix D : PM_{large} (2-16 μ m), Al, Fe, Ni, Sn, Ti and V.

In these figures, data is binned in 300 m x 300 m boxes. This grid size was chosen to best display data in the three primary neighborhoods of interest at a glance, with field data primarily along the main boulevards (spaced by around 800 m) and occasional areas of higher-density sampling, particularly in Compton and in Paramount (50 to 200 m city blocks). These maps are normalized by the number of datapoints in each bin. In this way, neighborhoods that were visited frequently are not over represented. The calculation has been done twice: once for normalized particulate matter mass (top), and once for the

normalized frequency of measured data points with mass above a given threshold (middle). The number of data points in each bin is shown (bottom) to give an idea of the representativeness of the measurement over the course of the campaign.

Thresholds for the frequency maps were chosen based on instrument performance and sensitivity. For the SJAC-LPAS measuring continuous Cr(VI), a detection threshold of 0.4 ng m^{-3} was used. Response to ambient concentrations below this threshold would have been difficult to distinguish from small fluctuations of the spectrometer lamp spectrum or detector response observed during actual operation. For the SP-AMS measuring Cr, a conservative threshold of 0.05 ng m^{-3} was chosen. This threshold just over three times the limit of detection (0.015 ug m^{-3}) of the SP-AMS for particulate matter Cr. Manual inspection of the mass spectra (as in Figure 6) for selected Cr events at or above this threshold was also done to confirm the presence of Cr and rule out potential interferences. SP-AMS data both pre and post lens change are used to construct these figures (see discussion in “AMS Detection of Cr”).

The frequency measure is particularly relevant for AMS metal results, since only single-second spikes were observed, and PM mass showed a large dynamic range. SJAC-LPAS data, which has a much longer time response, was further filtered to remove data where the AML was travelling faster than 50 km/hr. This aims to reduce artifacts from single enhancements “smearing” across the map when travelling fast.

These maps highlight areas of interest, some of which are discussed in detail in other sections of this report, notably West Rancho Dominguez, where Cr(VI) and some Cr were observed, and Longwood, where Cr and a number of other particulate matter metals were observed during a dedicated street-sweeper chase (no data reported from the SJAC-LPAS).

A significant enhancement of Cr(VI) was observed on Freeway 91, and in fact, throughout the campaign, several Cr(VI) enhancements were noted during highway drives. Appendix D, shows a zoomed-out map of Cr(VI) with enhancements on Highway 605 and Freeway 60. These highway Cr(VI) enhancements could not be definitively attributed to any one source, largely due to the time response of the SJAC-LPAS coupled with the speed of the mobile laboratory.

Other interesting source areas are also visible. In Paramount, for example, both Cr(VI) and Cr particulate matter was detected above their respective thresholds (middle panels, contrast enhanced by log scale), but looking at the normalized mass of particulate matter detected, these areas are not significantly enhanced overall (top panel, linear scale). Log scaling the mass concentration maps (top panels) does not change this conclusion. This means that those Cr(VI) and Cr enhancements detected in Paramount did not result in an enhanced average mass concentration above background levels. Conversely, areas that show enhancements in both metrics (mass concentration and frequency of detection) may indicate localized sources, and are explored in greater detail in the following sections.

SJAC Cr6

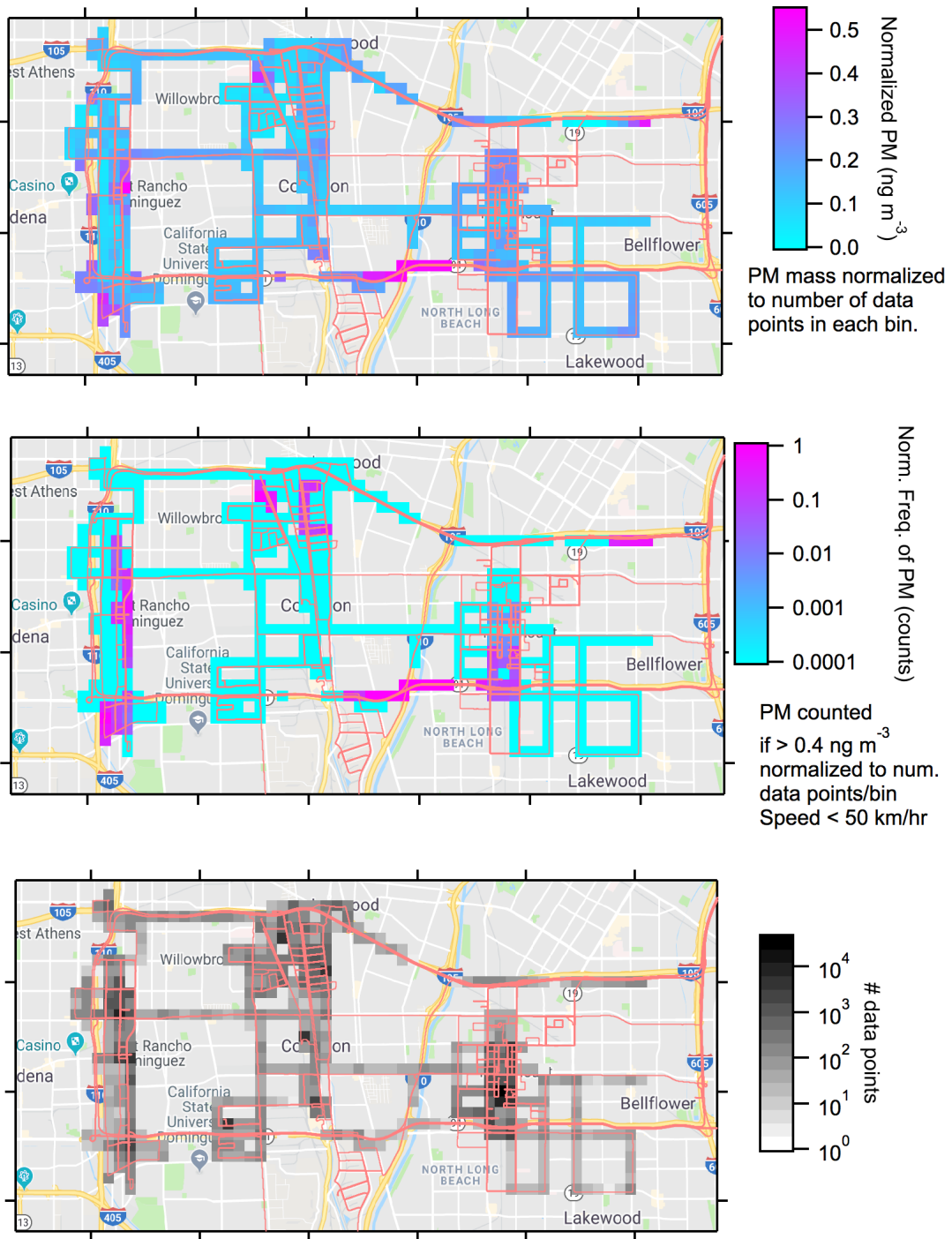


Figure 9. Particulate matter hexavalent chromium in the study region (Cr(VI) or Cr6 for short) is binned in 300m x 300m boxes and normalized by the number of data points per bin (bottom). PM mass concentration (top, linear scale) and the frequency of PM mass enhancements above a given threshold (middle, log scale). No data is shown for speeds $\geq 50 \text{ km/hr}$ or when the instrument was off. The red trace shows the AML route for the entire campaign.

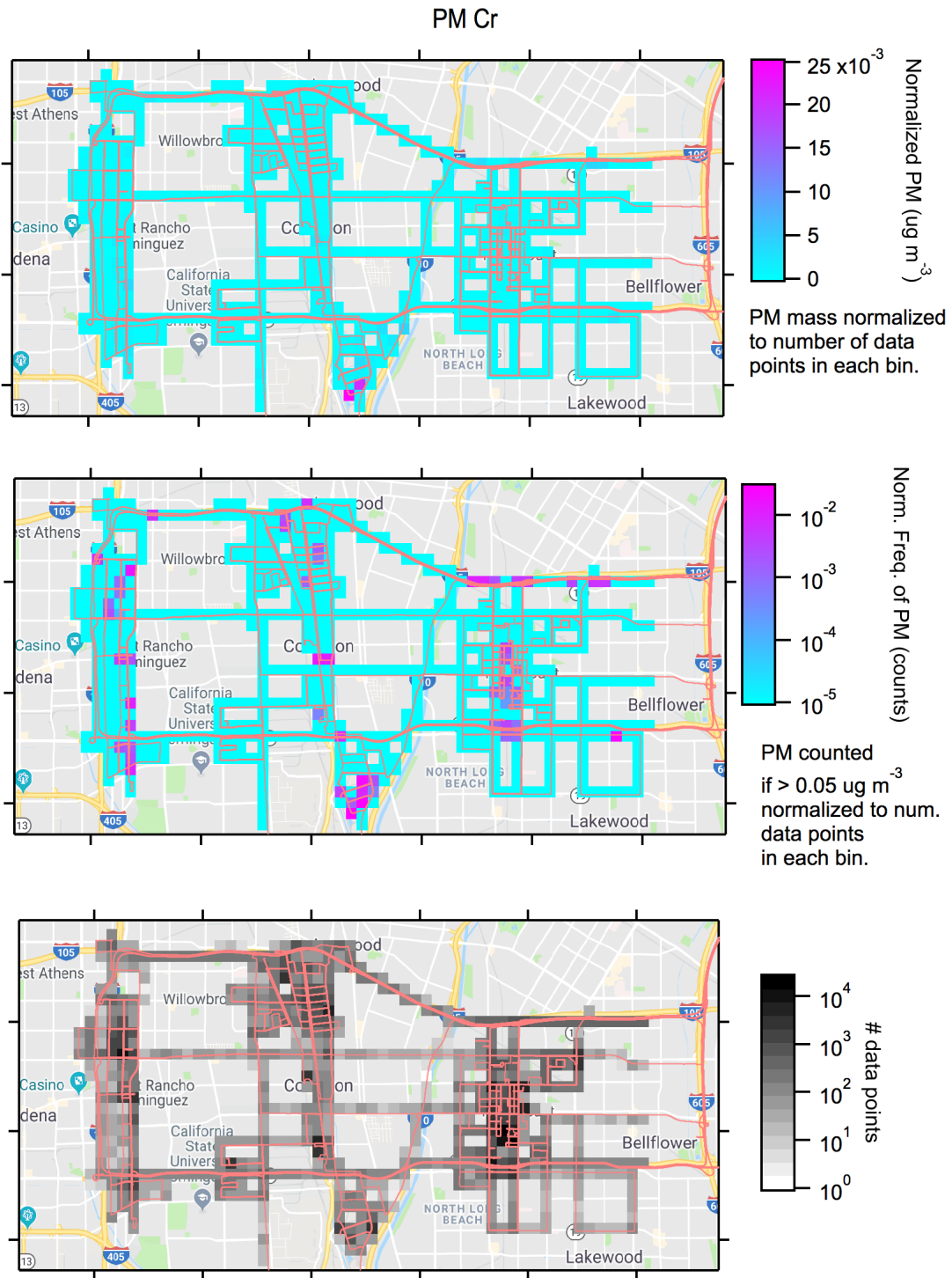


Figure 10. Particulate matter chromium in the study region is binned in 300m x 300m boxes and normalized by the number of data points per bin (bottom). PM mass concentration (top, linear scale) and the frequency of PM mass enhancements above a given threshold (middle, log scale). The red trace shows the AML route for the entire campaign.

SCAQMD analysis of data from the Cooper Xact monitor installed at the Paramount Hospital SCAQMD sampling site has found that Cr enhancements are often correlated with enhancements in V, Ni and Ti. For this reason, an investigation was undertaken of the similarity of the maps shown in Appendix D to Figure 10, with all species detected via AMS. These graphs were constructed by plotting the z-dimensions (color scales) of two maps. No correlation is observed for the normalized mass (Figure 11), nor for the normalized frequency (not shown). A significant amount of Fe is usually observed along with Cr, however, providing further evidence of the crustal nature of many of these particles.

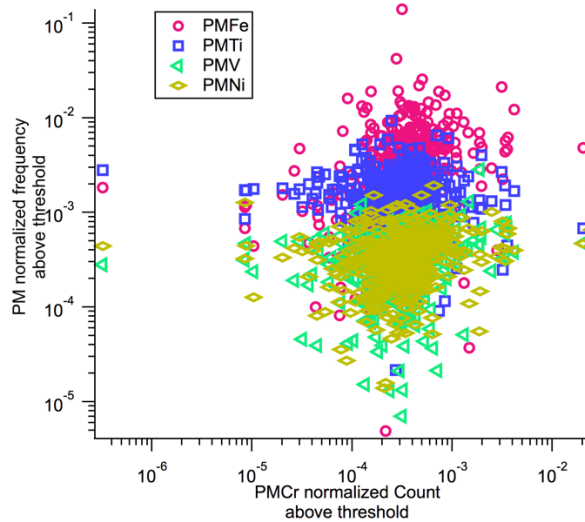


Figure 11. Correlation between selected PM metals enhancements above threshold versus PM Cr enhancements above threshold. Data is taken from the color scale of Figure 10 and the figures in Appendix D.

Street Sweeping

One notable area of enhanced particulate matter chromium (PM_{Cr}) occurred during a measurements where the AML followed a street sweeper in the Longwood neighborhood. This sampling strategy was attempted in order to verify the hypothesis that the PM_{Cr} enhancements observed by the SP-AMS were due to coarse mode crustal particles (i.e. dust that settles out of the air). Figure 12 shows a map of the normalized frequency of PM_{Cr} particles encountered during this period. When compared to Figure 10, and analogous figures in Appendix D showing other metals, we see that this area pops out over the rest of the studied areas in terms of enhanced PM metals detection with the AMS. Unfortunately, the SJAC-LPAS instrument, which quantifies hexavalent chromium (as opposed to atomic chromium) was not operational during this exercise.

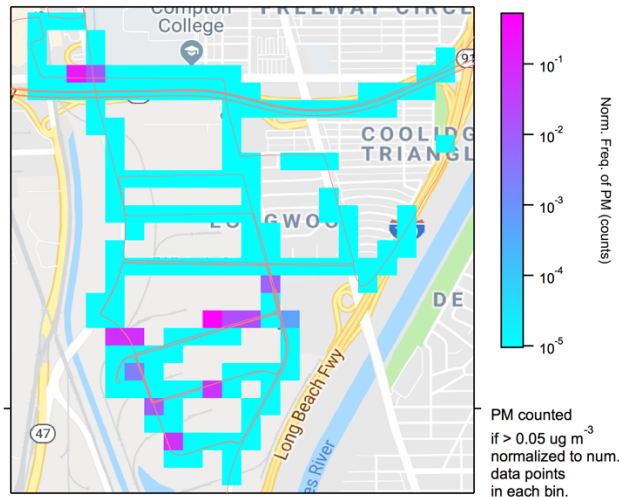


Figure 12. Particulate matter chromium during a street sweeper chase in Longwood. The frequency of PM mass enhancements above $0.05 \mu\text{g}/\text{m}^3$ is binned in $100\text{m} \times 100\text{m}$ boxes and normalized by the number of data points per bin (log scale). Figure 10 shows additional details over a broader area.

Paramount Odor Plume

At several points during the campaign, a very strong odor was noted in the neighborhood near the Promise Hospital, Paramount. The instrumentation responded at the same times that humans described an odor like burning plastic or burning electronics. During these encounters, the AMS detected very large amounts of organic PM with a unique signature. From a background below $1 \mu\text{g}/\text{m}^3$, we observed sustained enhancements, with maximum concentrations peaking at $250 \mu\text{g}/\text{m}^3$. The plume was wafting in and out of the AML inlet with variations in wind.

Figure 13 shows an overview of the region in question. The Promise Hospital and cul-de-sac parking spot on the right-hand side of the graph, east of the train tracks. Potential source areas are labeled A, B and C. A sample drive transect near these source areas is shown in green.



Figure 13. Map of apparent emission zones to the West of Promise Hospital, Paramount. The white lines represent the total project GPS track of the AML. The shaded data points (black-green-white color scale) are PM response for a period on April 5th, 2018. The red circled areas are potential source regions.

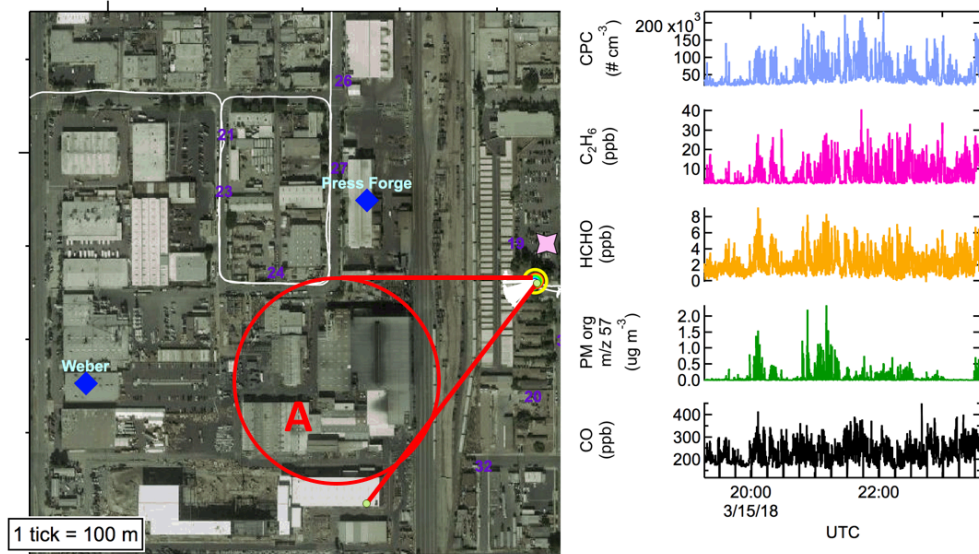


Figure 14. Data collected while stationary near hospital. The left panel is a map noting the same zone as in the prior figure with red lines projecting upwind. The right panel contains a time series from top to bottom of particle number, ethane, formaldehyde, AMS signal at $m/z=57$ and CO.

At various points during the campaign, the winds were from the south west, and the AML operated in the Paramount neighborhood east of the potential source region. A

receptor zone along Paramount Blvd, from Alondra Blvd to 70th St was chosen in order to synthesize observations throughout the campaign. A listing of approximate entry and exit times into this zone is tabulated in Table 2. A total of over 20 measurement hours were accumulated when the AML was located in this zone. The total aerosol organic loading ($\mu\text{g m}^{-3}$) has been spatially averaged and plotted (green) as a color map on Figure 15. A probability distribution (Figure 15, right) shows that organic aerosol loading in the eastern zone is shifted to the right relative to the total project data. This concentration map gives a good overview of the organic aerosol observations. However, the organic aerosol may not be chemically specific to the odor.

Table 2. Approximate time entering and exiting the eastern receptor zone along Paramount Blvd. The zone is shown in Figure 15.

UTC entering	UTC exiting
03/05/18 19:31	03/05/18 19:49
03/08/18 20:01	03/08/18 23:29
03/09/18 01:48	03/09/18 01:51
03/11/18 20:49	03/11/18 20:51
03/15/18 19:12	03/15/18 23:39
03/16/18 00:15	03/16/18 00:17
03/26/18 11:35	03/26/18 11:57
03/26/18 12:38	03/26/18 19:25
03/28/18 17:50	03/28/18 18:14
03/28/18 19:02	03/28/18 19:29
03/28/18 22:17	03/28/18 23:09
03/30/18 17:42	03/30/18 17:57
04/02/18 21:44	04/02/18 23:14

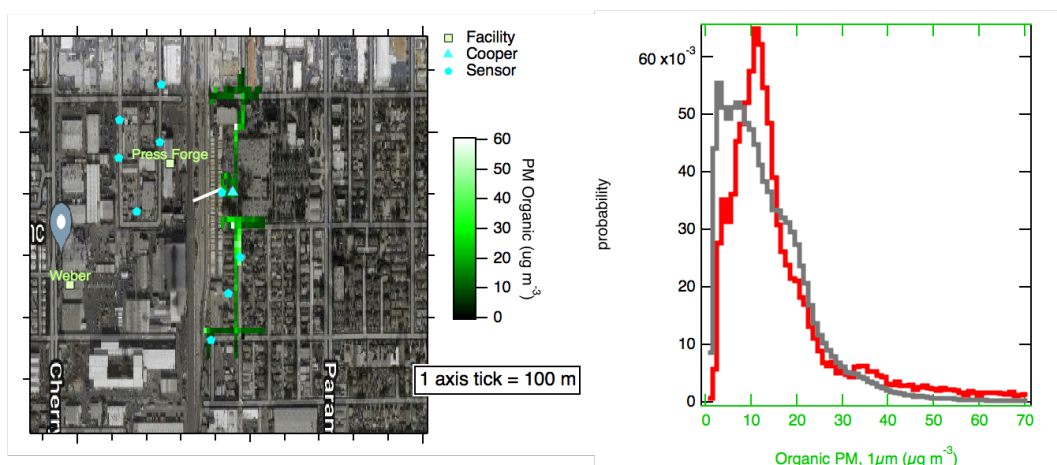


Figure 15. Organic Aerosol Loading downwind of industrial emissions. The left-hand panel is a map of organic aerosol concentrations, spatially averaging 20+ hours of data. The right-hand panel is a probability distribution of the data depicted as spatial average on the map (red distribution) and the total campaign (grey distribution).

The plume was not confined to the receptor zone described above. The downwind plume shown in Figure 16 shows how this emission travelled through downtown Paramount. In this example, the emissions on the map are colored by a particulate matter count, and other co-emitted species are shown in the time series (m/z 57 is shown as a proxy for the total organic particulate matter emission).

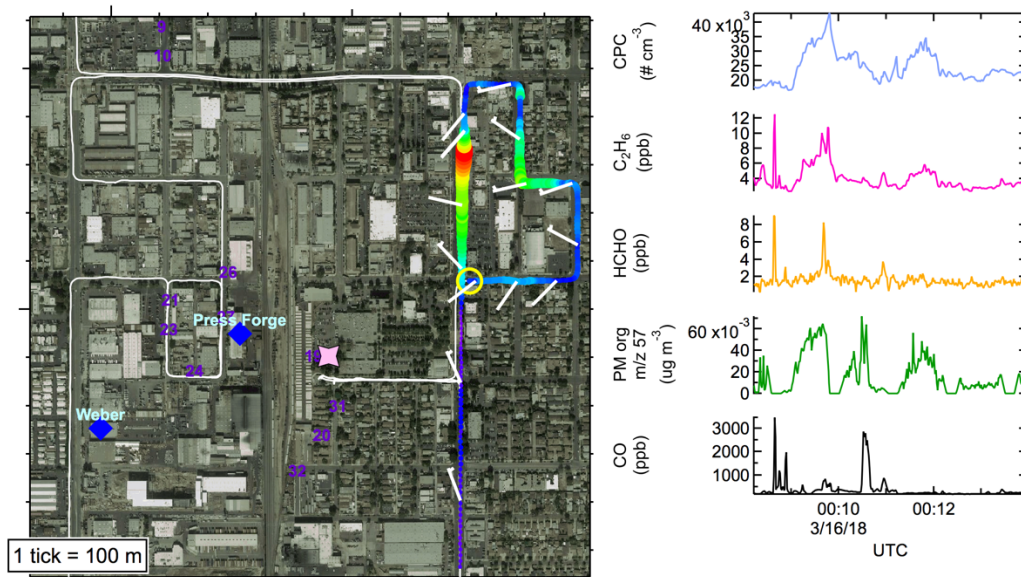


Figure 16. Emissions impact further downwind. The left-hand panel is a map track. The right-hand panel shows the associated time series of selected compounds. m/z 57 is shown as a proxy for total organic particulate matter (PM_{org}). The sharp encounters with CO are due to other traffic emissions.

The chemical composition of the odor plume was complex. As noted previously, organic particulate matter was measured by the AMS during the odor events. The specific ion at mass-to-charge ratio 57 (aka m/z 57) appeared elevated during the plume encounters. This m/z 57 signal can be due to ions from several fragments such as C₃H₅O⁺ and C₄H₉⁺.

Other combustion and hydrocarbon species were also elevated, showing a consistent chemical fingerprint (Figure 17). The roof-mounted small sensor (ARISense) showed particle sizes much smaller than coarse mode emissions. VOC investigation of the odor plume does not show elevation in any of the toxics that were selected for quantification by the quadrupole-based instrument. In fact, in some encounters with the odor plume, the mixing ratio of benzene is greater outside of the plume than within it, clearly originating from other sources.

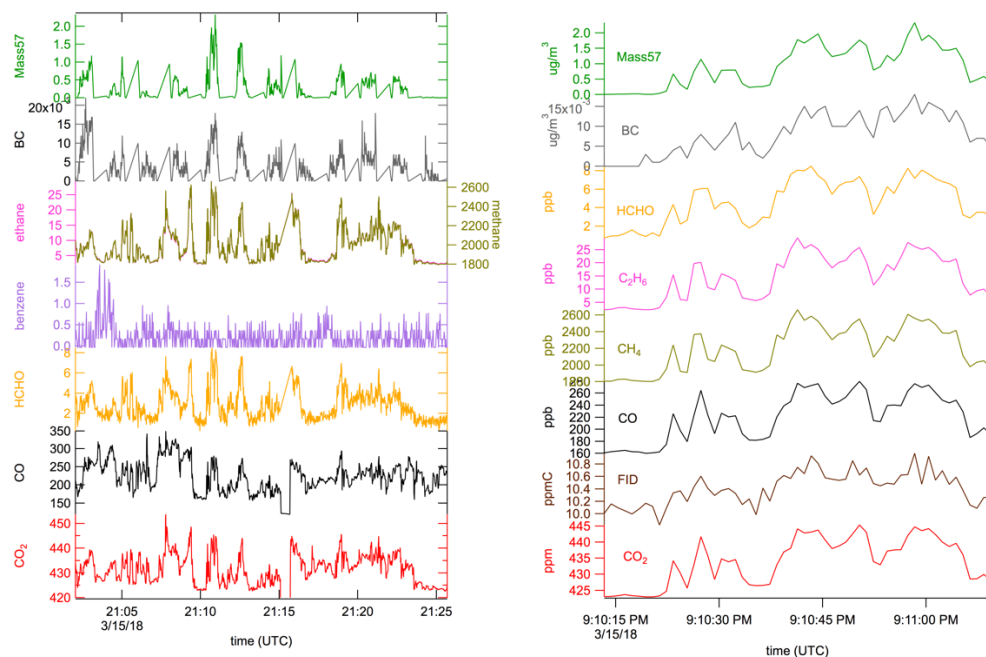


Figure 17. Example time series of other species emitted. The left-hand panel is a time series of data collected when the AML was sampling the odor plume. The fluctuations in amplitude are most likely driven by variability in the wind and dilution history of the emission plume, not variability in the emission rate itself. The species noted on this figure are: $m/z=57$ (aerosol fragment), black carbon signal, ethane & methane, benzene, formaldehyde, carbon monoxide, carbon dioxide. The right-hand panel depicts the same plume event over a shorter time scale.

The chemical composition of the plume provides some clues as to its source type. The combustion indicators CO and CO₂ exhibited periods of highly correlated variations (Figure 18), suggesting a combustion source. The presence of ethane and methane point to a natural gas fuel source and the presence of correlated formaldehyde indicates overall inefficiency in the combustion. One possible source could be the use of natural gas furnaces.

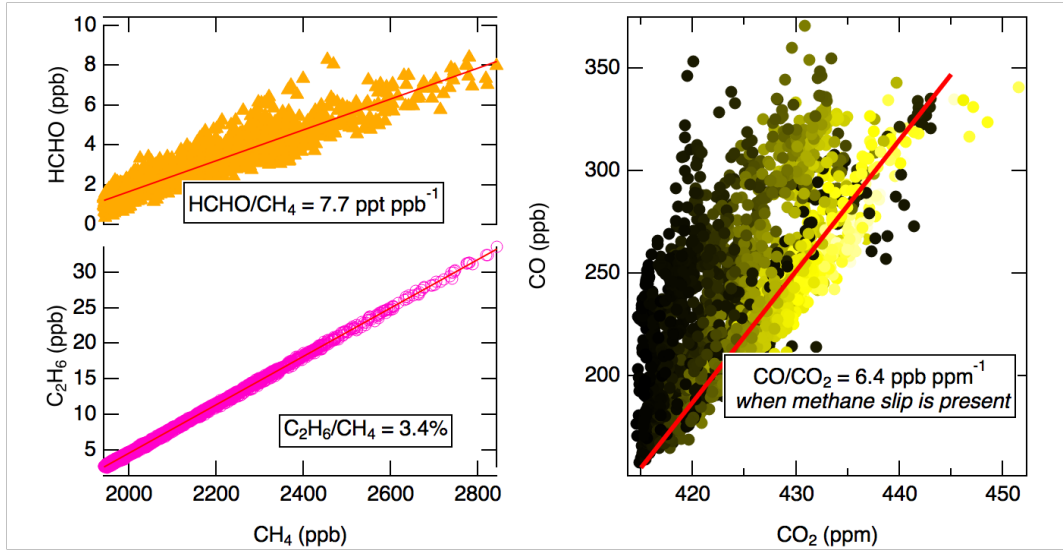


Figure 18. Correlation analysis of the emissions from the southern sector of Press Forge. The figure depicts correlations between formaldehyde and methane, ethane and methane and carbon monoxide and carbon dioxide. Note that the cited molar ratio between CO and CO₂ is estimated for the apparent presence unburned methane only.

The DRI hexavalent chromium measurement was functioning well during most of the total time period. The persistent odor plume did not show persistent and correlated elevations in Cr(VI). However, some enhancements in Cr(VI) were observed in Paramount in the receptor zone shown above, and are described in the section “Hexavalent Chromium at the Promise Hospital Site”.

Stationary Measurements at Promise Hospital

The map in Figure 19 shows the AML position relative to Promise Hospital. This parking location is near a cluster of SCAQMD’s portable samplers to the north and south. Sampling in the parking lot of this hospital allowed us to compare directly with the Cooper Xact monitor, which has observed elevated Cr signals during westerly winds at times. This location provided close access to multiple large facilities of interest over long periods of time (often several hours) in a secure location with some separation from nearby traffic. Geometry of the area relative to the parking lot allowed emissions to be more readily associated with a specific facility in certain wind directions.



Figure 19. Stationary measurement location near the Promise Hospital in Paramount. The AML parked in a cul-de-sac on Harrison street.

Table 3. Summary of Stationary Measurements at the Promise Hospital.

Measurement date	Winds	Observations
3/8/2018 (20:10 – 23:20 UTC)	Southerly	No significant enhancements.
3/15/2018 (19:15 – 23:30 UTC)	Westerly	Persistent odor plume. Single short enhancement of Cr(VI).
3/26/2018(12:45 – 19:00 UTC)	Northwesterly	Intercomparison with Cooper Xact monitor undertaken. Persistent odor plume. Several Cr(VI) enhancements.
4/3/2018 (17:00 – 21:00 UTC)	Westerly	CH ₄ and C ₂ H ₆ , occasional other VOCs. Persistent odor plume. Particulate organic matter emissions.

Table 3 summarizes the measurement observations at this location under different wind conditions. The odor plume is described in greater detail in the “Paramount Odor Plume Section”. In the following paragraphs, we describe intercomparison data and the Cr(VI) data.

PM Metal Intercomparisons

Figure 20 shows a comparison of particulate matter metal observations by the Aerodyne Aerosol Mass Spectrometer and SCAQMD’s Cooper Xact monitor during a 5-hour period on 3/26. The Cooper Xact monitor detects elemental metals using X-ray fluorescence of particulate matter samples collected on filter tape. The Aerodyne AMS, in addition to the more commonly measured organic or black carbon PM, can also detect metals via laser-induced vaporization of incoming particles. While the Cooper monitor is filter-based, the AMS is not, and has a particle size cutoff due to the presence of internal lenses (see the discussion section and the section “AMS Detection of Cr”). These differences will be particularly important if the metals occur in coarse particles (e.g. dust).

The difference in timescale between the Cooper data and the AMS data make comparisons over this time period difficult. Occasionally, box trucks and other vehicles could be seen driving up and down the lane for the storage company adjacent to the parking lot. Intermittent spiky combustion signals confirmed the nearby presence of passing trucks. Around 11am, we encountered a period of relatively steady wind out of the northwest. We noted the return of the odor plume (“Paramount Odor Plume”). We also note that visitors from SCAQMD installed an OmniTM FT sampler at the hospital site at one point on the morning of 3/26.

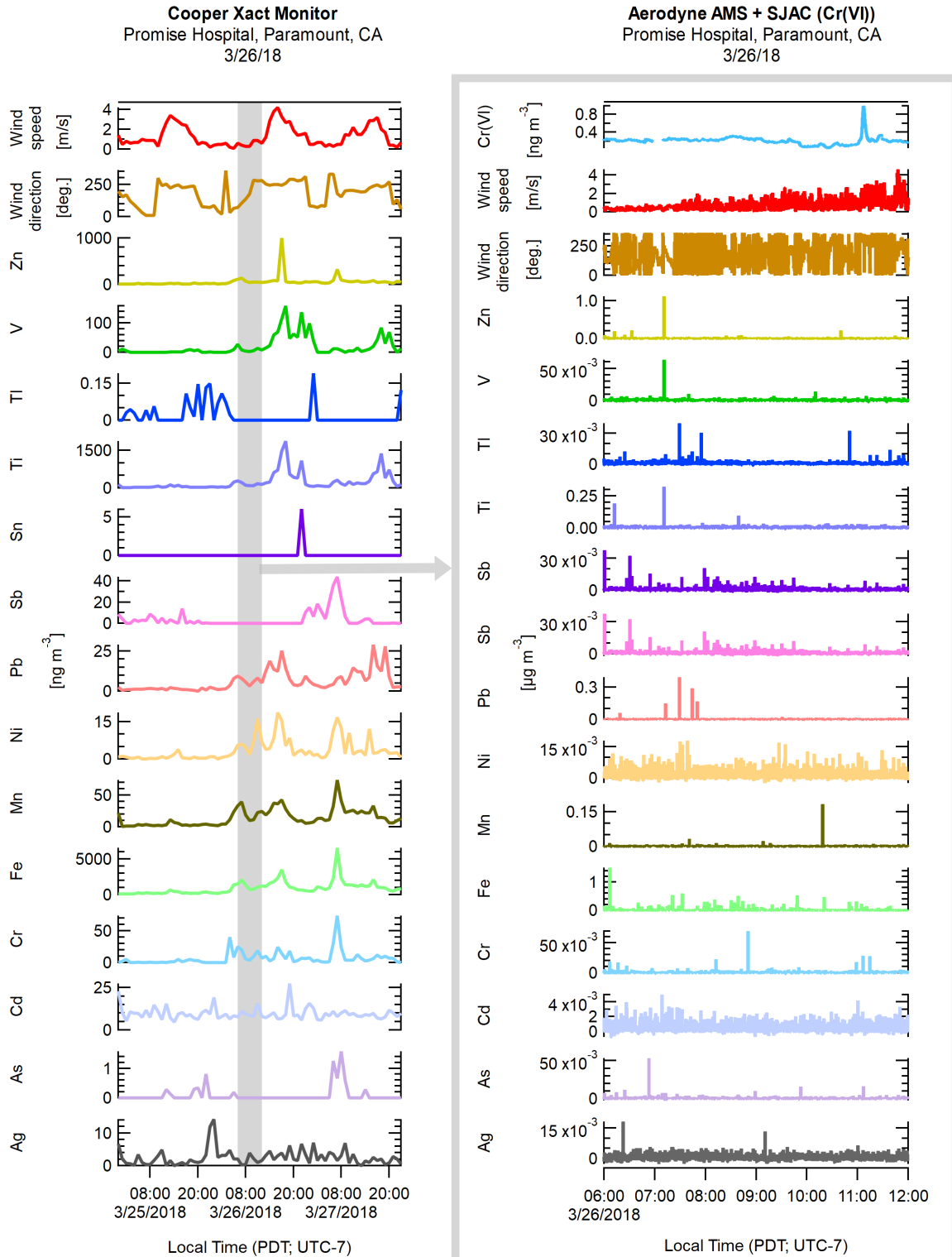


Figure 20. Stationary measurements of airborne metals collected during a side-by-side comparison of the Cooper Xact Monitor (hourly measurement; ng m^{-3}) and Aerodyne AMS (1 Hz; $\mu\text{g m}^{-3}$) instruments in the parking lot of Promise Hospital in Paramount, CA. A grey section shading the time traces of metals measured by the Cooper Xact monitor (left) from 6:00 AM to 12:00 PM on 3/26/2018 corresponds to results from the Aerodyne AMS (grey box on right).

Hexavalent Chromium at the Promise Hospital Site

A distinct Cr(VI) peak reaching $\sim 1 \text{ ng m}^{-3}$ was observed on 3/26 at $\sim 18:07 \text{ UTC}$ (11:07 AM local) with a smaller one about 20 min later, neither of which coincided with any of the measured pollutants (Figure 21; background around 0.12 ng m^{-3}). Met data from the SCAQMD site indicated light winds ($< 1 \text{ m/s}$) shifting from E at 14 UTC (7AM local) to W by 18 UTC (10AM local), putting the site downwind of Press Forge and adjacent railyard. This wind direction agrees with the measured wind on the AML shown as white wind barbs in (Figure 21).

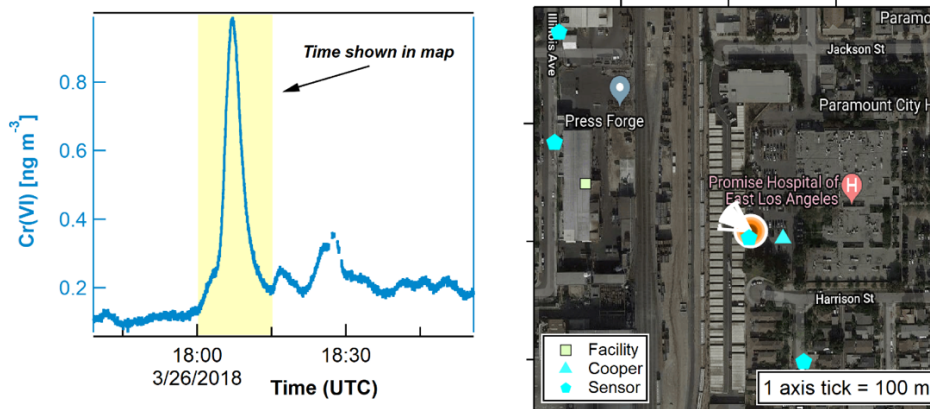


Figure 21. Observation of Cr(VI) enhancements measured while parked in the parking lot of the Promise Hospital. Peak occurs at $\sim 18:07 \text{ UTC}$ (11:07 AM local time).

The Cr(VI) trace has been mathematically deconvoluted in Figure 22 and Figure 23 (dark blue traces) to remove some of the smearing due to the mixing process in the SJAC (see Appendix C). The Cr(VI) emissions did not correlate with the PM_{org} and other tracers of the characteristic odor plume also observed in this area (see “Paramount Odor Plume” section). However, two periods of enhanced CO_2 and NO concentrations occurred at about the same time, but 3-4 min earlier (Figure 22). Time synchronization issues between the SJAC instrument and the gas phase tracers need to be verified. The CO_2 and NO peaks did not coincide with hydrocarbons or particulate matter Al, Cr and Fe metal measurements from the AMS. There is no obvious correlation with the hourly metals data from the collocated Xact monitor, although it did record an increase in total Cr for the 18 UTC hour (11AM local), see Figure 20.

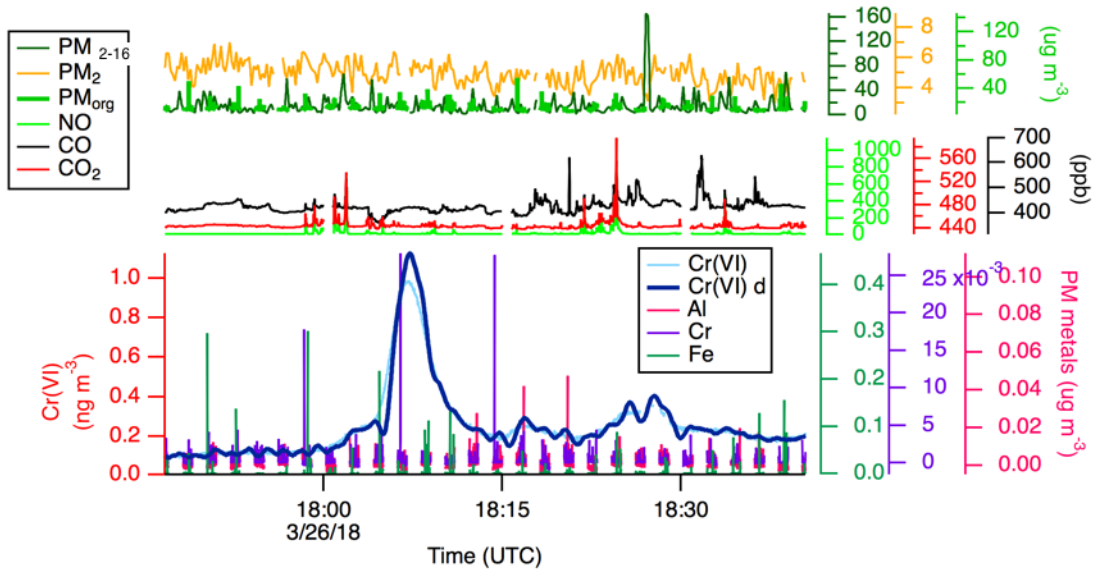


Figure 22. Promise Hospital Cr(VI) enhancements measured on 3/26/2018. Deconvoluted Cr(VI) data (dark blue, see Appendix C) is shown along with original data (pale blue).

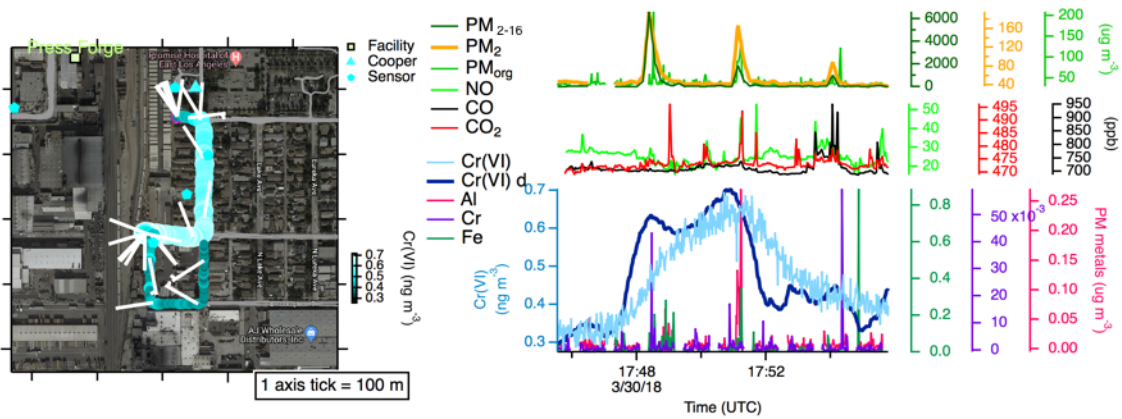


Figure 23. Promise Hospital Cr(VI) enhancements measured on 3/30/2018. Deconvoluted Cr(VI) data (dark blue, see Appendix C) is shown along with original data (pale blue).

VOC Emissions

Paramount Petroleum

There are two figures below from the Paramount Petroleum facility on Somerset in Paramount, which were obtained under light but persistent winds (03/11). There were two volatile organic hydrocarbon (VOC) signals that showed enhancements: ethanol and the sum of the methyl pentanes, for which sensitivity factors have been estimated (concentrations are tentative in figures below, but final corrected data has been produced). The sources are clearly spatially separated. The ethanol signal was less persistent than the alkane signature. There was no evidence of enhancements in any of the aromatics.

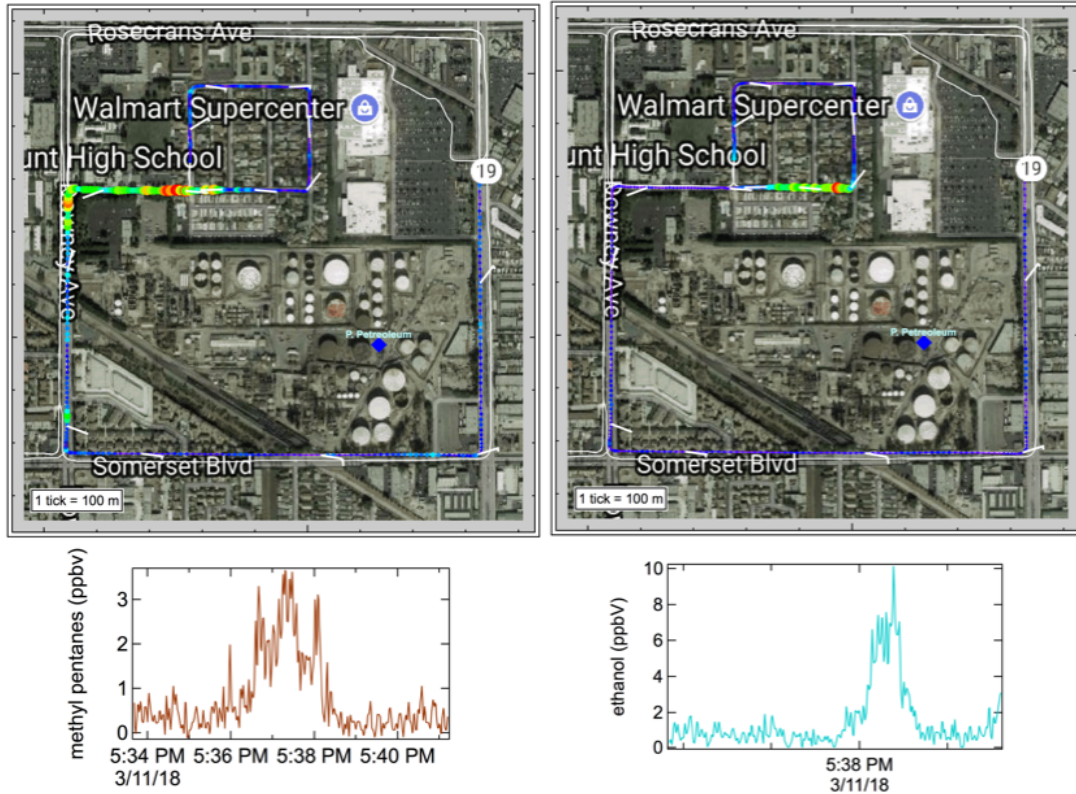


Figure 24. Emissions downwind of Paramount Petroleum. The maps (top) show the enhancements (green-red) of measured VOCs. Methylpentanes (left) or ethanol (right).

Paramount Styrene Plume

Styrene plumes were observed at a variety of locations throughout the study area. Analysis of the styrene plumes based on their location and relevant wind speed and direction, coupled with Google Street View, revealed that auto body repair and furniture manufacturing facilities were often found in close proximity. Both of these industries employ polyester resins, which contain styrene as a solvent. With the exception of one large plume of styrene (>150 ppb) observed downwind of the Peter Pepper furniture manufacturing facility in Compton, the remaining styrene plumes rarely exceeded 20 ppb.

The plume encounter with >150 ppb of styrene has a concentration at or near the odor threshold. The US EPA reports the odor threshold at 320 ppb (EPA, 2000), while the World Health Organization places the threshold at a lower value of 170 ppb (World Health Organization, 2000). Because the AML only performed a single survey of this facility, it is unknown whether the observed styrene concentration on this day is representative of the normal emissions for this facility.

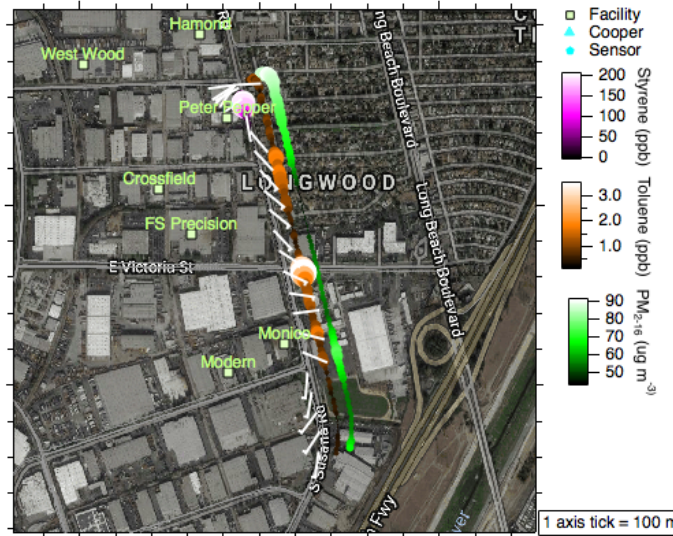


Figure 25. Map showing styrene enhancements (pink) near a furniture manufacturing facility. Toluene and large particulate matter (PM_{2.5-16}) are also shown.

Auto body shops appear to be responsible for most of the styrene emissions in Paramount, while furniture manufacturing facilities are the predominate contributors in Gardena. Compton has a much more diverse set of industries and there were numerous low-concentration plumes whose origin could not be assessed. Overall, the concentration of the styrene plumes originating from the auto body repair and furniture manufacturing facilities is substantially below the odor threshold and therefore they are less likely to be a source of community concern.

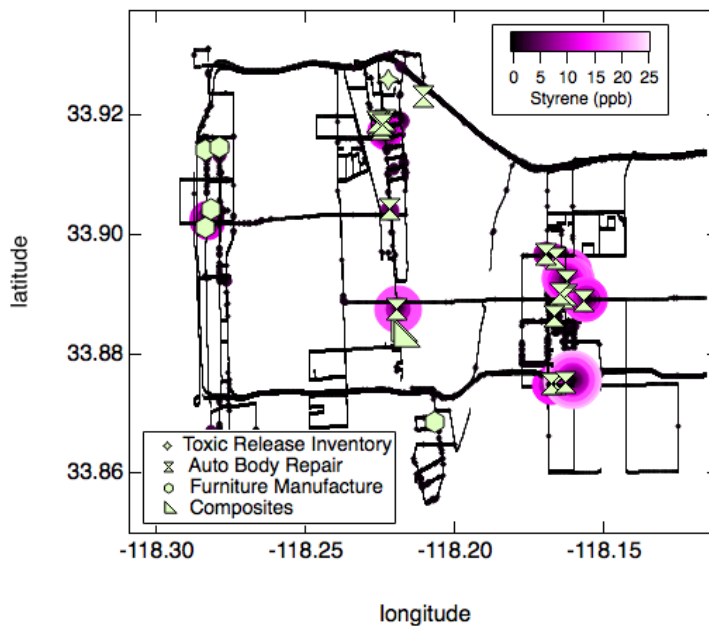


Figure 26. Measured styrene concentrations (pink) in the study area around Gardena (left), Compton (middle) and Paramount (right).

HCHO and Ethane in Paramount

On 03/05/2018, ethane enhancements indicative of point source(s) emissions downwind of Carleton Forge were observed. Figure 27 depicts the 1-second mixing ratio of ethane as a function of AML position. The ratio of ethane to methane in these enhancements was 3.1% indicating the source of the ethane was probably from a natural gas leak or combustion slip.

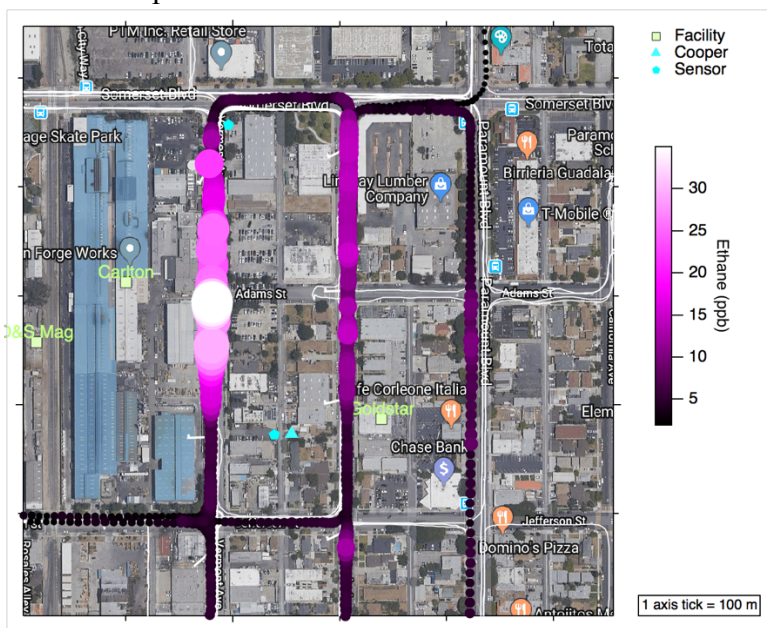


Figure 27. Ethane emissions from Carleton Forge. The wind was out of the west. A plume of ethane was reproducibly detected diluting with wind transport to the east.

Figure 28 examines the molar correlation of various species in this broad scale plume. Numerous CO_2 sources confound a clear assessment of a CO/CO_2 ratio, however the data suggests a somewhat low emission of CO (1.1 ppb ppm^{-1}). Paradoxically, the emissions of HCHO per CH_4 are greater than would be expected of a clean burning natural gas furnace (14 ppt ppb^{-1}). The spatial/temporal overlap of the observed HCHO with CH_4 is not perfect, suggesting the emission points for these species are not well co-located. The Carleton Forge website (<http://carltonforgeworks.com/products/>) does not provide any insight into how the metal alloy products are actually heated. It may be possible that another portion of the process is emitting formaldehyde at the site and the emissions of efficient natural gas combustion are being mixed prior to sampling with the AML. It is noteworthy that formaldehyde on 3/5/2018 from this source was detectable as a plume on Paramount Boulevard, 4 blocks downwind.

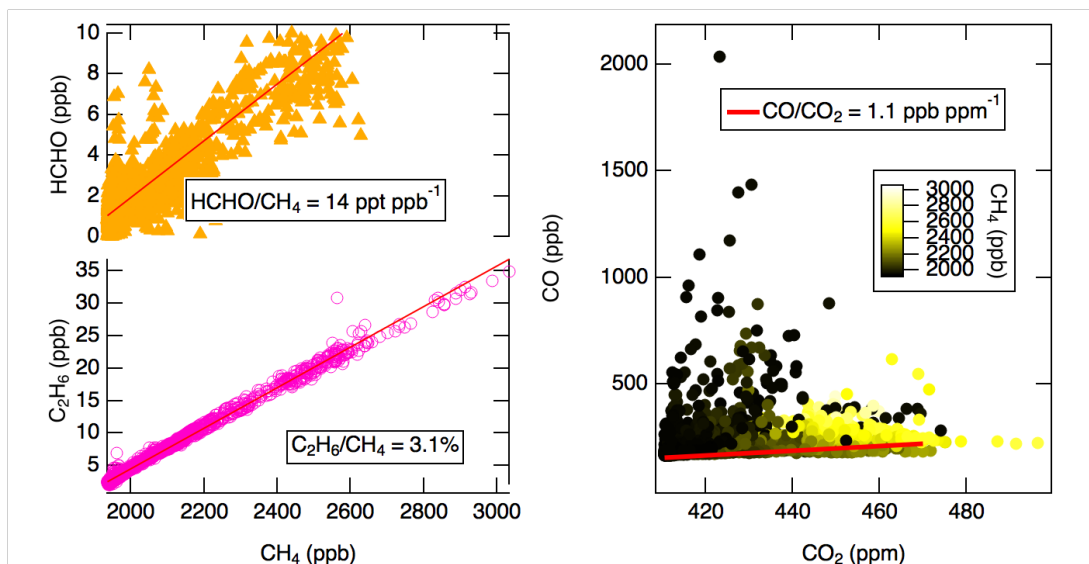


Figure 28. Correlation of species downwind of Carleton Forge. The left-hand panel shows the molar ratio of formaldehyde to methane and the ethane to methane ratio. The right-hand panel depicts a lack of correlation of CO with CO₂. The data points in the right-hand panel are colored by the concomitant methane mixing ratio.

Ambient Air Comparison

Several of the VOC compounds monitored (C3-alcohols, acetone, methyl ethyl ketone (MEK) and styrene) are not significant components in vehicle exhaust or their fuels and find their way into the atmosphere through fugitive sources. McDonald et al. refers to these as volatile chemical products, which are associated with coatings, printing inks, adhesives, cleaning agents and personal care products (McDonald et al., 2018). Inspection of the data reveals that numerous plumes of these fugitives were encountered during the AML surveys. GPS emission maps in concert with measured wind data allow one to deduce the geographical location of these emission vectors. Common solvents such as acetone, show the greatest prevalence, while MEK and styrene have fewer sources and are more constrained to specific source locations. It is not clear whether one can reliably extract background ambient concentration data from mobile area survey studies. In spite of this, it was deemed interesting to examine what the frequency distributions of the averaged data looked like and what they suggest might be representative ambient concentrations. The frequency distributions for the fugitives, with the exception of styrene, resulted in bimodal distributions where it is assumed that the distribution at the lower concentration was representative of the ambient. All of the frequency distributions are included in Appendix A. The histograms were fit to a Gaussian function with the centroid being taken as the most probable value. The figure below shows a plot of the AML data versus the VOC concentration data derived from the Pasadena ground site during the 2010 CalNex study (McDonald et al., 2018). The SCAQMD alcohol measurements differ significantly and are much lower than what was observed in the CalNex study. The present measurements for both alcohols differ by nearly a factor of 10 a result which cannot be easily rationalized by either photochemistry or errors in the estimated sensitivity factors. The remaining compounds all appear to correlate well albeit not with a one-to-one relationship.

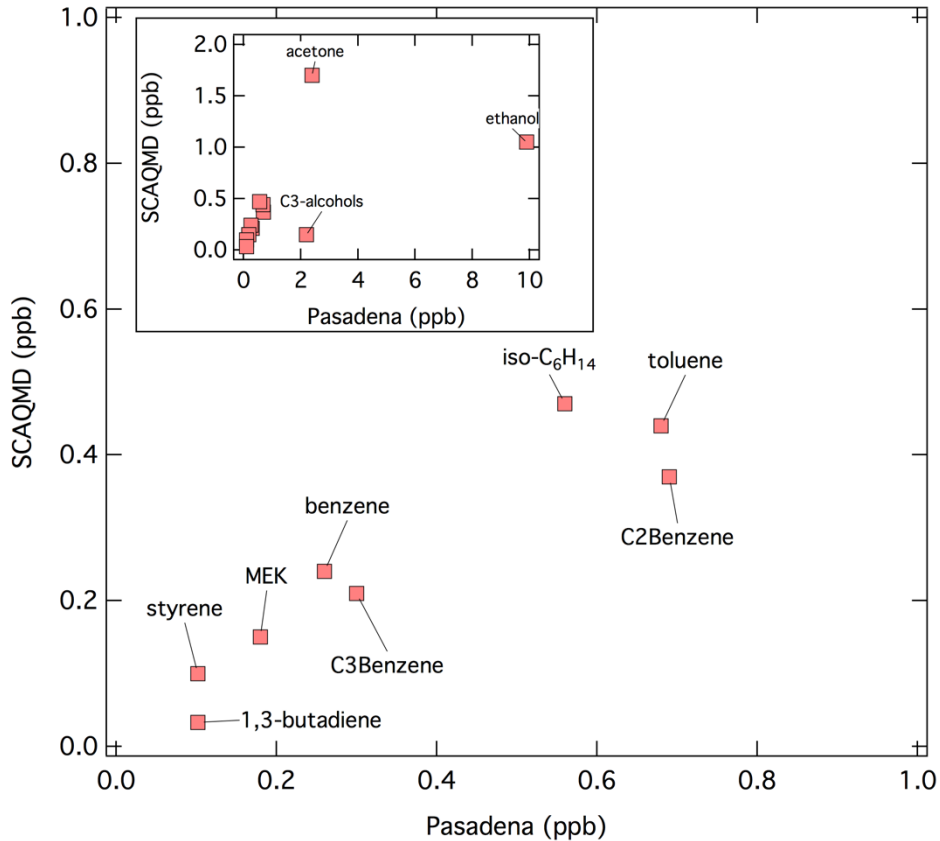


Figure 29. Comparison of ambient concentrations derived from AML survey data with those reported from 2010 CalNex Pasadena study (McDonald et al., 2018).

Exhaust Emissions

Vehicle Exhaust Comparison

Since the AML spent a significant amount of its time in transit on heavily trafficked roads, it is logical to examine how the VOCs measured during SCAQMD study compare with gasoline vehicle exhaust measurement from the Caldecott Tunnel (McDonald et al., 2018). Non-tailpipe emissions from liquid gasoline and evaporative emissions are also included. The PTR-MS data was first converted to 5-minute averages to improve integrity of the low concentration ambient background data. The averaged data is then examined as the ratio with respect to benzene through a correlation scatter plot and a histogram of the ratio computed by dividing each component by the benzene signal as is illustrated for toluene in Figure 30 below. The histogram is then fit to a Gaussian function in which the centroid is taken as the most probable ratio and the width is reflects the uncertainty.

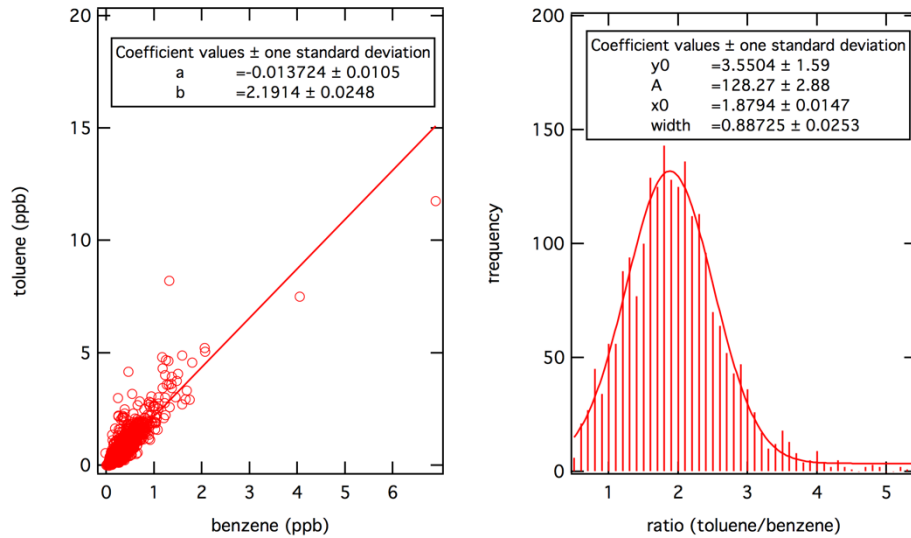


Figure 30. Analysis methods for determining the ratio of toluene to benzene for the SCAQMD study for comparison to VOC speciation profiles of gasoline vehicle exhaust.

Using the VOC speciation profiles reported within McDonald et al. (2018) molar ratios were computed for gasoline vehicle exhaust, liquid gasoline, gasoline vapors (evaporative emissions) and for ambient air. The profile for ambient emissions taken from McDonald et al. (2018) has been adjusted to account for photochemical aging (represents fresh emissions) and thus is not an exact representation of the daytime profile. These profiles along with those from the present study are examined in the figure below.

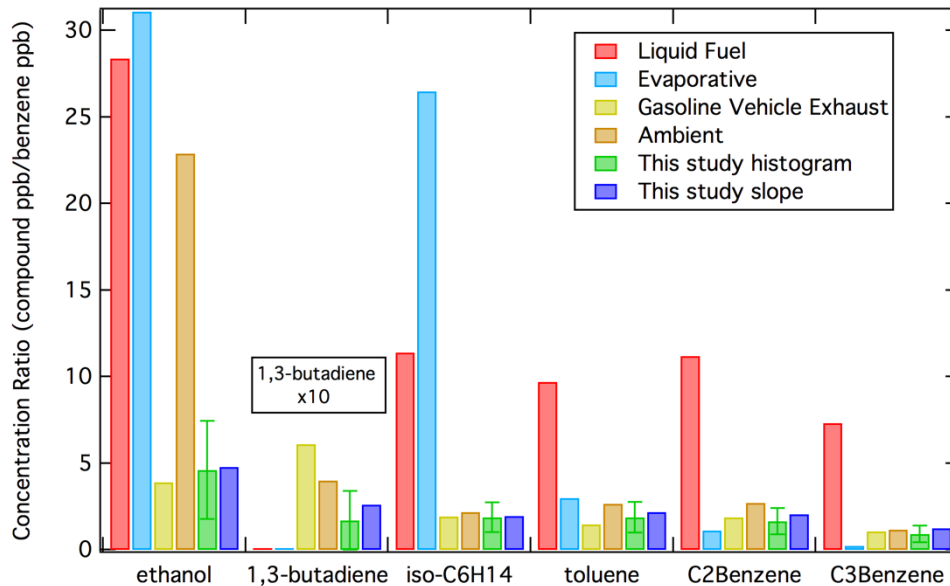


Figure 31. Comparison of SCAQMD study with reported VOC speciation profiles. Gasoline vehicle exhaust profile is from 2010 Caldecott Tunnel study (McDonald et al., 2018). Ambient profile is from 2010 CalNex Pasadena study (McDonald et al., 2018).

The current results compare most favorably the gasoline vehicle exhaust. Only 1,3-butadiene differs significantly. This result might be expected as 1,3-butadiene is readily

removed from the atmosphere by reaction with the hydroxyl radical. This analysis is not definitive, but it is suggestive that the calibration factors estimated for ethanol and C₆H₁₄ isoalkane isomers are reasonable. Except for ethanol the ambient and gasoline vehicle exhaust profiles are not significantly different and it is expected, and observed, that the data collected on-road by AML is similar to these profiles.

Truck Depots and Grocery Outlets

The Aerodyne Mobile Laboratory made several transects past the St. George Trucking Facility. Figure 32 highlights a plume measured downwind of the facility (to the NW). We observed enhancements in NO_x, total carbon, CO, CO₂, ultrafine particles, and formaldehyde. These are consistent with emissions from diesel combustion. Importantly, we also observed a depletion in ozone, consistent with NO→NO₂ oxidation between the facility and mobile laboratory. A correlation of NO₂ to O₃ indicates a slope of -1.1, consistent with the assignment of NO₂ to being derived from oxidation of NO via O₃ in transit to the laboratory. For the shown transect, wind speed was 0.9 m/s, corresponding to a total transit time of 130-500 seconds between emission and intercept. A correlation of total NO_x vs total carbon can provide a measure of NO_x emission index (EI(NO_x)). For this plume we find an EI(NO_x) of 6.9 g/kg. A second plume (not shown) measure two days later found an EI(NO_x) of 8.1 g/kg, consistent with the previous observation. From the road, it was not possible to judge how many trucks were running at the facility, or their operational state (cold started, long-running, etc). We note that there were no detectable emissions of aromatic VOCs from the facility. There were, however, correlated emissions of methane and ethane emitted (200 ppb methane, 10 ppb ethane enhancement). The 5% ethane/methane ratio is consistent with a natural gas source.

The Mobile Laboratory also spent time downwind of Ralphs grocery depot in Paramount. We were able to see into the lot, and saw regular semi-trailers, but no running refrigeration units. The facility was nominally open, with cars in the front lot and a security guard on duty. In general, there were low emissions from the depot, as shown in Figure 33. Mildly elevated NO_x and CO/CO₂ emissions indicate diesel activity, on a much smaller scale than at the St. George facility, despite being considerably closer to the site. The correlation of NO_x to total carbon indicate an emission index of 6.8 g/kg, consistent with the diesel truck observed elsewhere. There are no aromatic emissions (e.g. benzene, toluene, etc) associated with this facility. In addition, while there were correlated methane and ethane emissions from the site, they were relatively minor (20 ppb methane, 0.8 ppb ethane enhancement) as compared to the trucking facility.

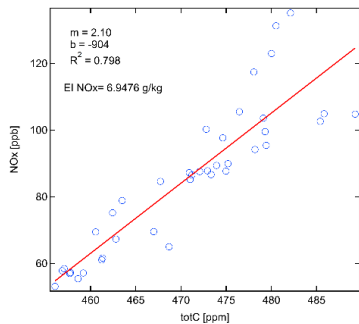
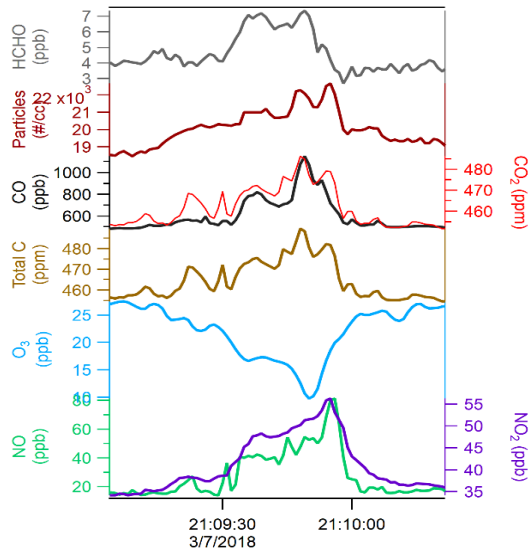


Figure 32. downwind plume from St. George trucking facility. Top: time traces for a variety of pollutants as the Mobile Laboratory transited to the northwest of the facility. Center: map of NO during the transect. White lines point into the prevailing wind direction. In this map the trucking facility is to the southeast. Bottom: NO_x vs total carbon correlation, indicating a NO_x emission index of 6.9 g/kg.

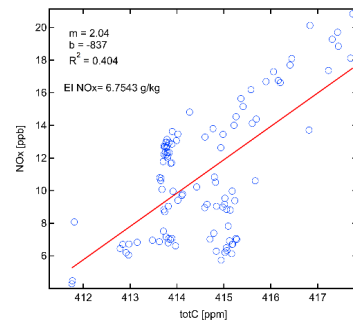
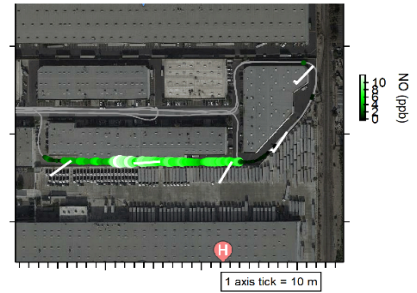
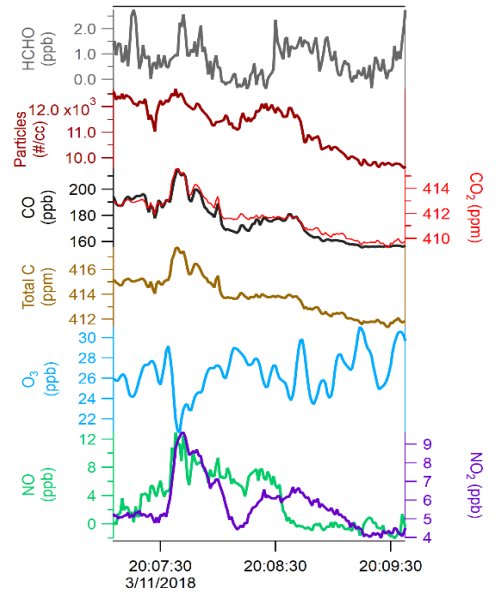


Figure 33. Measurements of pollutants while passing downwind of Ralph's grocery depot in Paramount. There are minor enhancements in NO_x, but comparatively less than at the St. George trucking facility. Top: time traces for a variety of pollutants as the Mobile Laboratory transited to the north of the depot. Center: map of NO during the transect. White lines point into the prevailing wind direction. In this map the depot is to the southwest of the transect. Bottom: NO_x vs total carbon correlation, indicating a NO_x emission index of 6.8 g/kg.

Chrome Plating/Grinding Facilities, and Cement Ready-Mix Facilities

Chrome plating/grinding and cement facilities have been combined in this sub-section because both are potential sources of chromium emissions, and both types of facilities were often present in together in the study area.

Cement is a fine powdered ingredient that turns into a paste when hydrated. Portland cement is the most common type of cement. Ready-mixed concrete, on the other hand, is made up of Portland cement, water and aggregate material like sand or crushed gravel. Several companies that produce ready-mix concrete were visited as a part of this field campaign.

Hexavalent chromium (Cr(VI)) is a known trace constituent in Portland cement. Its presence is caused by the manufacturing process.

Cr(VI) in West Rancho Dominguez

During transects in Gardena on 3/30, the SJAC saw multiple bursts of Cr(VI) signal over a 30-minute period. This was the first time this magnitude of recurring signal was observed. This same area was visited on 4/5, and again, repeated enhancements in Cr(VI) were observed (Figure 34).

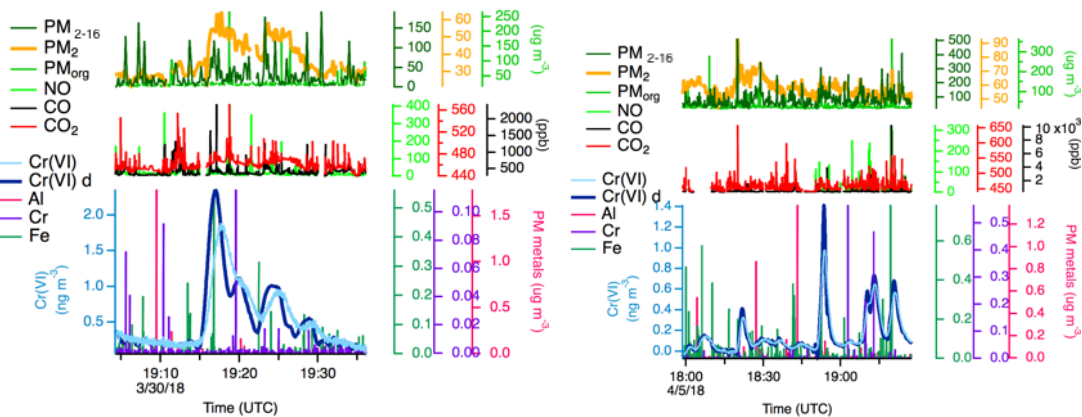


Figure 34. Recurring Cr(VI) signal on 3/30 and 4/5 in West Rancho Dominguez. Deconvoluted Cr(VI) data (navy blue trace, “Cr(VI) d”, see Appendix C) is shown alongside raw Cr(VI) data (pale blue, “Cr(VI)”).

It is notable that during these Cr(VI) enhancements, there were also single-second spikes noted in a variety of metals (Fe, Cr, Al, possibly others) as noted by the AMS. Some enhancements in large PM (PM_{2-16μm}) were also observed at the same time as Cr(VI) enhancements, and this correlation was better than for small particles (PM₂). On the other hand, there were also many spikes of AMS-measured PM metals that did not seem to coincide with enhancements of Cr(VI).

Two sample plumes from this set of measurements are below. The first (Figure 35) was taken in motion on 3/30; the second (Figure 36) was stationary on 4/5.

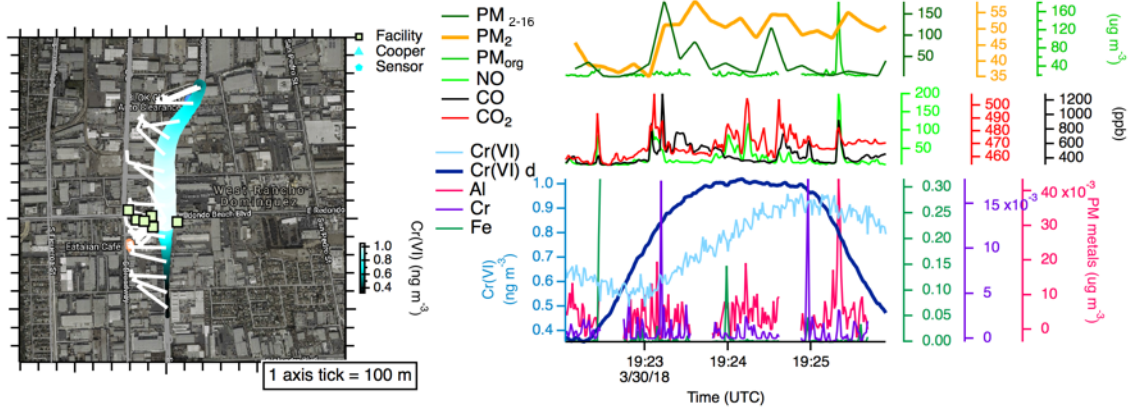


Figure 35. Detail on one of the Cr(VI) enhancements on 3/30. Deconvoluted Cr(VI) data (navy blue trace, “Cr(VI) d”, see Appendix C) is shown alongside raw Cr(VI) data (pale blue, “Cr(VI)?”). Local Time = UTC – 7h.

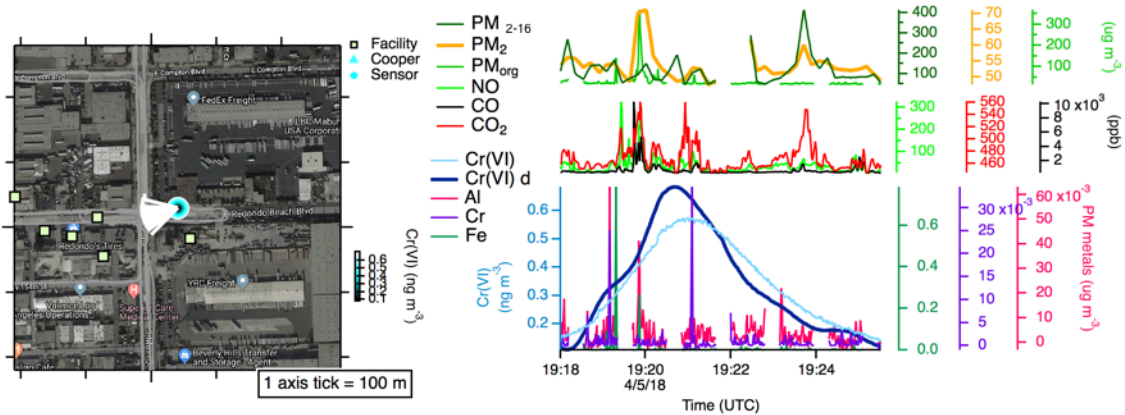


Figure 36. Detail of one of the Cr(VI) enhancements on 4/5. Deconvoluted Cr(VI) data (navy blue trace, “Cr(VI) d”, see Appendix C) is shown alongside raw Cr(VI) data (pale blue, “Cr(VI)?”). Local Time = UTC – 7h.

This data does not allow for conclusive identification of any specific industrial source of Cr(VI) emissions. However, searching publicly-available maps and listings reveals several business in this area (Table 4, Figure 37), most notably: Accu-Chrome Plating Co., A&A Ready Mixed Concrete, Rodco Precision Grinding, Redondo’s Tires, Mechanical Metal Finishing, and another unknown cement mixing facility on the E side of Main St. According to their website, Accu-Chrome performs precision grinding and applies hard chrome coatings on a variety of materials. OSHA documentation on Cr(VI) exposure in the workplace indicates that the risk of exposure is higher in hard-chrome operations than in decorative chrome operations (NIOSH, 2013).

Table 4. List of some of the businesses near the observed Cr(VI) enhancements in West Rancho Dominguez. No specific business could be conclusively identified as a Cr(VI) source.

Business Name	Latitude	Longitude
A&A Ready Mixed Concrete	33.892704	-118.2779
Accu-Chrome Plating Co.	33.89482	-118.27642
Rodco Precision Grinding	33.892904	-118.27703
Redondo's Tires	33.892641	-118.27745
Mechanical Metal Finishing Co.	33.893172	-118.2784
Unknown Concrete	33.892627	-118.27549

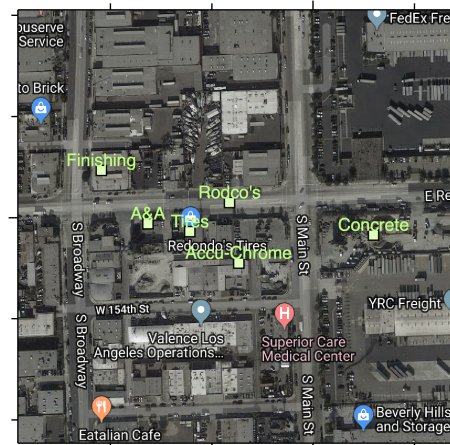


Figure 37. Map showing the locations of some of the businesses near the observed Cr(VI) enhancements in West Rancho Dominguez. No specific business could be conclusively identified as a Cr(VI) source.

During measurements on 4/5/2018, activity at the site was noted to diminish after 20 UTC (1 PM local time). The activity at other facilities in the area is not known. No further Cr(VI) events greater than 0.2 ng m^{-3} were observed between 19:30 and 20:15 UTC, at which point the AML left the area.

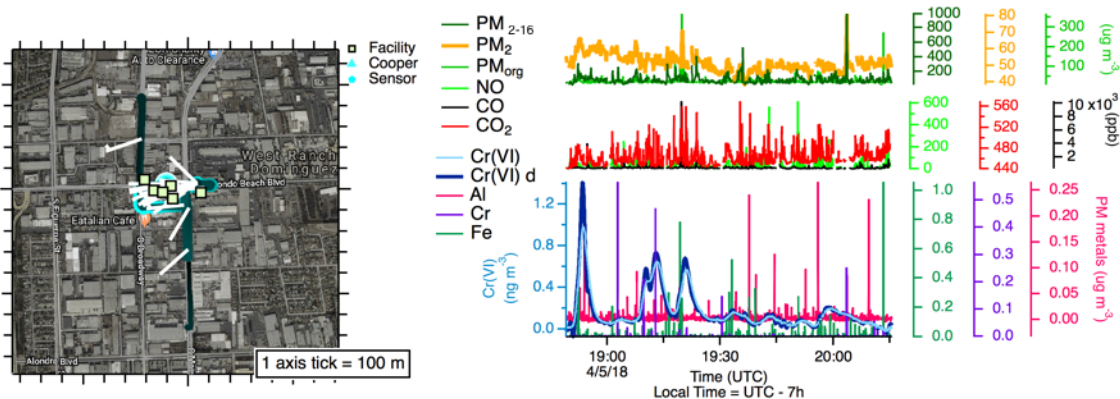


Figure 38. Detail of Cr(VI) enhancements on 4/5. Deconvoluted Cr(VI) data (navy blue trace, “Cr(VI) d”, see Appendix C) is shown alongside raw Cr(VI) data (pale blue, “Cr(VI)”).

While we are not able to definitively attribute the Cr(VI) enhancements in West Rancho Dominguez to any one facility, the repeat measurements of Cr(VI) in this area were notable. Additional Cr(VI) measurement efforts should be directed to this area.

Cadmium Plumes in the North Compton Area

The Aerodyne SP-AMS was run in 1 second mode throughout this campaign and a variety of different metals were sampled by with 1 second time resolution (see, for example, section “PM Metal Intercomparisons”). Cadmium (Cd) is a metal associated with electroplating used in the aircraft industry to reduce corrosion of steel components. OSHA states that exposure to cadmium can occur, among others, during cadmium electroplating or welding of cadmium-plated parts (OSHA, 2004). Sustained plumes of Cd were encountered on three separate occasions (3/7, 3/21, 4/4). Figure 39 shows sample high-resolution fits of the Cd signal.

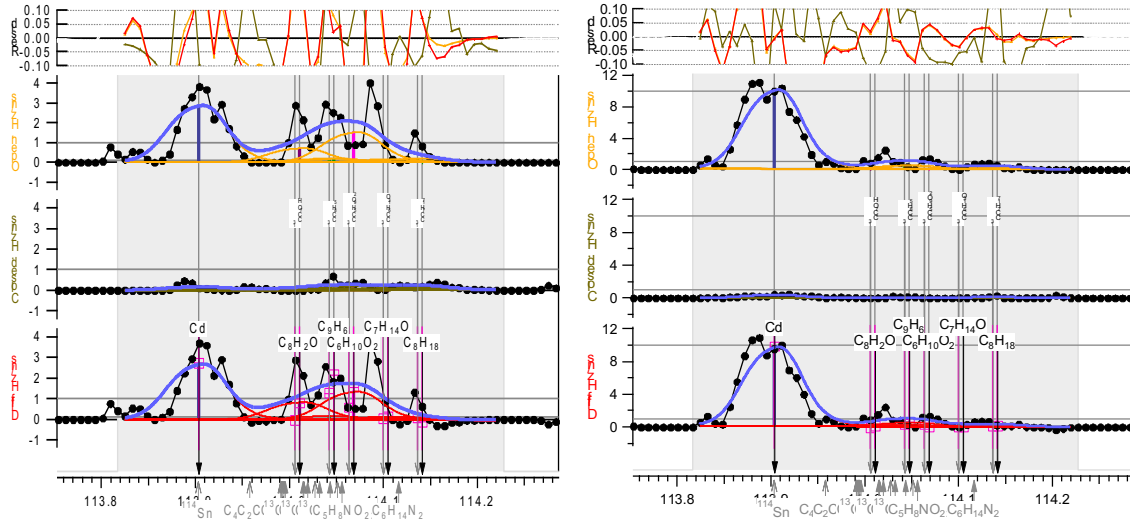


Figure 39. High-Resolution AMS fits of the Cd signal. The left and right plots show two time points in the plumes measured on 3/7/2018, showing that both moderate (left) and strong (right) Cd signals can be separated from nearby interferences.

These plumes were observed in the same area of North Compton bounded by North Alameda St., North Santa Fe Avenue, Euclid Avenue and Weber Avenue (Figure 40). It is important to note that we do not see multi-second plumes of cadmium at any other locations over this 5-week study. The fact that these sustained plumes were observed with the AMS with its $<1 \mu\text{m}$ or $<2.5 \mu\text{m}$ size cutoff, suggests that the Cd-containing particles are small, in contrast to other metals.

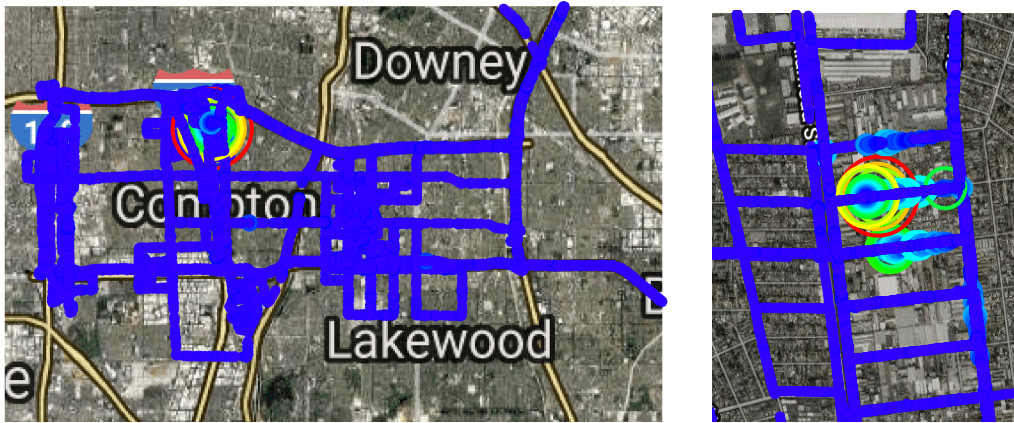


Figure 40. Cadmium measurements throughout the entire campaign (left) are depicted, with green-yellow-red circles indicating enhanced concentrations. A zoomed-in view (right) focuses on the North Compton area.

A sample Cd plume is shown in Figure 41 below. Other measurement days showed slightly different wind directions. When all of these plume encounters are considered, and assuming only a single source, the most probable source location would be the western part of the square block bounded by North Alameda St, Weber Ave, North Santa Fe Avenue and Banning Street. This is outlined in Figure 41. The highest 1-second average concentration of cadmium observed was approximately 80 ng m^{-3} . For reference, OSHA (2004) lists an “action level” where workplace air monitoring is needed at $2.5 \text{ } \mu\text{g m}^{-3}$, weighted over an 8-hour period (note: $1 \text{ } \mu\text{g} = 1000 \text{ ng}$).



Figure 41. Example Cd plume in North Compton. The suspected source location is inside the city block outlined in red. No specific business could be conclusively identified as a Cd source.

An industrial emission source of particulate matter Cd could not be conclusively identified. However, several businesses are present in the block highlighted in Figure 41. Examining this area on Google maps, reveals a preliminary list:

Table 5. Preliminary list of Compton businesses in the city block where a Cd emission source is suspected. No specific business could be conclusively identified as a Cd source.

Business Name	Note
BDC Body Shop	
Metal Movers	recycling center
Vasquez Trucking, Inc.	
Tadeo's Motor Oil	auto and truck lubricant supplier (https://tadeos-motor-oil.business.site)
Fleet Tech	truck repair shop (fleettechca.com)
Mistic Products	incense, candles
RND International	
Chino Steel, Inc.	steel fabricator or welding operation
Others	several pallet companies

Robertson's Ready Mix, Gardena and A&A Ready Mixed

Robertson's Ready Mix in Gardena, CA is a ready-mix cement facility that was visited on a few separate occasions. The facility and surrounding roads are covered in fine grey dust. Dry-sweeping of the road in front of the facility was observed. Many dust-covered RVs were parked on nearby roads, preventing the sweeper from accessing these areas. A flare can be seen through one of the openings (Figure 42). SCAQMD determined that this flare is a part-time flare permitted by the District. This area is home to the Brightburn oil fields, a few oil wells are located both on and off the property.



Figure 42. Robertson's Ready Mix in Gardena, CA. A permitted flare can be seen.

A first set of measurements were made on 03/13. Wind was from the west. Mixed plumes including ethane, methane (9% ethane/methane ratio), black carbon, and combustion tracers were observed. This mixed plume likely has contributions from a number of different nearby sources: the flare, the oil derricks, vehicles on site, and possibly the RVs. The Cr(VI) instrument was performing filter on-off experiments on this day, and the small amount of data that is available before it started to rain do not show enhancements above background.

A second visit to this site was made on 03/14. Winds were steady from the WSW. On this day, we observed a dust cloud coming from one of the towers on the facility. This cloud was not constantly emitted, rather it came in spurts from the sides. The towers can be seen in Figure 43 beyond the red-striped wall.



Figure 43. Aerodyne Mobile Laboratory performing stationary measurements downwind of Robertson’s Ready Mix in Gardena. Towers are seen in the distance.

During this dust event, we parked on a side street and sampled. The data from the roof-mounted ARISense showed high PM10 counts correlating with winds from the facility. The AMS did not appear to show any great enhancement in signal nor did the CPC but they are both on an inlet with a PM 2.5 cyclone. The SJAC detected a short pulse of Cr(VI) closely correlated in time with the “dust” events.

Stationary measurements downwind of Robertson’s Ready Mix in Gardena are shown below. A strong correlation is noted between integrated particulate matter mass (PM₂₋₁₆). Some hydrocarbons (CH₄ and C₂H₆ with a 8.3% C₂H₆/CH₄ ratio) were also noted, but were not well-correlated with the PM₂₋₁₆ enhancements, and likely originate from one of the previously noted nearby sources. A sample of roadside dust was taken at this location and given to SCAQMD.

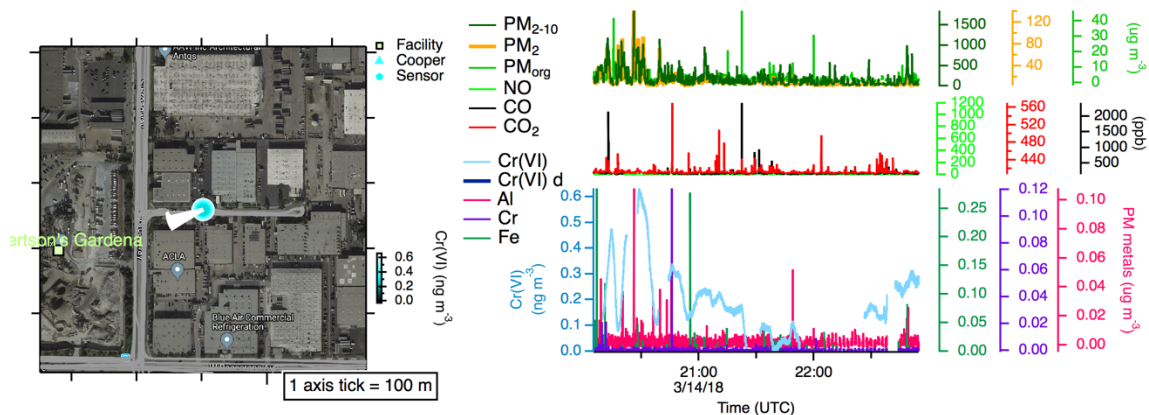


Figure 44. Detail of Cr(VI) measurements and selected PM and combustion tracer species on 03/14.

Transects of the same neighborhood on 03/19 included 15 minutes of data with active street sweeping. Brief enhancements of PM₂₋₁₆ were observed during these transects, but the Cr(VI) measurements do not show enhancements much above typical background concentrations (maximum ~ 0.25 ng m⁻³ versus the 0.6 ng m⁻³ previously). Stationary measurements on this day did not have favorable wind. No visible dust emission event was noted on this day.

Other examples of Cr(VI) enhancements nearby were noted (see section, “Cr(VI) in West Rancho Dominguez”), and another enhancement close to Robertson’s Ready Mix was noted on 03/28.

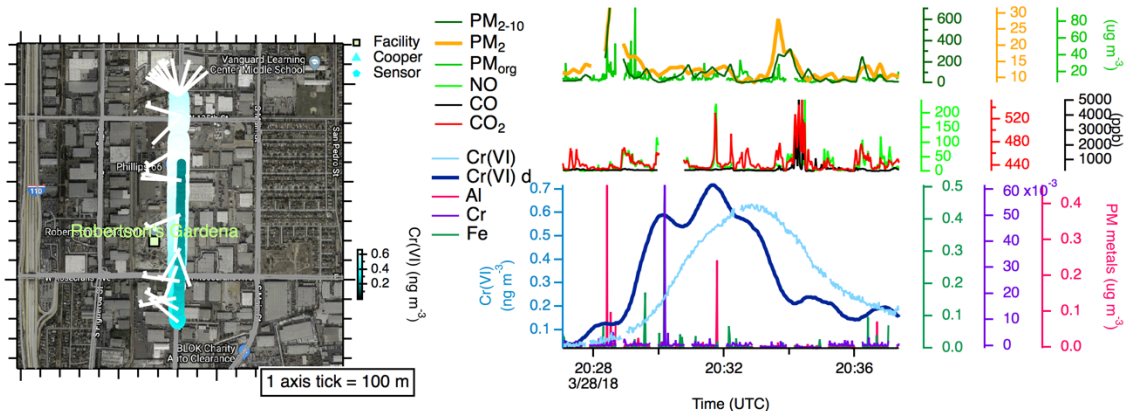


Figure 45. Enhancement of Cr(VI) on 3/28/2018

Foundries

On 3/21/18, we visited the Fontana area and collected stationary data near various foundries at the suggestion of SCAQMD. SCAQMD personnel were also present and collected samples nearby. Hartman Industries and Vista Metals Co., two steel-based operations, provided no notable signal during close transects. Given the NW wind and impenetrable block of industry to the SE of these business, we could not get downwind at any reasonable distance. At another nearby facility using steel, California Steel Industries, we observed emissions black smoke from two tall stacks into a weak wind. A massive facility with limited fence line access (up against speedway and busy roads), we had few options but to observe at a distance on Banana Avenue amongst other active industrial and freight operations in untenable wind conditions. We surveyed the nearby Fontana Foundry Corp. in a light rain and noted the challenge of navigating around the business in the largely residential area.

Table 6. List of foundries visited, primarily in Fontana, CA and Ontario, CA

3/21/2018	
17:00 UTC	Hartman Industries
18:00 UTC	Vista Metals Co.
19:00 UTC	California Steel Industries
20:00 UTC	Fontana Foundry Corp.
3/23/2018	
12:00 UTC	Leerock Foundry
13:00 UTC	California Die and Casting Inc.
14:00 UTC	Calidad, Inc.
16:00 UTC	Alum-Alloy Co. Inc.
17:00 UTC	United Castings
4/3/2018	
22:00 UTC	Angelus Foundry

Observations of a foundry in City of Industry can be found in section: “Custom Alloy Light Metals, City of Industry”. Several visits were made (3/16/18, 3/17/18, and 4/2/18) attempting to characterize emissions.

On Friday, 3/23/18, we visited the Ontario area early in morning, starting around 5:00am local time. Leerock Foundry (also near R&S Machine & Mold and Performance Aluminum Products), did not appear to be operating that early so we moved on. At California Die and Casting Inc., sampling occurred from an adjacent parking lot separated from their lower parking lot by a short wall. Activity on-site involved forklifts driving around, while cars arrived and departing (possibly indicating a shift change). An occasional metallic odor was noted. At one point, we saw a small increase in nickel and chromium concentrations concurrent with similarly minor increases in aromatics, manganese, and titanium. We left to go to Calidad which performs "investment casting" of non-ferrous aluminum. Activity was confirmed via cars in the small parking lot. Odors were noted at times, but no metal signal enhancements measured. This site was proximate to the Ontario Airport and the frequently departing aircraft nearby. At Alum-Alloy Co. Inc., mobile sampling revealed elevated organics associated with metallic odors, but little else. Activity inside or outside the facility could not be detected. The final stop of the day, United Castings, appeared active based on sounds from the facility. However, nothing notable in terms of emissions was observed.

On Saturday, 4/3/18, we briefly visited Angelus Foundry in East Los Angeles. It appeared the small facility may be closed though the measurement conditions were unfavorable. A SW wind made it difficult to get close to the facility while remaining downwind.

Custom Alloy Light Metals, City of Industry

Custom Alloy Light Metals, a metal foundry in the City of Industry specializing in recycled aluminum, was visited on several occasions. On 03/16, winds were too light to

pinpoint any emission sources. A white billowy cloud emanating from the foundry was noted, which disappeared later in the day. On 03/17 and 3/29, the facility was visited again, with more billowy emissions from the stacks. Emissions were measured on both days and a slight odor was noted (sweet and metallic, like soldering). A final visit on 04/02 showed no emissions despite a clear sampling wind and repeated transects. Images taken on 3/29 and 4/2 show the rooftop of the foundry with and without the white billowy cloud.

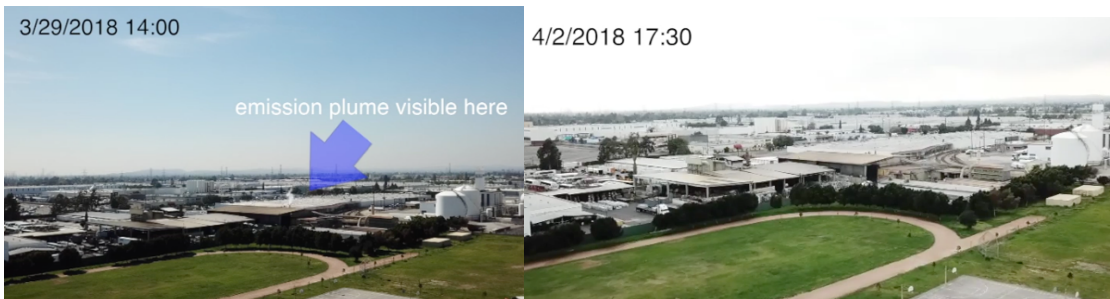


Figure 46. Images show the presence (left, 3/29) and absence (right, 4/2) of a billowy white cloud emanating from the foundry.

Measured emissions were first noticed from the enhancements at mass 36 in the AMS. This mass is typically associated with black carbon emissions due to C_3 . However, closer examination revealed two peaks at mass-to-charge ratios 36 and 38 as well as a negative mass defect, both clear indicators that this signal is due to HCl. The presence of particulate matter ammonium (NH_4) was also observed with HCl. The measured chloride and HCl peaks (magenta, Chl) show the expected isotope pattern for chlorine; the isotopic reference pattern for HCl (pale pink) is also depicted, highlighting this agreement (Figure 47).

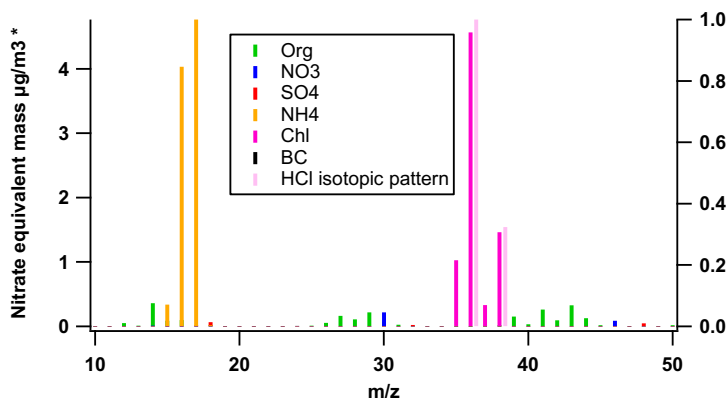


Figure 47. The high-resolution mass spectrum of the AMS while transiting through an HCl plume. Particulate matter chloride (Chl, magenta) and ammonium (NH_4 , yellow) are elevated. The reference mass spectrum for HCl is shown for comparison (pale pink), showing an isotope pattern that is expected.

The observations in Figure 47 are consistent with observations of a particulate matter plume of ammonium chloride (NH_4Cl), with fragmentation patterns and ratios within the range expected based NH_4Cl calibrations of similar instruments. NH_4Cl is used as a flux in soldering (Engineering360, 2018) and in metal casting (Hill and Griffith Company, 2017) operations.

The figure below shows a wind rose the chloride emissions measured on 03/17 (m/z 36). The gas manufacturer Linde was to the north of the foundry, but most of the density in the wind rose plot is coming from further south. NO, NO₂ and small particle number count were also elevated in this plume. The SJAC instrument did not see any Cr(VI) elevations above background during any of these measurements. No sustained multi-second-long plumes of aluminum or other metals were noted by the AMS.

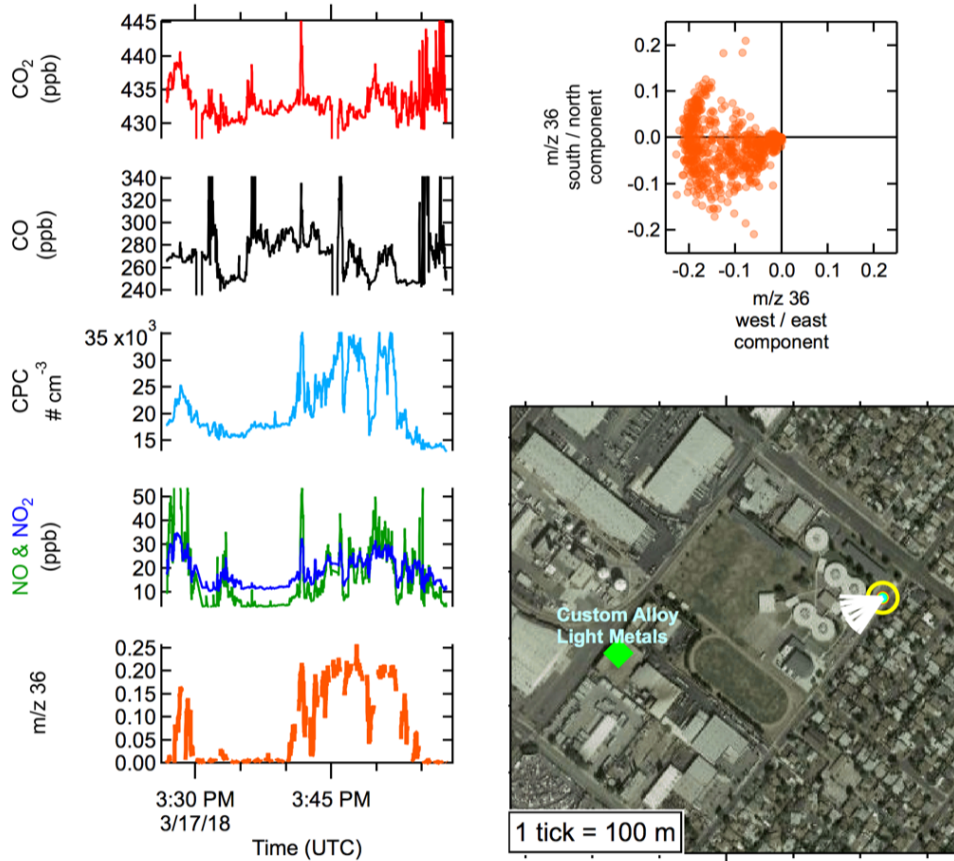


Figure 48. Stationary measurements downwind of Custom Alloy Light Metals.

Discussion

The experimental plan going into this project was to use the Aerosol Mass Spectrometer's (AMS) fast detection capabilities (1 second response) to monitor real-time emissions of particulate matter chromium. When emissions were detected, then the slower (~15-minute response) SJAC-LPAS system would be able to determine whether the chromium was hexavalent in nature. In actuality, no sustained plumes of particulate matter chromium were detected with the AMS. Additionally, enhancements of Cr(VI) were rare in the initial neighborhoods of interest (Compton and Paramount). The experiment goals and design were altered as a result, performing neighborhood surveys "blind", and analyzing any Cr(VI) enhancements after the fact. Many stationary measurements were also undertaken in order allow the SJAC-LPAS system time to positively identify signals without the complication of motion. Finally, the full capabilities of the mobile lab in detecting other hazardous and nuisance species (e.g. styrene, formaldehyde, benzene) was leveraged in order to identify other air quality concerns in the studied areas.

The potential emission vectors for chromium in the study region included dust from certain concrete ready-mix facilities, and (unconfirmed) grinding of hard-chrome parts or hard-chrome metal plating. Concrete and metal grinding emission vectors are coarse-mode in nature (i.e. Cr in soil or metal dust and not Cr-containing "fumes"). Even chrome plating is expected to yield emissions in the 0.75 - 6.4 μm range (see Section "Industrial Sources of Hexavalent Chromium"). Indeed, these large particle sizes are the current hypothesis for why fast AMS measurements with particle size cutoffs of <1 or <2.5 μm did not show sustained plumes of particulate matter chromium.

Coarse mode particles consist of 1-100 μm particles generated through a mechanical processes like winds lifting dust (Hinds, 1999), or, in this hypothesis, industrial activities related to metal grinding or cement. Large particles settle quickly out of the air and also have poor conductance through sampling lines. Both these considerations will impact the signal sampled through the SJAC-LPAS and the SP-AMS inlet lines (though the SP-AMS inlet was run with a <2.5 μm cyclone, whereas the SJAC-LPAS was not). The nature of SJAC-LPAS detection means that a single 1-second spike of Cr(VI) particulate matter would get broadened over several minutes. Thus, while it is possible that the SP-AMS is missing large particles in sustained Cr(VI) plumes due to size cutoffs, it is also possible that the SJAC-LPAS is responding to single-second Cr(VI) events, and that no sustained minute-scale Cr(VI) plumes were present in this study.

In several examples, single-second enhancements in AMS-measured metal particles were observed at the same time as SJAC-LPAS Cr(VI) enhancements, most notably in West Rancho Dominguez near a number of metal grinding operations and cement facilities. The ARISense small sensor, which counts particles up to 16 μm , also showed suggestive enhancements in particle count during certain sustained plumes of hexavalent chromium from the SJAC system, most notably at cement ready mix facilities.

Sustained plumes of particulate matter cadmium (Cd) were observed by the AMS during this study, in stark contrast to AMS-measured chromium and other metals, which showed only single-second spikes. Particulate matter Cd enhancements were confined to a single small area in Compton, and were observed on three different days. The fact that these sustained plumes were observed with the AMS suggests that the Cd-containing

particles are small, in contrast to other metals, notably Cr, where we hypothesize a coarse-mode source like dust or grinding.

A number of previous studies have measured particulate matter Cr(VI) with some degree of size specificity.

Venter et al. (2016) collected particulate matter samples using filters at a background site in South Africa, in an area influenced by major chromite mineral extraction and associated ferrochromium industries. They found elevated Cr(VI) concentrations in PM_{2.5} particles over PM_{2.5-10} for airmasses passing over the source region. The authors attribute this observation to two factors: the dominant source types expected, which include offgassing of fine particles from furnaces, and the short atmospheric lifetime of larger particles produced from mechanical processes like milling. This African region is vastly different from the urban areas discussed in this report.

In conference proceedings, Catrambone et al. (2013) report 24 hr filter-based measurements at three sites in Italy, electrochemically analyzed for Cr(VI), Cr(III) and total chromium. At one site, size-specific PM measurements were also done, and found Cr(VI) in all size ranges measured (<0.18 µm to <18 µm), with a broad peak between 0.32 and 5.6 µm. The authors do not describe the industrial sites sampled, and do not further speculate on potential source types.

Yu et al. (2014) describe another set of 24 - 72 hr filter-based measurements at two sites in New Jersey, one near a highway and one near a waste facility for chromium ore processing residue. The authors found that photochemical processes that convert ambient Cr(III) into Cr(VI) were important in explaining the concentration enhancements observed in the summertime, and that Cr(VI) was present in larger amounts in particles sized between 1.0 and 5.6 µm. Humidity levels were also noted to play an important role in the observed particle sizes.

The sizing information in these previous studies (Catrambone et al., 2013; Yu et al., 2014) tends to suggest higher Cr(VI) content in PM_{2.5} than in PM_{2.5-10}. However, these long averaging time studies (24 hours or longer) cannot distinguish slow enhancements in background particulate matter concentrations (from photochemistry or regional transport, e.g.) from short-duration high-concentration events. Though we have observed no evidence of direct industrial emissions of fine Cr-containing particles, we cannot say with absolute certainty that no such short-duration events occurred during the study period. This study also cannot assess slow changes in ambient background fine particle Cr(VI), which might be more apparent in filter measurements. Previous studies may also be less sensitive to coarse-mode particle emission or resuspension events at localized sources, due to stationary samplers coupled with short residence times of coarse particles in the atmosphere.

The particulate matter measurements done as part of this campaign used numerous different types of instrumentation and co-located for part of the time with SCAQMD filter and metals analysis sampling sites. Using multiple measurement technologies was crucial in forming the hypothesis that Cr(VI) is present in large dust particles. Even still, there remain unknowns related to these particles.

SCAQMD intensive monitoring activities may have impacted emissions, particularly in Compton and Paramount, where an extensive network of SCAQMD's portable samplers had been deployed. Indeed, the few instances reproducible Cr(VI)

enhancements on repeated transects were observed outside of these neighborhoods. The Aerodyne Mobile Laboratory itself is also fairly conspicuous (the vehicle is clearly labeled, and inlets and wind measurement devices are visible) and may have resulted in some degree of activity change in those areas which were visited repeatedly over the month-long measurement period.

In the results section, whenever possible, measured emissions were traced back to individual sources or source areas. This type of source triangulation is very difficult using stationary data, especially in complex environments with multiple potential sources. The ability of the mobile laboratory to drive around a neighborhood, identify a hotspot, and then follow those emissions as the winds bring them through the neighborhood provides valuable data in source identification. Similarly, null measurements where emissions were suspected but none detected provide equally valuable information in the effort to identify and mitigate emissions.

Though the campaign was focused on industrial emission sources, and daily measurement activities were planned with these in mind, surveys drives of neighborhoods were also very fruitful. In a few cases, they turned up unanticipated emissions that could be of concern to the community. Most notable was an odor plume in Paramount, which propagated through the neighborhood, including along the commercial main street lined with restaurants. This plume's characteristic signature allowed us to measure it on multiple occasions.

The AML was measuring an enormous number of different species at the same time during this campaign. In general, we were very successful at identifying emission signals in real-time and could adapt daily measurement goals in response. In at least one case, however, a clear emission signature was identified only in post-analysis (the particulate matter cadmium emission). This highlights the benefits of an instrumentation suite with broad coverage, combined with a measurement plan that includes neighborhood surveys.

The dataset produced as part of this study contains a vast amount of data on particulate matter speciation, VOCs and others. There are likely additional stories to be gleaned beyond what has been presented here. For example, air quality mapping activities were undertaken around a number of schools in the neighborhoods of interest. These time periods could be mined in HAPS exposure studies or other efforts. Measurements were also conducted for an entire month, leading to variations in wind and metrology. Eliminating the sources nearby and focusing on the background concentrations could also be interesting for investigation of regional pollution or transport.

Conclusions

A month-long campaign was staged in a complicated source region home to a variety of sources, including industrial facilities (cement ready-mix facilities; foundries; metal plating) traffic, natural gas and solvent use. Numerous different types of emissions were measured and characterized, including particulate matter emissions (metals, hexavalent chromium, organics), combustion emissions, and volatile organic hydrocarbons (including nuisance compounds like styrene).

The results in this report suggests that chromium and hexavalent chromium emissions are present as coarse-mode particulate matter, defined as particles with diameters

between 1-100 μm . This evidence includes: 1) no sustained multi-second long Cr emissions detected with the AMS; 2) sustained plumes of metals are observable with the AMS, as demonstrated for cadmium; 3) increased Cr detection when AMS lens was changed from 1 to 2.5 μm cutoff; 4) increased Cr concentrations noted when following street-sweepers; 5) Cr(VI) enhancements were short in duration and did not persist; 6) Cr(VI) detected near cement ready-mix facility, and hard chrome plating/grinding facility. The exact particle size distribution of detected hexavalent chromium is not known.

Cr(VI) enhancements were generally of short duration, consistent with the coarse-mode particulate matter hypothesis. However, this also implies that the elevated concentrations detected by SCAQMD fixed-site 24-hour monitors may have been due either to short-duration events of very high concentrations (higher than measured by the SJAC-LPAS during this study) or to re-suspended coarse-mode particles too large and/or insoluble to be detected by our instruments.

Recommendations for Future Studies

There are still many basic questions related to the nature of particulate matter emissions of Cr(VI): their emission vectors, the size distribution of the particles. Future field studies should include additional soil and dust testing efforts due to the suspected large-particle nature of the emissions. Collaboration with industry, including knowledge of daily operations and access to process areas would also help pinpoint the nature of these emissions.

Deployment of a broad range of particulate matter sampling technologies to any future study is crucial until the nature of these chromium particles is well understood. For example, inclusion of regular filter measurements aboard the mobile laboratory would help bridge the gap between the stationary SCAQMD filter samplers and the live instrumentation. Other particulate matter instrumentation may also be of value, particularly those aimed at larger particulate sizes or at single-particle characterization.

Optimizing inlet microphysics to favor large particle detection is a particularly valuable goal for future studies focused on coarse-mode emissions. Eliminating bends in the inlet lines and greatly reducing their length (by exiting the AML through a side port instead of the front bulkhead, for example) would favor large particle detection. Modifying flows to the inlets could also improve particle transmission.

Several modifications to the current AMS could also be made for better large particle detection. A cyclone, which eliminates large particles and lets small particles through, must be used on the AMS inlet in order to prevent clogging of the instrument. In this campaign, cyclone with a 2.5 μm cut was operated to specification. However, it is possible to relax the particle size cutoff by changing the bypass flow on the cyclone. This procedure could let through a larger fraction of particles around $\sim 2.5 \mu\text{m}$ without eliminating the cyclone entirely, which would run the risk of damaging the instrument. Improvements to the live data acquisition software on the AMS could also be made to allow for live streaming of sub-mass-resolution peaks, and easier live detection of short-duration events with neighboring interferences in the mass-spectrum.

Although the SJAC-LPAS as utilized in this study was able to detect short duration Cr(VI) events at quite low concentrations, the slow response time and broad smearing of peaks made it difficult to correlate those events with other parameters measured in real-time and to precisely identify the location where evanescent Cr(VI) concentrations were encountered during mobile monitoring. It may be possible to significantly improve the response time of the instrument by replacing the current steam-jet aerosol collector with an impactor whose surface is continuously flushed with liquid. This would reduce the volume of liquid required by the cyclone to prevent entrainment of air bubbles into the analytical system. Potential benefits of this modification are:

- more precisely characterized measurement lag time
- improve sensitivity to short-duration concentration spikes
- allow to operate for longer periods unattended, for better intercomparison with fixed site monitors
- faster startup and reduced power consumption and heat generation

Another area in which utility of the continuous Cr(VI) could be advanced would be in identification or development of external sources that would provide a steady detectable signal to the monitor. This would allow us to characterize the response to aerosol particles in different size ranges, by changing the inlet size fractionator, to determine the characteristics and relative strength of interferences from broad-spectrum light absorbing aerosols (EC or brown carbon).

Future studies should continue to emphasize mobile data, if possible. It is much easier to map emission hotspots and pinpoint potential emission sources with drive data. Though it may be more complicated initially, surveys where a meandering path is driven through a community under a variety of wind conditions can be an efficient way to identify problems and motivate additional monitoring activities.

The results presented here suggest that additional Cr(VI) monitoring be undertaken in West Rancho Dominguez and Gardena, where there is a high density of both concrete and metal grinding operations, including one “hard chrome” facility. Measurements of Cr(VI) in this area showed enhancements and were reproducible over two different visits. On the other hand, numerous chrome plating facilities in Compton and Paramount, where SCAQMD monitoring activities were well established, did not show repeated enhancements of Cr(VI) above background concentrations.

Future work in urban/industrial areas will benefit from the measurement of speciated volatile organic hydrocarbons, VOCs, using the PTR-MS or next-generation instruments like the VOCUS (Aerodyne Research, 2018). This technology has the potential to measure BTEX and many other HAPS species, including nuisance odor compounds like styrene. At the same time, measurements of combustion species, ethane, methane, and others are needed in order to identify commonly observed emissions like vehicle exhaust and natural gas leaks and distinguish them from industrial emissions.

List of Appendices

- Appendix A: Histograms of VOC concentrations – 5 minute averages.
- Appendix B : Aerodyne Quality Assurance Document
- Appendix C : DRI Instrument Overview
- Appendix D: Overview Maps for PM Metals

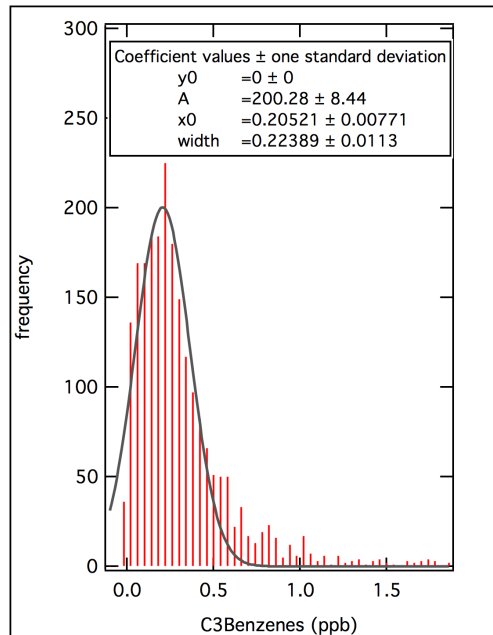
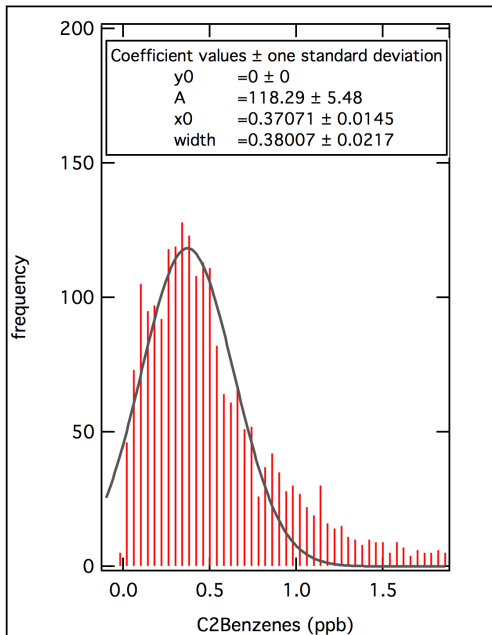
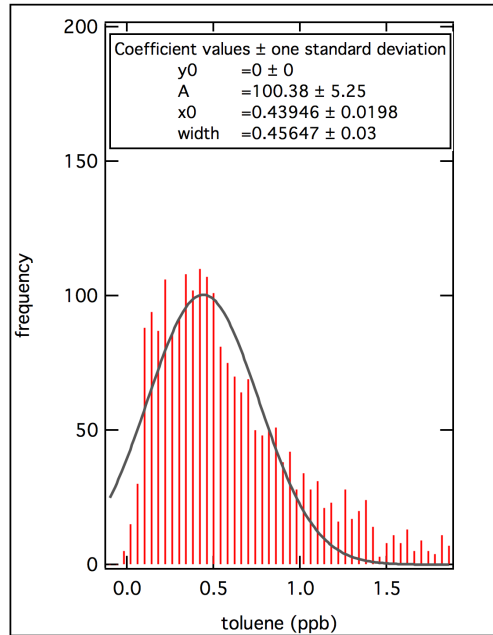
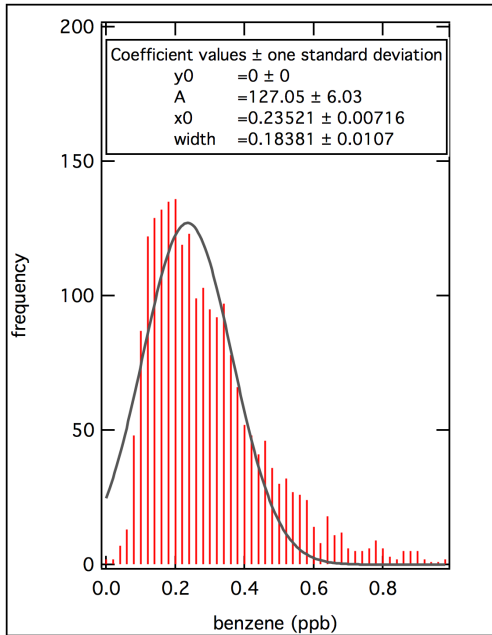
References

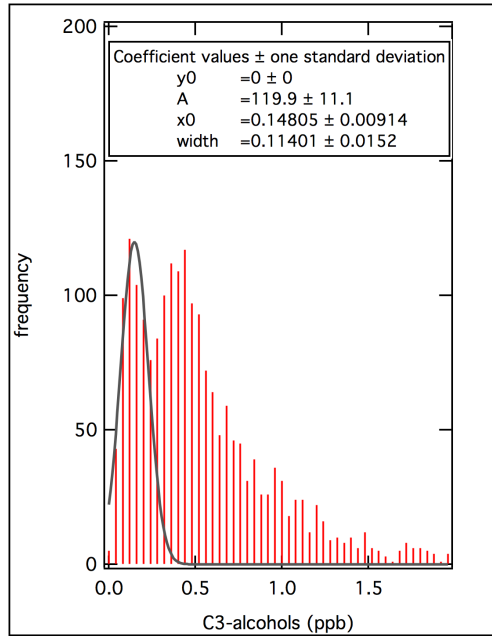
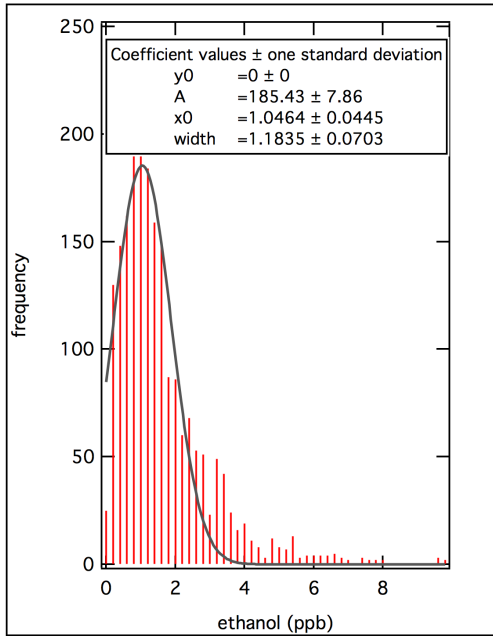
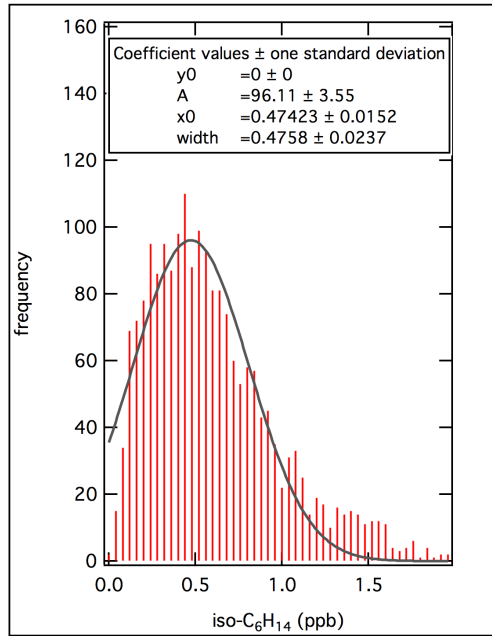
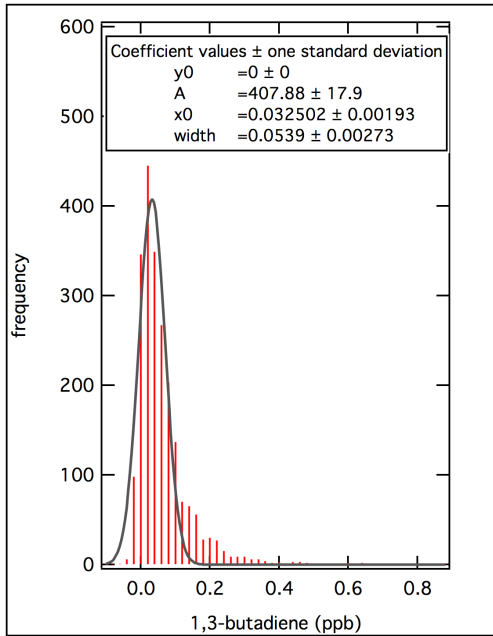
1994. Metallurgical industry. *AP 42: Compilation of air pollutant emission factors*. 5th ed. Research Triangle Park, NC: U.S. Environmental Protection Agency. Available at <http://www.epa.gov/ttn/chief/ap42/ch12> Accessed 12/01/2008.
- Abelson J. 2008. Hexavalent chromium: What you need to know. Donaldson Filtration Solutions. Available at <https://www.donaldson.com/en-us/industrial-dust-fume-mist/technical-articles/hexavalent-chromium/>.
- Aerodyne Research. 2018. Vocus-PTR. Available at <http://www.aerodyne.com/products/vocus-ptr>. Accessed 09/12/2018.
- Bae S, Hikaru F, Kanematsu M, Yoshizawa C, Noguchi T, Yu Y, Ha J. 2018. Removal of hexavalent chromium in Portland cement using ground granulated blast-furnace slag powder. *Materials* **11**(1): 11. DOI:10.3390/ma11010011.
- Bonin MP, Flower WL, Renzi RF, Peng LW. 1995. Size and concentration measurements of particles produced in commercial chromium plating processes. *J Air Waste Manage Assoc* **45**(11): 902-907. DOI:10.1080/10473289.1995.10467422.
- C-ADD Mapei. Technical notebook: Hexavalent chromium reducing agents for portland cements and cement-based materials. Available at <http://cadd.mapei.com/wp-content/uploads/2016/02/mapei-dam-cement-reducing-agents-technical-notebook.pdf>. Accessed 09/12/2018.
- Catrambone M, Canepari S, Perrino C. 2013. Determination of Cr(III), Cr(VI) and total chromium in atmospheric aerosol samples. E3S Web of Conferences; EDP Sciences. 1: 07005. DOI:10.1051/e3sconf/20130107005.
- CSTEE. 2002. Opinion on risks to health from chromium VI in cement Brussels: Scientific Committee on Toxicity Ecotoxicity and the Environment (CSTEE). Available at http://ec.europa.eu/health/ph_risk/committees/sct/documents/out158_en.pdf. Accessed 09/12/2018.
- Engineering360. 2018. Fluxes information. Available at https://www.globalspec.com/learnmore/manufacturing_process_equipment/welding_equipment_supplies/fluxes. Accessed 09/10/2018.

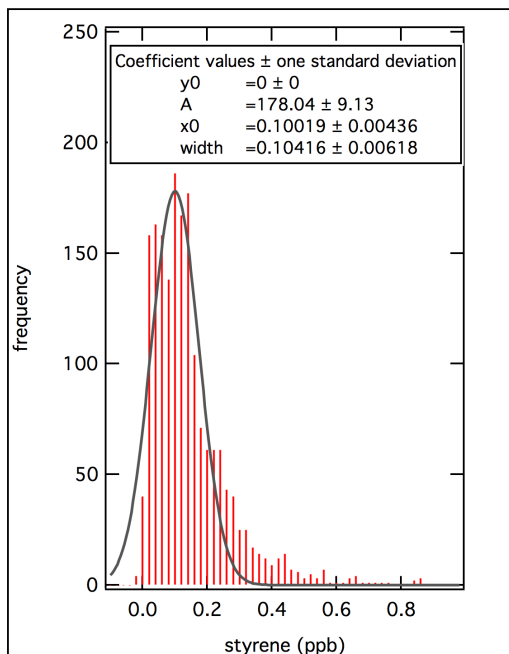
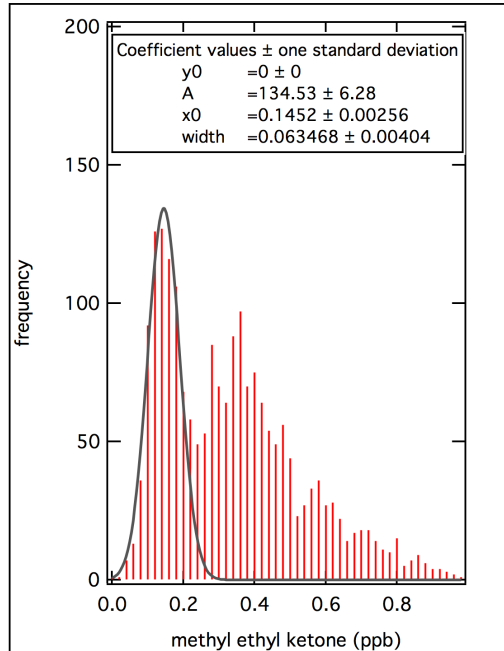
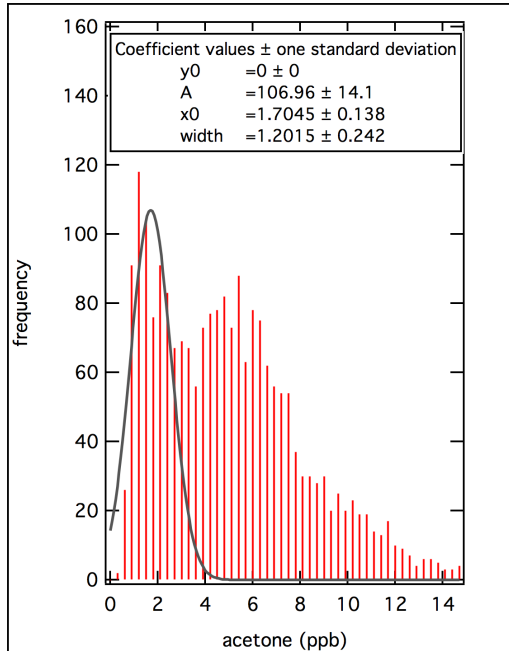
- EPA. 2000. Styrene. Available at <https://www.epa.gov/sites/production/files/2016-09/documents/styrene.pdf>. Accessed 08/02/2018.
- Eštoková A, Palaščáková L, Singovszká E, Holub M. 2012. Analysis of the chromium concentrations in cement materials. *Procedia Engineering* **42**: 123-130. DOI:10.1016/j.proeng.2012.07.402.
- Foulke EG. 2007. Inspection procedures for construction sites using Portland cement: Occupational Safety and Health Administration. Available at https://www.osha.gov/dep/hexchrom/BCTD_settlement_memo_20070416.html. Accessed 09/12/2018.
- Frias M, Sánchez de Rojas MI. 2002. Total and soluble chromium, nickel and cobalt content in the main materials used in the manufacturing of Spain commercial cements. *Cement and Concrete Composites* **32**: 435-550.
- Heung W, Yun M-J, Chang DPY, Green PG, Halm C. 2007. Emissions of chromium (VI) from arc welding. *J Air Waste Manage Assoc* **57**(2): 252-260. DOI:10.1080/10473289.2007.10465314.
- Hill and Griffith Company. 2017. Foundry additives glossary. Available at <http://www.hillandgriffith.com/green-sand-metalcasting-foundry-news/foundry-additives-glossary>. Accessed 09/10/2018.
- Hinds WC. 1999. *Aerosol technology: Properties, behavior and measurement of airborne particles*. 2nd ed.
- Khlystov A, Wyers GP, Slanina J. 1995. The steam-jet aerosol collector. *Atmos Environ* **29**(17): 2229-234.
- Klemm W. 1994. Hexavalent chromium in Portland cement. *Cement, Concrete and Aggregates* **16**(1): 43-47. DOI:10.1520/CCA10560J.
- Liu PSK, Deng R, Smith KA, Williams LR, Jayne JT, Canagaratna MR, Moore K, Onasch TB, Worsnop DR, Deshler T. 2007. Transmission efficiency of an aerodynamic focusing lens system: Comparison of model calculations and laboratory measurements for the aerodyne aerosol mass spectrometer. *Aerosol Sci Technol* **41**(8): 721-733. DOI:10.1080/02786820701422278.
- McDonald BC, de Gouw JA, Gilman JB, Shantanu HJ, Akherati A, D. CC, Jimenez JL, Lee-Taylor J, Hayes PL, McKeen SA, Cui YY, Kim S-W, Gentner DR, Isaacman-VanWertz G, Goldstein AH, Harley RA, Frost GJ, Roberts JM, Ryerson TB, Trainer M. 2018. Volatile chemical products emerging as largest petrochemical source of urban organic emissions. *Science* **359**(6377): 760-764. DOI:10.1126/science.aaq0524.
- NEWMOA. 2010. Pollution prevention technology profile: Trivalent chromium replacements for hexavalent chromium plating. Northeast Waste Management Officials' Association. Available at <http://www.newmoa.org/prevention/p2tech/TriChromeFinal.pdf>. Accessed 09/14/2018.
- NIOSH. 2013. Criteria for a recommended standard occupational exposure to hexavalent chromium: Department of Health and Human Services; Centers for Disease Control and Prevention; National Institute for Occupational Safety and Health. DHHS (NIOSH) Publication No. 2013-128. Available at https://www.cdc.gov/niosh/docs/2013-128/pdfs/2013_128.pdf. Accessed 08/01/2018.

- OSHA. Osha fact sheet: Controlling hexavalent chromium exposures during electroplating. Available at https://www.osha.gov/Publications/OSHA_FS-3648_Electroplating.pdf. Accessed 09/12/2018.
- OSHA. 2004. Cadmium: Occupational Safety and Health Administration. OSHA 3136-06R 2004. Available at <https://www.osha.gov/Publications/osha3136.pdf>. Accessed 8/6/2018.
- Pilat MJ, Pegnam RC. 2006. Particle emissions from chrome plating. *Aerosol Sci Technol* **40**(8): 639-648. DOI:10.1080/02786820600763020.
- Serageldin M, Reeves DW. 2009. Development of welding emission factors for Cr and Cr(VI) with a confidence level. *J Air Waste Manage Assoc* **59**(5): 619-626. DOI:10.3155/1047-3289.59.5.619.
- Tandos R, Aarts B. 1993. Chromium, nickel and cobalt contents of some australian cements. *Contact Dermatitis* **28**(4): 201-205. DOI:doi:10.1111/j.1600-0536.1993.tb03401.x.
- Venter AD, Beukes JP, Gideon van Zyl P, Josipovic M, Jaars K, Vakkari V. 2016. Regional atmospheric Cr(VI) pollution from the bushveld complex, south africa. *Atmos Pollut Res* **7**(5): 762-767. DOI:10.1016/j.apr.2016.03.009.
- Wahlberg JE, Lindesedt G, Einarsson O. 1977. Chromium, cobalt and nickel in swedish cement, detergent, mould and cutting oils. *Berufsdermatosen* **25**: 220-228.
- World Health Organization. 2000. Styrene. *Air quality guidelines for Europe*. 2nd ed. Copenhagen: WHO Regional Publications. Available at http://www.euro.who.int/_data/assets/pdf_file/0018/123066/AQG2ndEd_5_12Styrene.pdf?ua=1. Accessed 08/01/2018.
- Yu CH, Huang L, Shin JY, Artigas F, Fan Z-h. 2014. Characterization of concentration, particle size distribution, and contributing factors to ambient hexavalent chromium in an area with multiple emission sources. *Atmos Environ* **94**: 701-708. DOI:10.1016/j.atmosenv.2014.06.004.

Appendix A: Histograms of VOC concentrations – 5 minute averages.







Appendix B: SCAQMD Cr(VI) Project

Quality Assurance Notes

Prepared by Aerodyne Research, Inc.

Last Updated: 2018/05/07

Contents

Contents	1
Mobile Data	3
Data Access.....	3
crvi_datetimeUTC, crvi_LocalTime	4
Location Wind Weather.....	4
crvi_Latitude, Longitude	4
crvi_Easting, crvi_Northing, crvi_Zone	4
crvi_wind_degrees, crvi_wind_metersPerSecond.....	4
crvi_truckSpeed_kmph	5
crvi_SolarElevAngle	5
crvi_solar.....	5
crvi_StrictBackgroundMask	5
crvi_temperature_C	6
crvi_truckHeading	6
crvi_wind_E_meters, crvi_wind_N_meters	6
crvi_truckPitch_deg, crvi_truckRoll_deg, crvi_truckHeave_m	6
Trace Gases and Combustion Tracers	7
crvi_CO2_ppm.....	7

crvi_CO.....	7
crvi_CO_background.....	8
crvi_N2O.....	9
crvi_H2O.....	9
crvi_RH.....	9
crvi_NO	9
crvi_NO2.....	10
crvi_O3	12
crvi_CH4, crvi_C2H6.....	13
crvi_THC_ppm.....	13
crvi_HCHO	16
Particulate Matter	17
crvi_PM2, crvi_PM10, crvi_PMlarge	17
crvi_PMorg, crvi_PMSO4, crvi_PMNO3, crvi_PMNH4, crvi_PMchl, crvi_PMBC	18
crvi_CPC.....	19
Volatile Organic Hydrocarbons	19
crvi_ethanol.....	20
crvi_C3alcohols.....	20
crvi_butadiene.....	21
crvi_benzene	21
crvi_C6H14isoalkanes.....	21
crvi_acetone	21
crvi_toluene.....	22
crvi_MEK	22

Appendix C: SJAC-LPAS Instrument Details

Prepared by Andrey Khlystov and David Campbell, Desert Research Institute
Edited and formatted by Tara Yacovitch, Aerodyne Research Inc.

Instrument description

The schematic of steam jet aerosol collector long pathlength absorbance spectroscopy (SJAC-LPAS) system is shown in Figure C1. Aerosol particles are collected with the Steam-Jet Aerosol Collector (SJAC) (Khlystov et al., 1995). The SJAC operates by injecting steam into the sampled air stream, which causes water vapor to condense on the sampled aerosol particles. Particles grow due to water condensation to a size of at least $1\mu\text{m}$ in diameter and are collected by a cyclone. The SJAC quantitatively collects particles down to a few nanometers in diameter (collection efficiency 99%) (Khlystov et al., 1995). The collected liquid containing dissolved aerosol species is continuously pumped out and mixed with diphenylcarbazide (DPC) reagent for colorimetric determination of Cr(VI) (Allen, 1958). To increase sensitivity, a liquid waveguide capillary cell (LWCC) is used to increase the sensitivity.

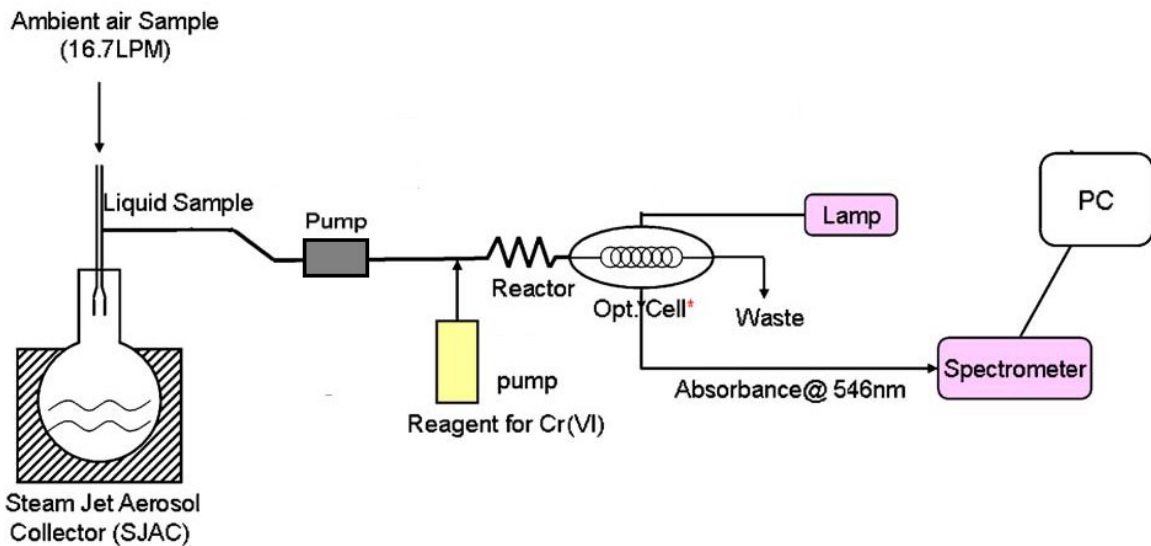


Figure C1. Instrument diagram of the SJAC-LPAS System.

Laboratory characterization

Prior to field deployment, the instrument was tested to determine its sensitivity, stability, and response time using potassium dichromate solutions of various concentrations within the range anticipated to occur during ambient monitoring. Spectra of transmitted light through the LWCC filled with water and a Cr(VI)-DPC solution are shown in Figure C2.

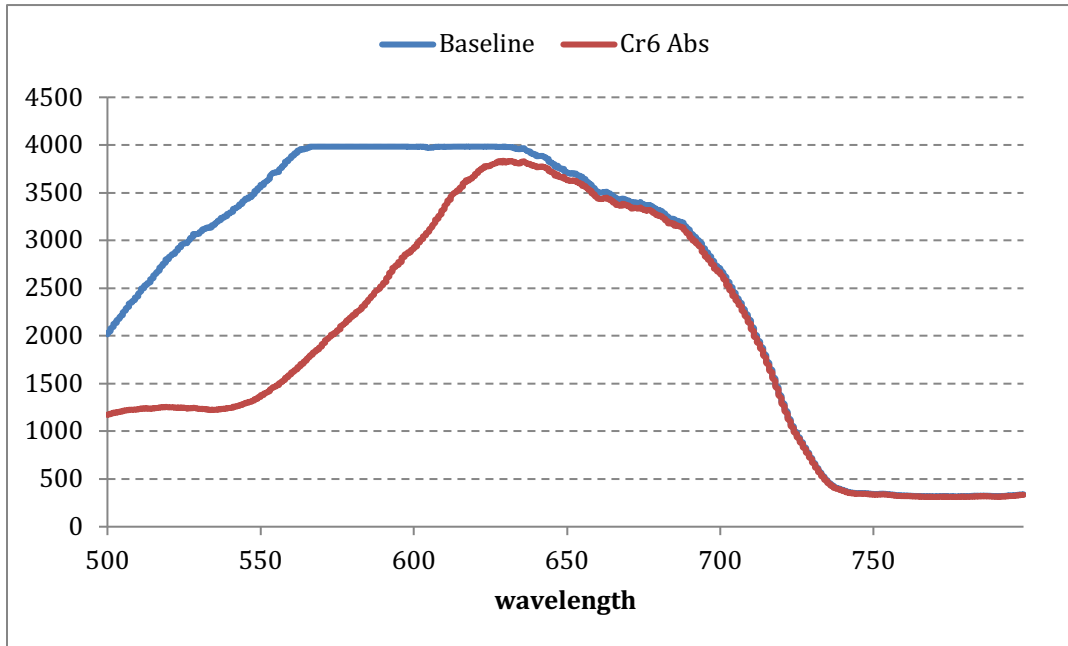


Figure C2. Spectra measured for pure water (baseline) and a Cr(VI)-DPC solution.

Step inputs of Cr(VI) solution were used to determine response characteristics of the analytical part of the instrument. The residence time distribution (RTD) was determined by differentiating the instrument response to a step input. The observed RTD was found to be stable and reproducible on several test days (Figure C3).

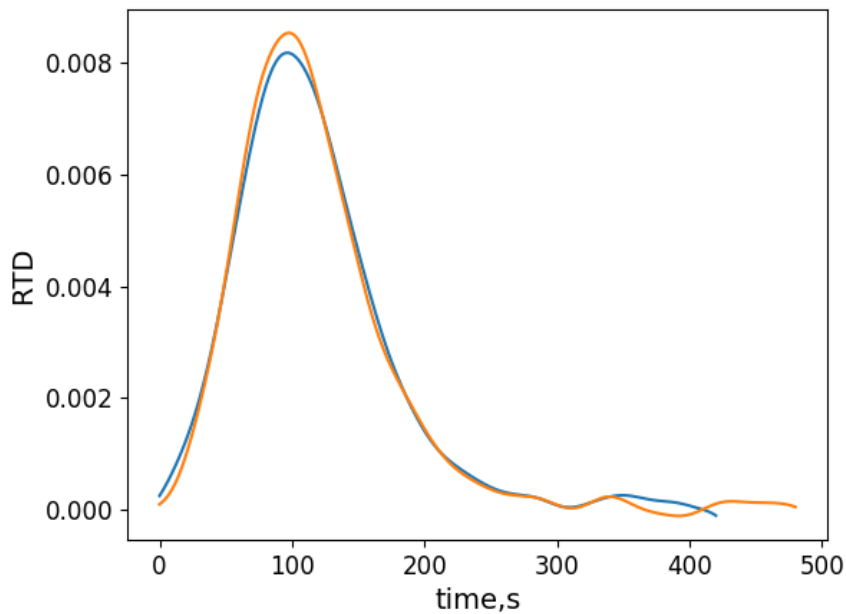


Figure C3. Residence time distribution (RTD) of the analytical part of the instrument.

Calculation of Cr(VI) concentrations

The concentration of Cr(VI) at a specific time was determined from the ratio of the measured intensity of light at 546 nm transmitted through the LWCC (I) to the intensity that would be transmitted in the absence of Cr(VI) (I_0), as per the well-known Beer-Lambert absorbance equation. Since only a single light source and detector were used, the value of I_0 could only be directly measured during periodic zero checks, when ultra-pure water was supplied to the detector in place of water from the SJAC by switching on a solenoid valve. To correct for temporal variations in the baseline intensity between these zero checks the transmitted intensity at a reference wavelength (700 nm, which is not significantly affected by the presence of Cr(VI)) was multiplied by the ratio I_{546}/I_{700} measured during zero checks and the result used as I_0 for each 1 second measurement. Measured absorbance values were converted to ambient concentrations of Cr(VI) by multiplying by a factor determined from the daily three-point calibrations (Figure C4), then dividing by the inlet air flow rate (16.7 ± 0.3 lpm) which was measured with an external flow meter during zero checks.

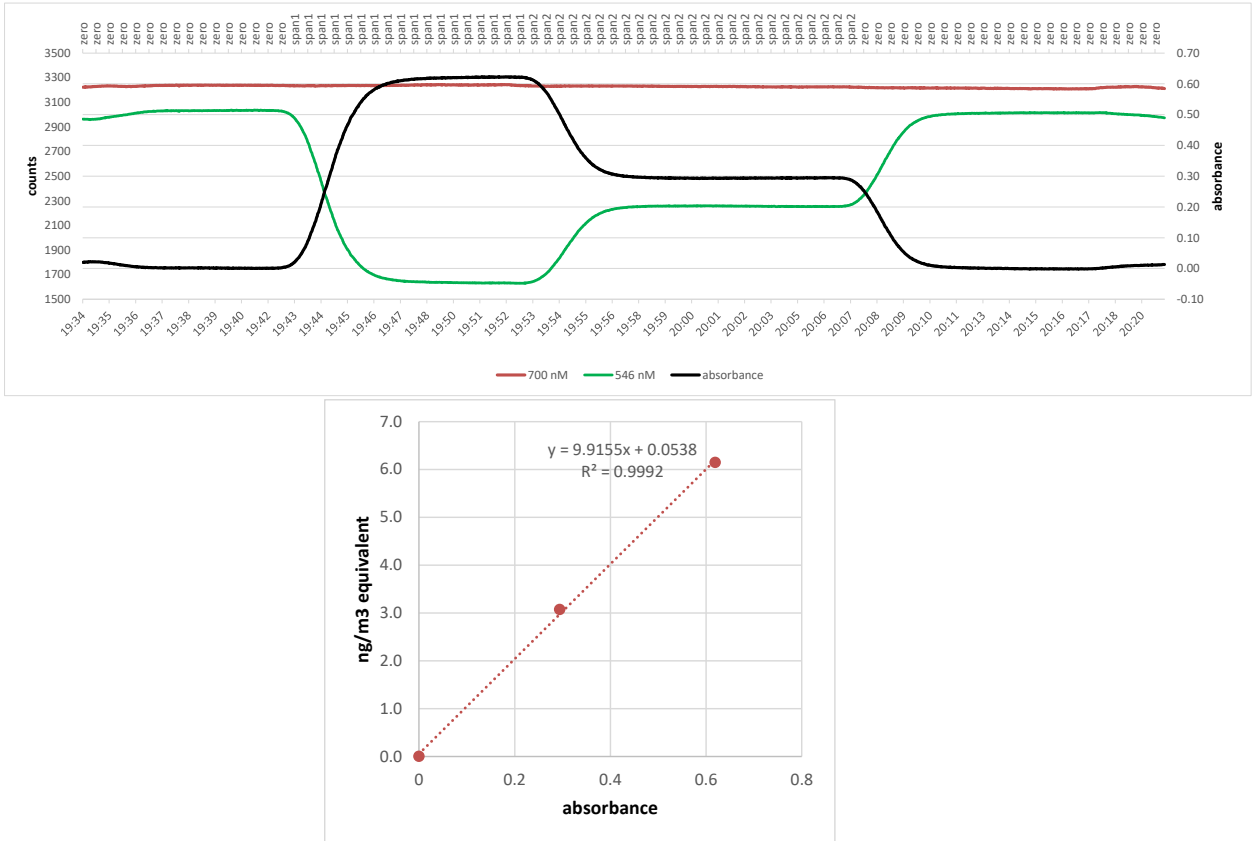


Figure C4. Example of daily 3-point calibration data and calibration curve.

Deconvolution

Due to the mixing processes in the SJAC-LPAS, the measured Cr(VI) signal appears to be smeared-out. To correct for this smearing and to restore the measurements closer to

the original signal, a deconvolution procedure was used that is briefly described here. First, the residence time distribution (RTD) of the SJAC was measured by subjecting it to a step input of a Cr(VI) solution. The RTD was calculated by differentiating the observed signal with respect to time. The measured RTD could be closely approximated as a combination of two gaussian distributions (Figure C5). The RTD was then used to restore the measured signal with Wiener deconvolution (Gonzalez et al., 2003). Using an analytical approximation of the RTD allowed for the reduction of noise amplification during the deconvolution process.

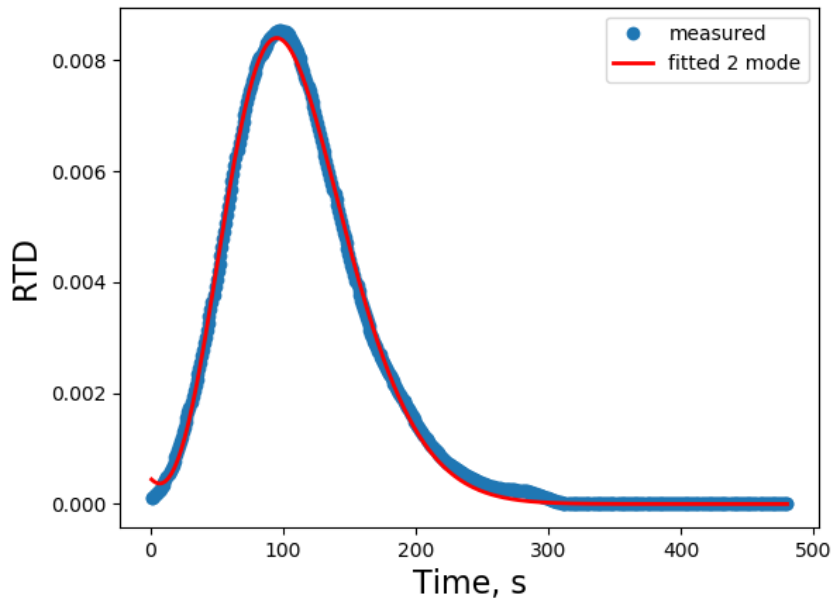


Figure C5. Measured RTD of the SJAC-LPAS and a two-mode gaussian fit.

QA/QC

The instrument was calibrated daily by direct injection of ultra-pure water and potassium dichromate solution at 2 known concentrations (initially 2.7 nM and 27.1 nM, later reduced to 4.1 and 8.2 nM to be closer to observed levels) in place of the SJAC output (Figure C4). In addition, the instrument zero was regularly checked when ultra-pure water was supplied to the detector in place of water from the SJAC by switching on a solenoid valve.

Since the AML frequently parked for periods of time during each survey we were able to gauge the effect of the considerable vibration inside the vehicle while driving on the measurement stability. As shown in Figure C6 there was a small increase in high-frequency noise when in motion, but this had little effect on the calculated Cr(VI) concentrations. Effective measurement sensitivity is $< 1 \text{ ng/m}^3$ but due to fluctuations in the baseline transmittance intensity, accuracy is estimated to be $\pm 0.2 \text{ } \mu\text{g/m}^3$ giving an effective LOQ of $0.4 \text{ } \mu\text{g/m}^3$ for the 1-second averages. Time averaging of data and peak

deconvolution can yield improved performance for time periods when persistent elevated concentrations are observed.

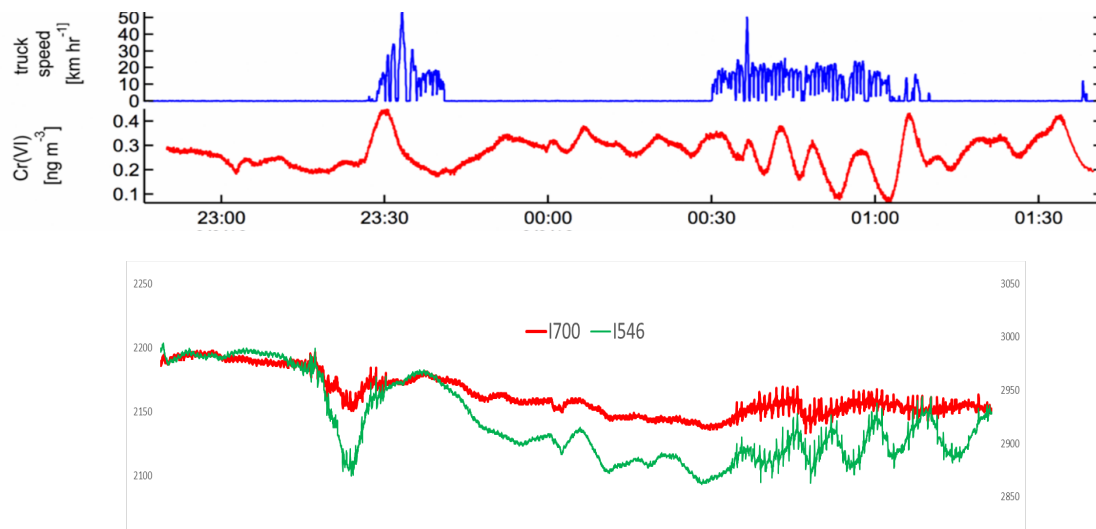


Figure C6. Time-series plots of 1-second raw (lower) and processed (upper red line) Cr(VI) data when AML was stationary and while driving.

Deconvolution was done for a subset of the data. This data has been output along with the original time trace in the final data deliverable. To request additional periods of deconvolution, please contact Andrey Khlystov.

In an attempt to confirm the accuracy of the monitor in actual use, one of the filter samplers used by the AQMD to make time-integrated Cr(VI) measurements at fixed sites (BGI PQ-100) was installed in the AML and operated with equivalent inlet and air flow rate to the continuous monitor for ~6 hr periods on 2 days. Unfortunately, the average concentrations of Cr(VI) on those days were too low ($< .02 \text{ ng/m}^3$) to allow meaningful inter-comparison. For similar purpose the AML also parked adjacent to the AQMD's site at the Paramount hospital for 4 to 6 hours on 2 days, however, pollutant levels were low again and no obvious correlation between the near-background Cr(VI) concentrations and hourly total Cr from the site's continuous XRF monitor was observed. Also, the stationary measurements collected by the AML at the hospital did not correspond to every-third day sample collection schedule for the AQMD's Cr(VI) filter measurements.

Since no consistently elevated ambient concentrations of Cr(VI) were encountered during the study it was not possible to determine the measurement lag time by observing the response after attaching a particle filter to the monitor inlet, as we had intended. Instead, a small amount of potassium chromate solution was injected directly into the steam jet of the aerosol collector and the lag time before a response was observed by the detector was measured. Since the transit time of aerosol particles from the external inlet to the SJAC can be calculated to be only a few seconds at the air flow rate of ~17 lpm, this approach is expected to be sufficiently accurate.

Measurement lag time was determined to be 330 seconds but could increase or decrease somewhat as the solution flow rate was adjusted to compensate for variations in liquid collection by the SJAC cyclone. In order to more accurately determine the actual time when the Cr(VI) aerosol creating an observed signal reached the monitor inlet, the internal volume of the liquid flow path in the monitor was calculated from the measured lag time and pumping rates. Second-by-second pump flow rates recorded in the datalogs were summed until the necessary volume was reached and the number of seconds required was used to adjust the timestamp of each data point.

Data recovery

Due to damage to a major component, the liquid waveguide capillary cell (LWCC), during transport from DRI to the project site the Cr(VI) monitor was not operable for the first few days of scheduled mobile monitoring. A replacement LWCC was obtained and installed on Mar. 6, allowing measurements to commence on Mar. 7. After that the monitor was operated during all mobile surveys with the exception of days when measurable Cr(VI) aerosol concentrations were unlikely due to rain or absence of activity at the source facilities (e.g. Sundays). In total, we collected mobile data on 21 days from March 7 to April 5.

References

- Allen TL. 1958. Microdetermination of chromium with 1,5-diphenylcarbohydrazide. *Anal Chem* **30**: 447-450.
- Gonzalez R, Woods R, Eddins S. 2003. *Digital image processing using Matlab*. Prentice Hall.
- Khlystov A, Wyers GP, Slanina J. 1995. The steam-jet aerosol collector. *Atmos Environ* **29**(17): 2229-234.

crvi_styrene.....	22
crvi_C2benzene.....	22
crvi_C3benzene.....	22
PM Metals or Salts.....	23
Hexavalent Chromium.....	24
crvi_cr6_ngm3	24
References.....	25

Mobile Data

The data in question for this document include Aerodyne mobile data during March and the first few days of April, 2018. Data was taken in the greater Los Angeles area, focusing on Paramount, Compton and Gardena. A single time base is used throughout, covering the entire campaign. Data reported here includes only mobile data taken 30 meters or more away from the overnight parking location at SCAQMD headquarters.

There are two reasons for pairing down the data in this way:

1. Some instruments were not collecting data overnight. This includes particulate matter speciation data from the Aerosol Mass Spectrometer (AMS), volatile organic hydrocarbon data (VOC) from the proton-transfer mass spectrometer (PTR-MS) and hexavalent chromium data from collaborators at the Desert Research Institute.
2. Excluding overnight data allows for the creation of comma-separated-value (csv) files that have few enough rows to be opened in Microsoft Excel. This makes these data files easily accessible to future researchers and collaborators using a variety of analysis tools.

This data includes 26 driving days between Sunday March 3rd and Wednesday April 5th, 2018.

A subset of instruments collected stationary data at the SCAQMD parking lot between drives, for the period spanning Thursday March 1st to Wednesday April 5th, 2018. This data is not reported here for the reasons above.

Data Access

Data is stored on a shared drive specific to this project located at <https://herndon.homeunix.net/owncloud/index.php/f/211027>

This drive is password-protected. All project collaborators have been given a user name and password. Contact tyacovitch@aerodyne.com for access. Comma-separated-value files (.csv) are named as follows, where *yyyymmdd* indicates the year, month and day of the file revision.

- crvi_LocationWindWeather_yyyymmdd.csv*
- crvi_TraceGasesAndCombustion_yyyymmdd.csv*
- crvi_VolatileOrganicHydrocarbons_yyyymmdd.csv*
- crvi_ParticulateMatter_yyyymmdd.csv*

Each file starts with a column for datetime in UTC and Local time. Null data is reported as blank. All data columns are described below.

Duplicate data are output in a subfolder of the data share called “IgorMobileData”. These files are Igor binary files (.ibw) and can be directly loaded into Igor Pro software.

crvi_datetimeUTC, crvi_LocalTime

The data interval for these results is 1-second. Gaps in time are included and indicate overnight parking periods.

crvi_datetimeUTC is in universal coordinated time (UTC). UTC is 8 hours ahead of PST and 7 hours ahead of PDT.

crvi_LocalTime is in local time, either as Pacific Standard Time (PST, first part of campaign) or Pacific Daylight Time (PDT, second part of campaign). Daylight savings time occurred during the campaign on March 11, 2:00 AM, 2018.

Location Wind Weather

crvi_Latitude, Longitude

The position (latitude and longitude in decimal degrees) of the Aerodyne Mobile Lab (AML) are reported. This data was collected using a Hemisphere GPS Vector v103 Compass.

crvi_Easting, crvi_Northing, crvi_Zone

The GPS location of the measurements are also reported as easting and northing (in meters), using the WGS84 coordinate system. The zone is always 11 for the dataset in question.

crvi_wind_degrees, crvi_wind_metersPerSecond

Incident wind direction in degrees clockwise from true north. A 90 degree wind direction indicates a wind from the east. Wind speed, in meters per second.

Apparent wind data was collected on a RMYoung 2D anemometer mounted to the roofline of the truck. This data was then corrected for truck bearing and speed using heading and speed data from the Hemisphere GPS Vector v103 Compass. Uncertainties in wind speed and direction are larger for low wind speeds and fast truck speed.

crvi_truckSpeed_kmph

Truck speed in kilometers per hour. This data was collected using the Hemisphere GPS Vector v103 Compass.

crvi_SolarElevAngle

The solar elevation angle was computed for the entirety of the campaign using the GPS location of the truck and the time of day. Solar elevation angle is reported in azimuthal degrees.

crvi_solar

Insolation, arbitrary units.

Solar insolation was measured with the ARISense unit mounted to the roof of the AML. Since the ARISense unit was mounted flat against the roof, the sky-facing port was facing forward. A quantitative insolation value is thus not possible. This metric still allows for a comparison between sunny and cloudy/dark times. This metric will be affected by any overhead obstruction like trees, overpasses, building shadows or overhangs.

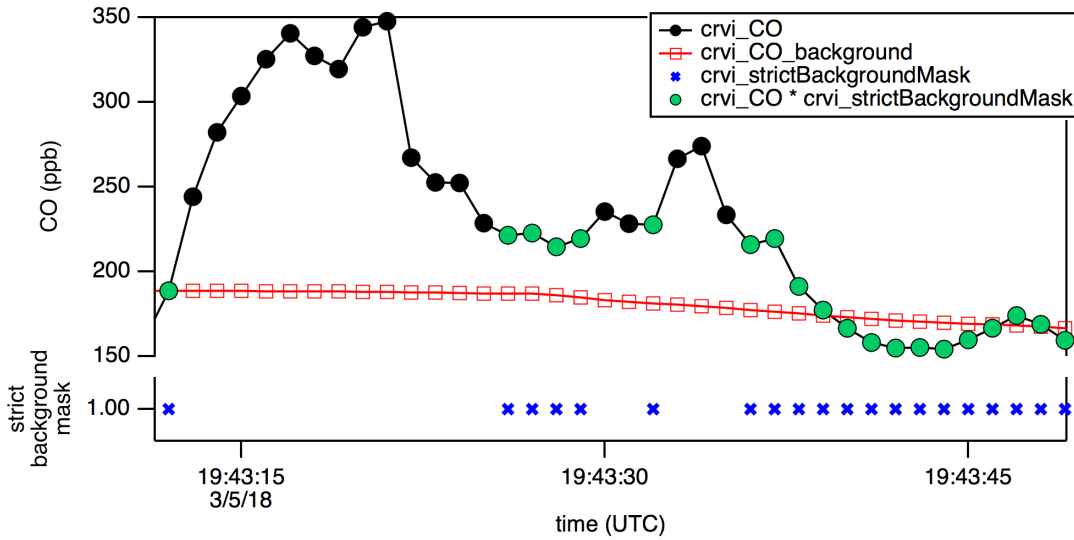
crvi_StrictBackgroundMask

Mask wave (1 or NaN) meant to indicate periods of regional background sampling (1) versus periods of potential local source contamination (NaN).

This mask was calculated by setting to NaN any data where the 1-second CO data exceeds the CO_background data by more than 50 ppb (see also crvi_CO_background section).

To use this mask, you can simply multiply the 1-second data by the mask.

The graph below shows an example of applying this strict background mask to the fast CO data.



crvi_temperature_C

Outdoor temperature in degrees Celsius. This data was collected on the RMYoung 3D Sonic anemometer mounted to the mobile lab boom. There may be a slight humidity dependence to this measurement, but no major issues have been observed when comparing it to nearby airport temperatures in previous campaigns.

crvi_truckHeading

Heading of the mobile lab, in degrees clockwise from true north. This measurement was taken with the v103 GPS unit. A heading of 180 points south.

crvi_wind_E_meters, crvi_wind_N_meters

Incident wind components, in meters per second from the east or north. This vector-style data is output for ease of plotting, but it is identical to the wind_degrees and wind_metersPerSecond data described earlier.

crvi_truckPitch_deg, crvi_truckRoll_deg, crvi_truckHeave_m

Pitch (front/back motion, in degrees), roll (side-to-side rocking, in degrees) and heave (bouncing, in meters) of the truck. These data were collected with the v103 GPS unit mounted to the truck roof. They are best used to diagnose instrument sensitivity to motion.

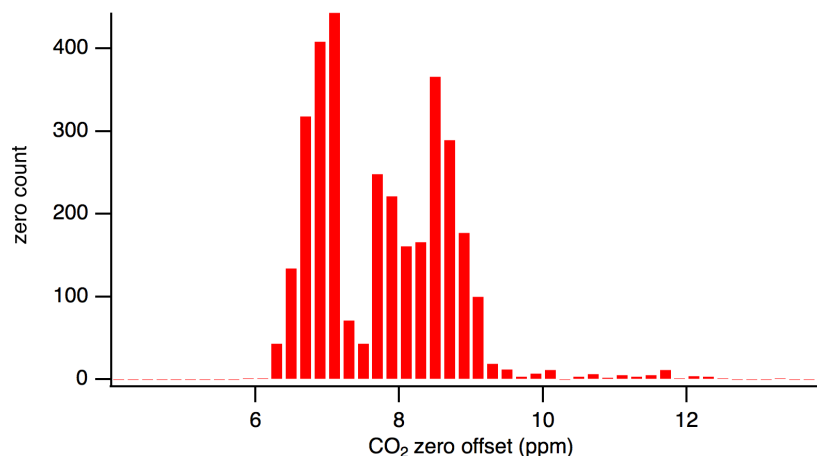
Trace Gases and Combustion Tracers

crvi_CO2_ppm

Carbon dioxide (ppm) on the gas-phase inlet was measured using a LI-6262 CO₂/H₂O analyzer (NDIR) from LI-COR, Inc.

No calibration factor was applied ($m = 1.0$; measured = standard * m) with a 2% uncertainty.

The zero offset of this instrument was corrected via linear interpolation between neighboring 15-minute zeroes. The magnitude of the zero correction was usually between 6 and 9 ppm, as the histogram below shows. Most variation in zeroes appears to occur over the course of the day, possibly correlating with temperature, as opposed to clear trends related to the purity of zero air tanks.



crvi_CO

Carbon monoxide mixing ratio (ppb). This is an absorption measurement taken with a TILDAS instrument in the 2200 cm⁻¹ region. Mixing ratios are not corrected for the water content of air.

No calibration factor has been applied. 6 calibration factors were done throughout the campaign, with an average of 0.996 and a standard deviation of 0.02. This average is not representative of the entire campaign because of tuning rate drift. There is a maximum possible low bias in CO of 4.5% during periods with poor tuning rate.

The full dataset is output as *crvi_CO*. Known periods of self-sampling have been removed. However, an exhaustive check of self-sampling periods remains to be done. This dataset includes traffic signatures and other CO enhancements that may not be desirable for photochemical analysis.

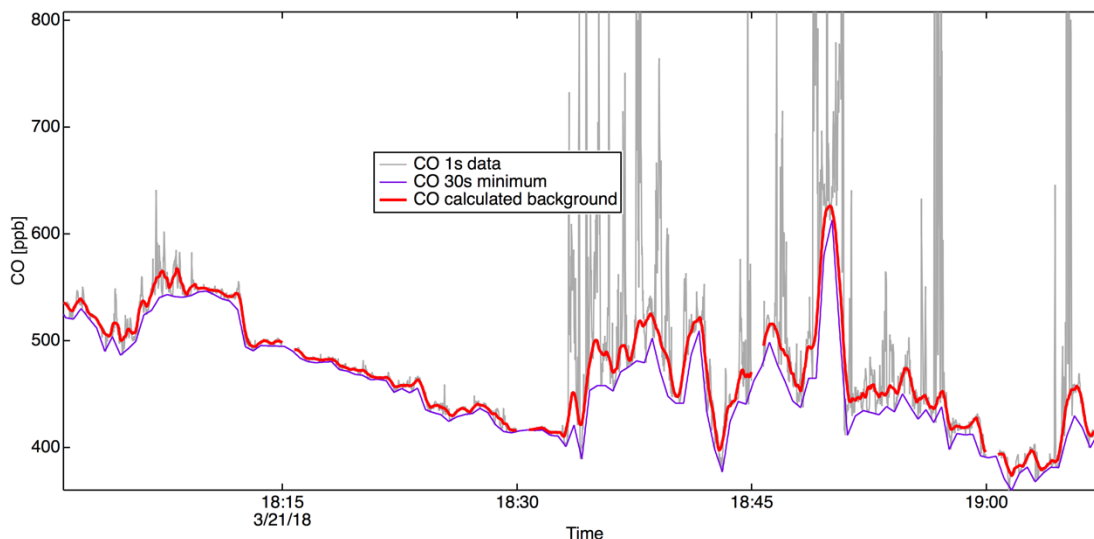
crvi_CO_background

Carbon monoxide mixing ratio (ppb), background levels only. Mixing ratios are not corrected for the water content of air.

Data represents the background CO concentrations without the fast enhancements due to local sources like traffic. This trace is calculated from the quality-assured crvi_CO data above.

A 30-second minimum was calculated. The difference between the fast CO trace and this running minimum was taken. Any time this fast enhancement exceeded 50 ppb, the fast CO data was thrown out. The fast CO data was smoothed (30-point box smoothing). The resulting trace is called crvi_CO_background. This algorithm keeps as much data as possible. A stricter algorithm has been used to output a mask wave that can be applied more generally to 1-minute data. See crvi_StrictBackgroundMask.

The figure below illustrates the difference between crvi_CO (grey) and crvi_CO_background (red). The 30-second minimum used for processing is shown in purple.



The Igor code used to take this background used the function “QAQCw_FiveMinMinimum” and is reproduced below. The functions used have been saved to the Igor software called QAQCw_waveTools.ipf.

```
QAQCw_ResetListWaves("CO")
QAQCw_NaNZeroes(1,0,tokens="CO");
QAQCw_NanThisClass("Blacklist;SelfSampling")
QAQCw_NaNLargeDataGaps("CO",5)
QAQCw_FiveMinMinimum(GetXwaveRef4Token("CO"),
$(getFullWaveStr("CO","YWAVE",era_datetime=datetime)+"_NaNed"),
resolution=30, avgTime=30)
setdatafolder root:a_tdlCO
duplicate/o tdl3_conc_Naned_5minmin delta
delta = tdl3_conc_Naned - tdl3_conc_Naned_5minmin
QAQCw_clipIntensity("deltaCO","CO",0,50,time2inletTF=0)
QAQCw_interpOverNaNs("CO")
Duplicate/O tdl3_conc_Naned,CObkg_smooth;Smooth/EVEN/B 30, CObkg_smooth
QAQCw_ResetListWaves("CO")
```

```
QAQCw_NaNZeroes(1,0,tokens="CO");
QAQCw_NanThisClass("Blacklist;SelfSampling")
QAQCw_NaNLargeDataGaps("CO",5)
CObkg_smooth = numtype(tdl3_conc_NaNed[p]) == 2 ? NaN : cobkg_smooth[p]
```

crvi_N2O

Nitrous oxide mixing ratio (ppb). This is an absorption measurement taken with a TILDAS instrument in the 2200 cm⁻¹ region. Mixing ratios are not corrected for the water content of air.

No calibration factor has been applied.

crvi_H2O

Water mixing ratio (ppb). This is an absorption measurement taken with a TILDAS instrument in the 2200 cm⁻¹ region.

No calibration factor has been applied.

crvi_RH

Relative humidity, in percent (%).

This was measured in the flow cell of the ARISense unit.

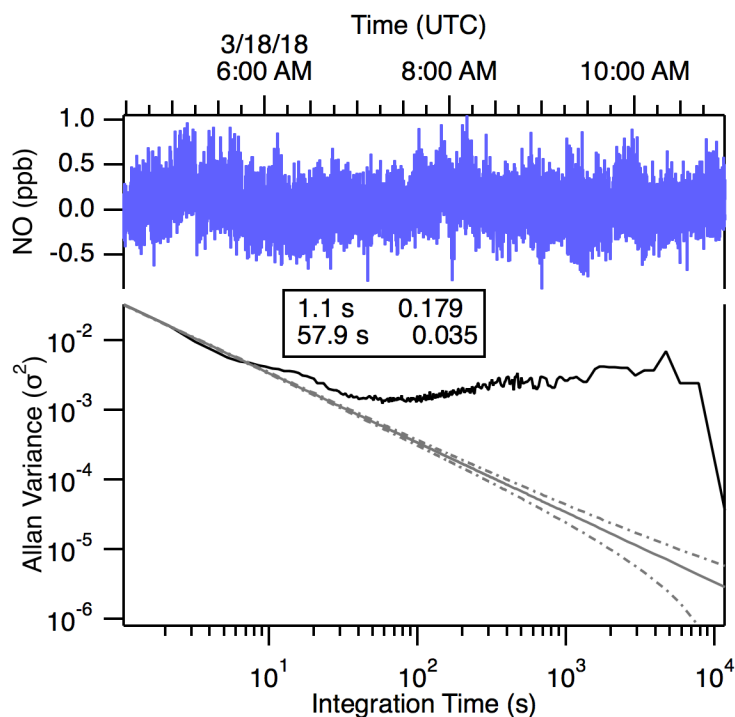
crvi_NO

Nitrogen oxide (NO) in ppb.

This was measured by a TILDAS instrument. Mixing ratios are not corrected for the water content of air.

A calibration factor of $m=0.85$ was applied ($\text{true} = m * \text{meas} + b$). This calibration factor is the average of 4 calibrations taken over the course of the campaign (0.91, 0.81, 0.85, 0.85). The 1-sigma uncertainty on calibration accuracy is 4%. A tuning rate adjustment was done on 03/17/2018, after which the calibration factor stabilized to 0.85 for the remainder of the campaign. There is insufficient evidence to motivate using different calibration factors early on in the campaign.

The short-term noise performance of the instrument was quantified via an Allan variance plot, shown below. The 1-sigma noise at 1 second was 0.18 ppb, averaging down to 0.035 ppb at 1 minute.



One problem encountered during this study was a loss of frequency-locking capability during certain periods, resulting in peak position errors that are far enough away from the true positions that it was difficult to identify the correct position during refitting of the data. This was dealt with as follows: the spectral data was refit with floated peak position at 2 minute averaged intervals. This allowed the spectrum to average the noise down, and to be influenced by large self-sampling events, so that the NO spectral doublet could be easily identified. The peak position derived from this first fit was then used as a legitimate peak position in a subsequent fit, if the average NO concentration was >25 ppb over the 2 minute interval. If the NO concentration was below 25 ppb during the interval, the most recent interval with >25 ppb NO was used. The spectra were then refit at 1-second intervals with NO fixed at these new peak positions.

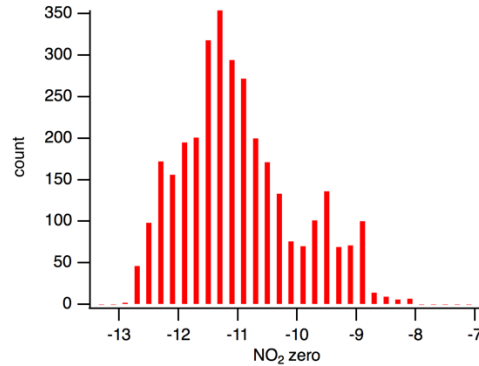
While this resolved the majority of the fitting issues, there are still periods where the NO value goes below zero, likely due to bad instrument zeroing events, or drift in the laser frequency in between the lock intervals described above. Rather than eliminate that unphysical data, which is still of value for plume-based analyses, we include it in the analyzed data, with the caveat that the zero level is incorrect.

crvi_NO2

Nitrogen dioxide, NO₂, in ppb.

This was collected with an Aerodyne CAPS-NO₂ instrument. The unit was run with an approximately 10 second time constant in the optical cell.

Zero corrections were done by interpolating between subsequent zeroes. Zero values fluctuated about -11 ppb (see graph below).

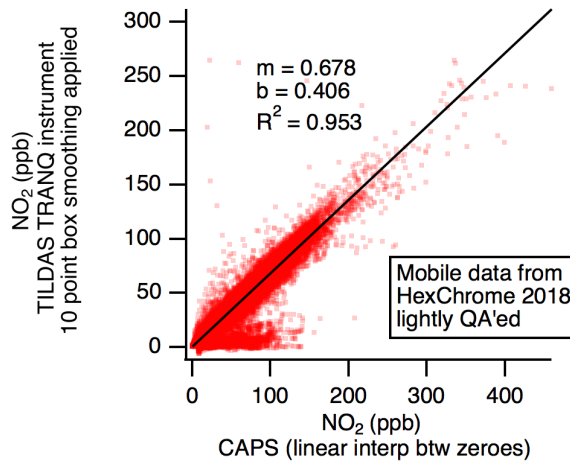


Faster time-response data was taken with a TILDAS instrument (the same one that collected NO data). This TILDAS instrument suffered a larger number of data drop-outs, and so CAPS data is reported as primary NO₂.

This instrument appeared delayed versus the other instruments in the AML by about 5 seconds. This 5-second time difference has been corrected in the output data.

No calibration factor was applied because a recently-calibrated NO₂ cylinder was not available.

An intercomparison was done with the TILDAS instrument (no calibrations applied to either dataset). This graph shows that the CAPS reports lower mixing ratios than the TILDAS instrument by 32%.



This TILDAS instrument, with an NO₂ laser that has since been replaced, had an NO₂ calibration factor of 1.08 versus the “FIREX CO₂” calibration tank in January 2018. This TILDAS instrument with the current NO₂ laser, has a calibration factor of 0.504 versus the “FIREX CO₂” calibration tank in June 2018; the current CAPS-NO₂ unit has a calibration factor of 0.566 for this June calibration (for a TILDAS vs CAPS ratio of 0.89).

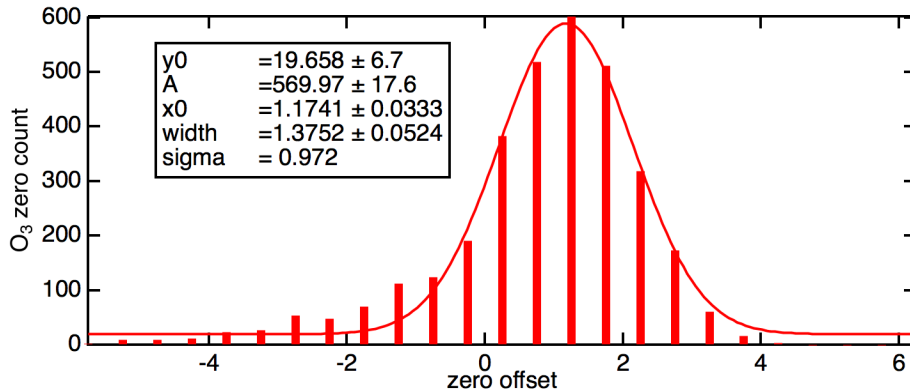
This calibration history reveals that new calibrations are required on both the TILDAS and CAPS-NO₂ units, and the calibrations should use either a new and trusted calibration tank, or a NO + O₃ titration strategy. Reported NO₂ concentrations will be updated once this has been done.

crvi_03

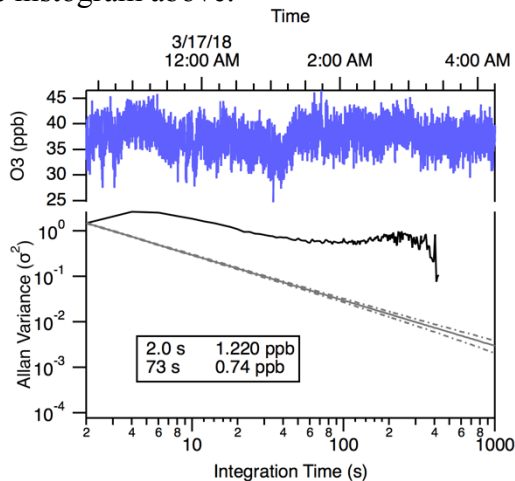
Ozone, O₃, in ppb.

This data was collected with a 2B Technologies, Inc. Ozone Monitor, Model 205. Data from this instrument was offset in time by -4.4 seconds to account for an inlet lag and in order to match the zero timing of the gas-phase inlet CO₂ measurement.

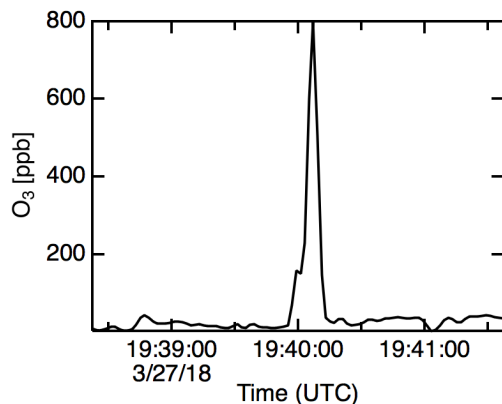
No calibration has been applied to this instrument. Zero offsets were computed during the zero overblows every 15 minutes. The average zero offset is 1.2 ppb, and the distribution of these zeroes is shown in the histogram below. Zero offsets were corrected by linearly extrapolating between subsequent zeroes.



The data rate of this instrument is one data point every 2 seconds (0.5 Hz). The 2s noise is approximately 1.2 ppb, based on limited data when concentrations were somewhat stable, see figure below. This is fairly close to the 1-sigma variation in zeroes (0.97 ppb) that was calculated in the histogram above.



There was one instance of a suspiciously high O₃ plume, correlating with C₂H₆ and N₂O. This plume was left in the data for the time being but more QA is required to assess its validity. Known interferences to this UV absorption instrument include sulfur dioxide, aromatic hydrocarbons and others. (Spicer et al., 2010) Unfortunately, no VOC data was acquired during this period.



crvi_CH4, crvi_C2H6

Methane, CH₄, and ethane, C₂H₆, in ppb.

This data was collected on a TILDAS instrument operated at 2998 cm⁻¹, with a wide laser scan. Mixing ratios are not corrected for the water content of air.

A calibration factor of $m=0.847$ for C₂H₆ and $m=0.925$ for CH₄ have been applied to the data, where $\text{true} = m * \text{meas} + b$. There is a 1-sigma standard deviation between these calibrations of 0.013 for C₂H₆ and 0.002 for CH₄.

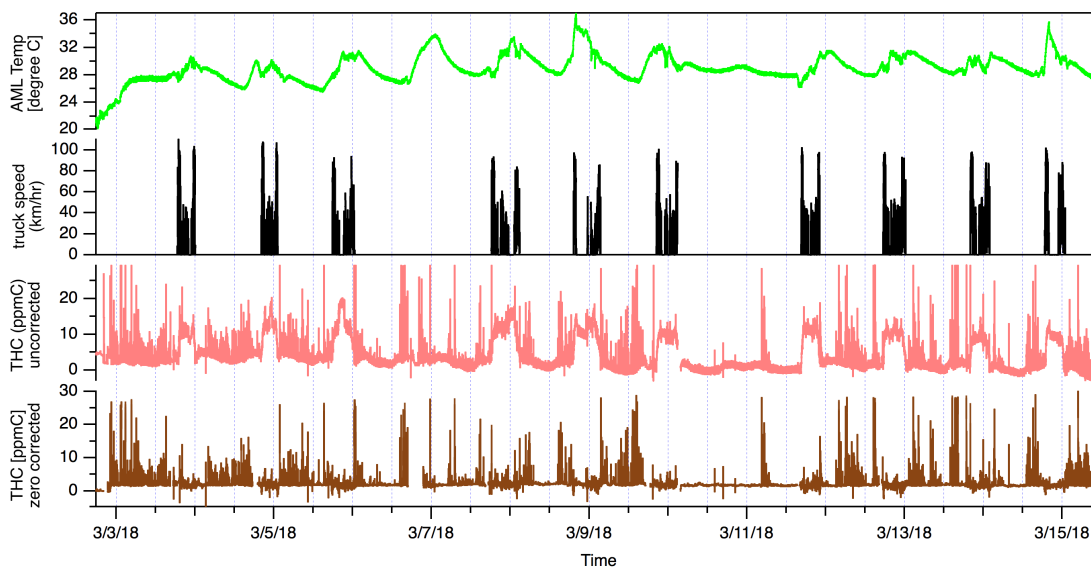
Overnight data was contaminated by emissions from the LNG fueling station in the SCAQMD Diamond Bar parking lot. Methane and ethane also have numerous sources in this study. For this reason, there is no period of “quiet” data that is appropriate for a statistical analysis of instrument noise. The estimated performance of this instrument is a 1-sigma, 1-second noise better than 70 ppt for C₂H₆ and better than 1.5 ppb for CH₄.

crvi_THC_ppm

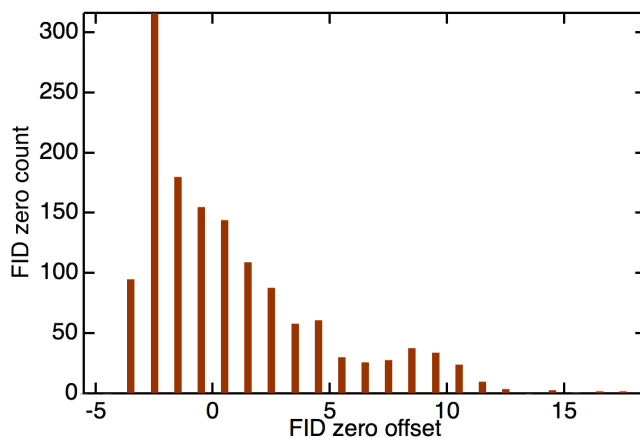
Total hydrocarbons, in ppm of Carbon (methane equivalent). This is a relative measurement and should not be used to determine baseline carbon content.

A CAI flame ionization detector (FID) was used. The instrument was set to “Range 1” for the entire campaign (0 – 29 ppm). Measurements above 29 ppm max out and have been set to NaN. Similarly, the instrument bottoms out at a response level of -3 ppm and this data has been set to NaN.

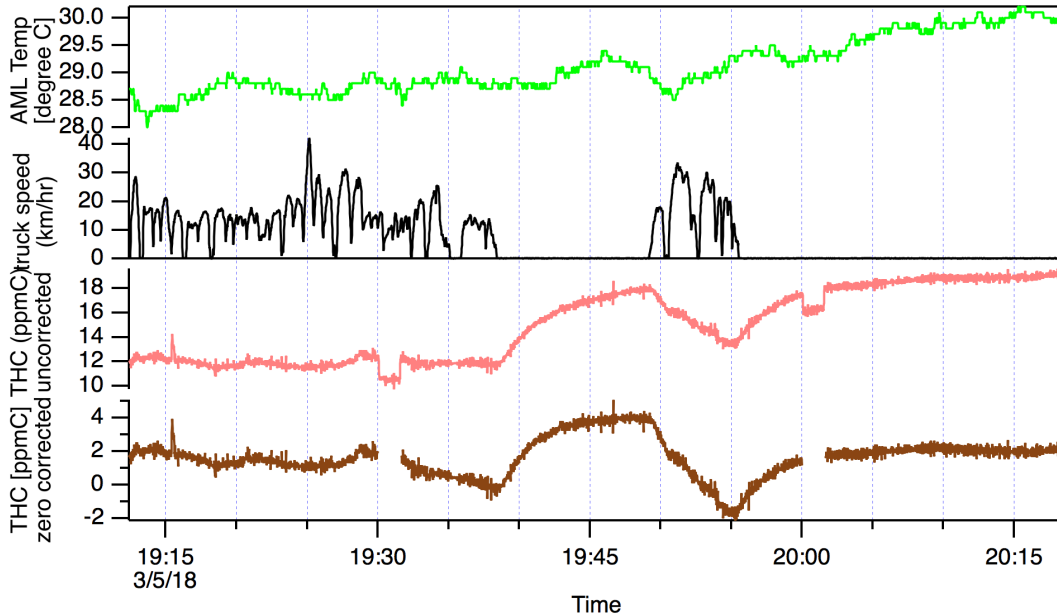
This instrument showed sensitivity to truck motion. Baselines tended to drift up, up to raw response levels of 10-15 ppm, when in motion. Conversely, when the truck was stationary, response levels drifted back down to 0-2 ppm, and occasionally bottomed out below the -3 ppm limit, precluding any data reporting for these periods. The figure below compares raw data (pink) with truck speed (black), showing the sensitivity to motion. The instrument’s relative insensitivity to truck temperature (green) can also be seen.



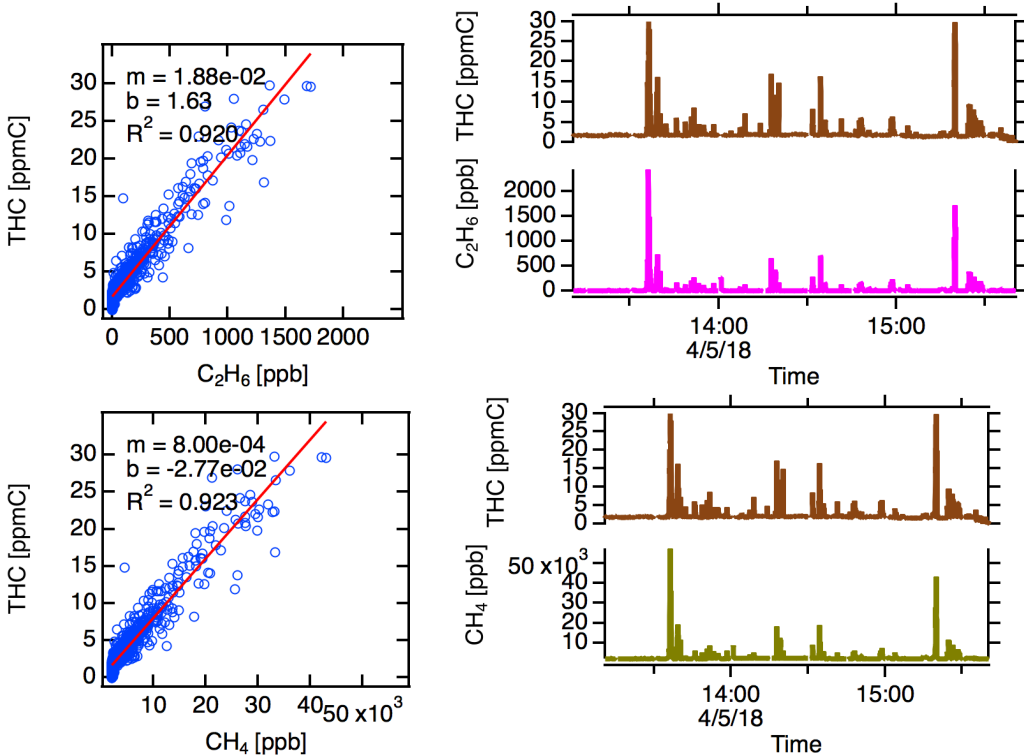
Instrument zeroes were corrected using the every-30-minute delivery of air from the zero air generator (ZAG). The ZAG uses a heated catalyst to convert VOCs to CO₂. It is quite efficient for aromatics and larger VOCs but does not effectively convert methane or ethane. For this reason, this data should not be used to determine baseline carbon content of the air. The figure below shows a histogram of zeroes acquired during the campaign. Note that the zero drift does not go below -3 since the instrument bottoms out at this response level.



Even with zero correction, there remain periods of data with significant baseline drift. Such periods should be ignored.



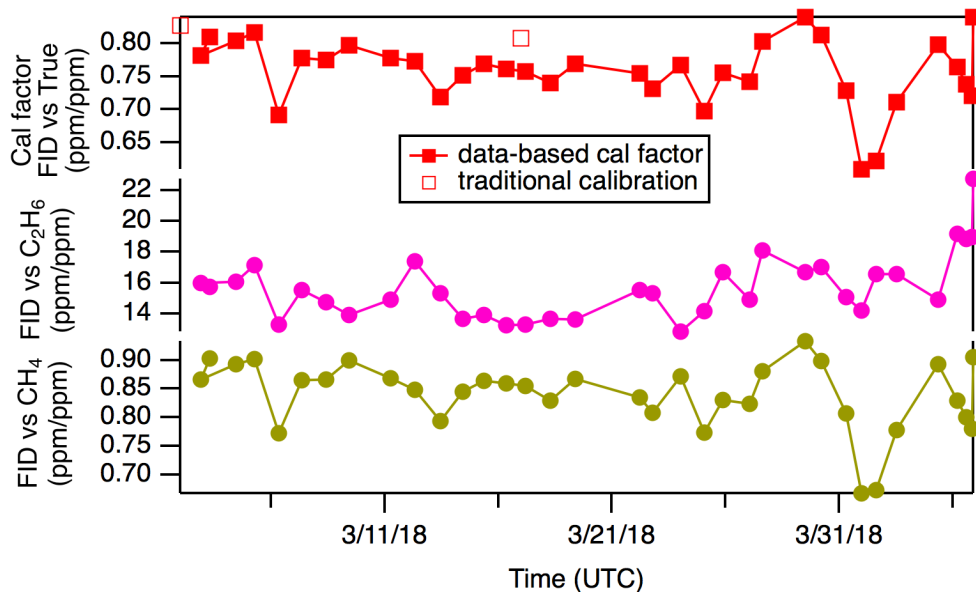
Overnight measurements were impacted by a leak from the natural gas fueling station in the SCAQMD Diamond bar parking lot. This fortuitous data can be used to calibrate the response of the FID instrument. The graphs below show one of many overnight data segments where the FID response (total hydrocarbons, THC) is correlated to methane and ethane.



These two ratios can be combined to give a data-based FID cal factor (red squares, figure below):

$$\text{ratioFIDcal} = 1/(1/(\text{ratioFIDtoCH}_4 * 1000) + 2 * 1/(\text{ratioFIDtoC}_2\text{H}_6 * 1000))$$

which agrees well with the traditional calibration factors done via dilution of a high-concentration methane and acetylene tank into ZAG air (open squares).

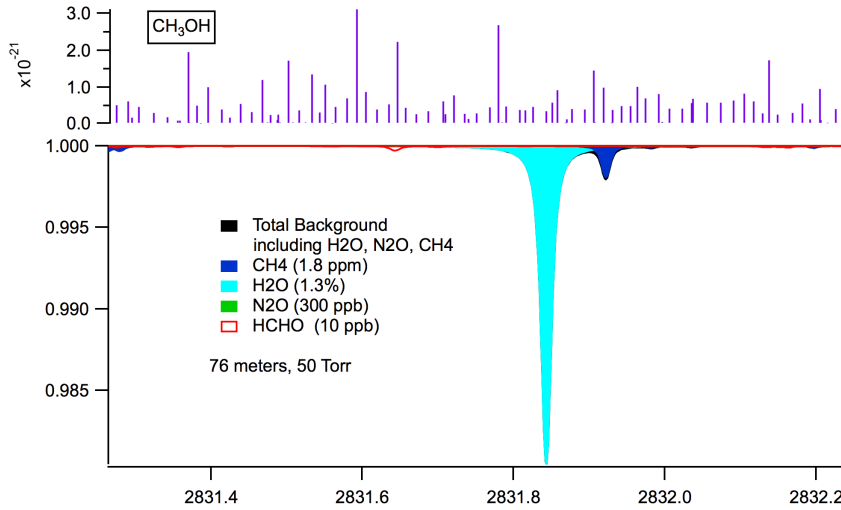


These data-based calibration factors were linearly interpolated onto the common time base and applied to the final data.

crvi_HCHO

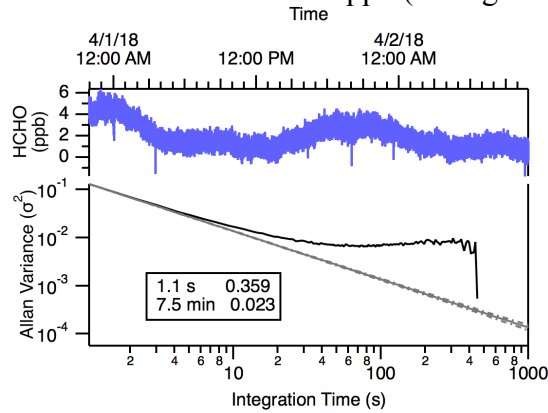
Formaldehyde, HCHO, in ppb.

This data was collected on a TILDAS instrument operated at 2831 cm⁻¹. Mixing ratios are not corrected for the water content of air.



No calibration factor has been applied.

This instrument had a 1-second noise around 0.35 ppb (see figure below).



Particulate Matter

crvi_PM2, crvi_PM10, crvi_PMLarge

Particulate matter mass, in units of micrograms per meter cubed ($\mu\text{g}/\text{m}^3$).

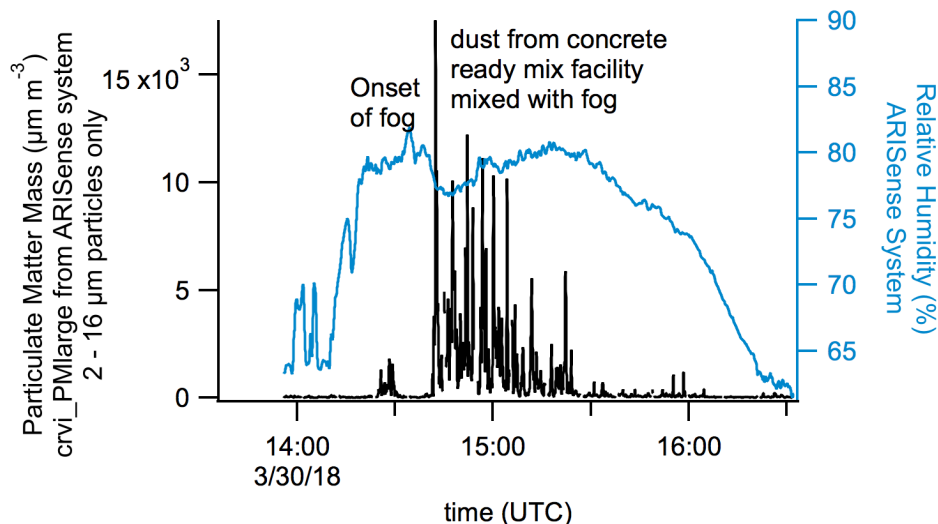
These data were acquired with the ARISense system mounted to the roof of the AML, using its internal OPC (Alphasense model OPC-N2). This unit reports data at a rate of once every 10 seconds.

The OPC reports data as particle counts (number concentration). Internal firmware (not controlled by Aerodyne) classifies each raw scattered light signal into 16 distinct particle size bins (0.4 to 16 microns). The size distribution is then further analyzed to provide integrated number and mass concentration metrics. PM2 and PM10 waves were calculated by first assuming that all detected particles were spherical with a density of 1.65 grams per cubic centimeter. The resultant mass distributions were then integrated

between 0.4-2 μm for PM2 and 0.4-10 μm for PM10. No size-dependent collection efficiency corrections were applied to the PM2 and PM10 outputs.

The PMLarge data trace includes only particles with sizes between 2 μm and 16 μm . This is distinct from the typical PM10 metric, for example, which includes all particles smaller than 10 μm .

These large particle measurements will include the droplet mode. During the campaign, the mobile lab sometimes sampled in foggy conditions, and on one occasion (see figure below), sampled a dust plume from a concrete facility in the fog. It is recommended to use the relative humidity measurement from the ARISense (*crvi_RH*), or the water mixing ratio measurement (*crvi_H2O*) from the gas phase inlet, to understand and identify these droplet mode time periods and distinguish them from dust.

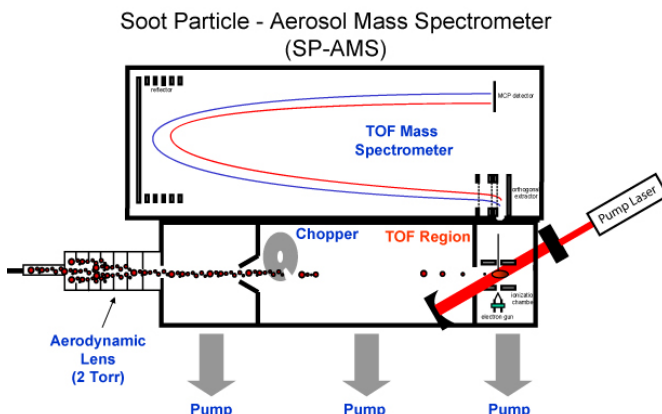


For 3 days near the end of the campaign (3/23/18 11:58 UTC to 3/26/2018 14:33 UTC), there was a power or logging problem and the data from this instrument was not logged.

crvi_PMorg, crvi_PMSO4, crvi_PMNO3, crvi_PMNH4, crvi_PMchl, crvi_PMBC

Particulate Matter mass, in micrograms per meter cubed ($\mu\text{g m}^{-3}$), speciated.

This data was collected on an Aerodyne Soot-Particle Aerosol Mass Spectrometer (SP-AMS) equipped with a high-resolution time-of-flight mass spectrometer (HR-ToF). This instrument combines the Single Particle Soot Photometer (SP2, Droplet Measurement Technologies) (Schwarz et al., 2006) and the High Resolution Time-of-Flight Aerosol Mass Spectrometer (HR-ToF-AMS, Aerodyne Research, Inc.) (DeCarlo et al., 2006).



These species waves listed below have all had the necessary corrections applied to them (ionization efficiency, relative ionization efficiency, collection efficiency and airbeam corrections). These waves should be considered final in units of $\mu\text{g m}^{-3}$. This data considers only small particles ($<1 \mu\text{m}$ initially, then $<2.5 \mu\text{m}$ after 3/18/2018). See final report for a discussion of particle sizes and coarse-mode aerosols.

The speciated particles are defined as:

Org Organic
 SO4 Sulfate
 NO3 Nitrate
 NH4 Ammonium
 Chl Chloride
 BC Black Carbon

crvi_CPC

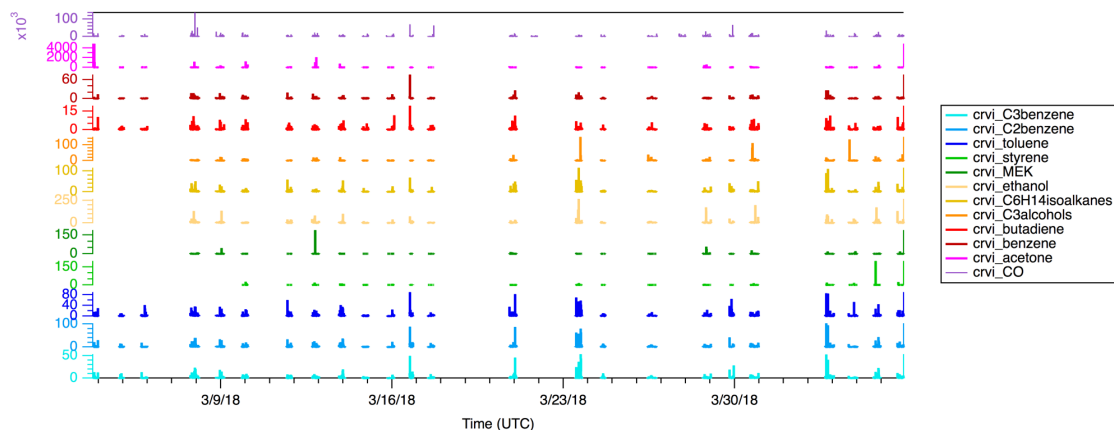
Particulate matter count, in number of particles per centimeter cubed, or $\# \text{cm}^{-3}$
 Measured with a Condensation Particle Counter.

This data considers only small particles ($<2.5 \mu\text{m}$). See final report for a discussion of particle sizes and coarse-mode aerosols.

Volatile Organic Hydrocarbons

These measurements were taken by a Proton Transfer Mass Spectrometer (PTR-MS) operated in NO^+ mode. The list of measured ions was finalized on 3/9/2018 after initial surveys of the study area. For this reason, some species have no reported data in early days. The data rate of the instrument is typically 0.1 Hz (one data point every 10 seconds). For the purpose of putting data on a common time base, the data has been

linearly interpolated onto 1-second base. In the latter portion of the 3/5/2018 data, data is reported at a 0.05 Hz data rate (one data point every 10 seconds), since data was collected in full mass spectrum mode to evaluate the presence of any important ions that may not have been on our radar. No data from this instrument was acquired on two of the drive days (3/21 and 3/27) due to operator error. The graph below gives an overview of the data coverage of this instrument relative to carbon monoxide (crvi_CO, violet) which has coverage for the full period.



crvi_ethanol

Ethanol, in ppb, was measured by the Proton Transfer Mass Spectrometer operated in NO⁺ mode.

The ion at mass 45 is attributed to the hydride abstraction product (M-H)⁺ of ethanol. Koss et al. in their speciated analysis of this ion indicate that virtually all of its intensity can be attributed to ethanol. (Koss et al., 2016) Ethanol is a significant component in California reformulated gasoline. (McDonald et al., 2018) This ion was first included in the measurement list on 3/7.

crvi_C3alcohols

C3 alcohols (isopropanol and *n*-propanol), in ppb, were measured by the Proton Transfer Mass Spectrometer operated in NO⁺ mode.

The ion at mass 59 is attributed to the hydride abstraction product (M-H)⁺ of the C3-alcohols (isopropanol and propanol). (Koss et al., 2016) Acetone arising from proton transfer (MH⁺) with the residual H₃O⁺(H₂O) represents an interference. Approximately 0.8% of acetone signal is detected at m/z 59 and no effort has been made to correct for this interference. Koss et al. in their speciated analysis of this ion do not report any additional interferences. (Koss et al., 2016) This ion was first included in the measurement list on 3/7.

crvi_butadiene

1,3-butadiene, in ppb, was measured by the Proton Transfer Mass Spectrometer operated in NO⁺ mode.

The ion at mass 54 is attributed to the charge exchange product (M⁺) of 1,3-butadiene. Knighton et al. have previously measured 1,3-butadiene in ambient and polluted atmospheres assuming that m/z 54 is from 1,3-butadiene. (Knighton et al., 2009; Knighton et al., 2012) Koss et al. report that m/z 54 arises from propyne (MW 40) and vinyl acetylene (MW 52). (Koss et al., 2016) This would appear to be an error as there is no logical ionization scheme whereby either of these compounds could produce an ion at m/z 54.

crvi_benzene

Benzene, in ppb, was measured by the Proton Transfer Mass Spectrometer operated in NO⁺ mode.

The ion at mass 78 is attributed to the charge exchange product (M⁺) of benzene. There are no known interferences to the determination of benzene at this mass-to-charge ratio. (Koss et al., 2016)

crvi_C6H14isoalkanes

Isoalkanes with the chemical formula C₆H₁₄, in ppb, were measured by the Proton Transfer Mass Spectrometer operated in NO⁺ mode.

The ion at mass 85 is attributed to the hydride abstraction product (M-H)⁺ of C₆H₁₄ isoalkanes, which include 2-methylpentane, 3-methylpentane, 2,2-dimethylbutane and 2,3-dimethylbutane. (Koss et al., 2016) There are other interferences including the C₅aldehydes (hydride abstraction) and fragmentation products of larger alkanes. (Koss et al., 2016) While there may be interferences, this mass was selected to help distinguish between fuel leaks and evaporative fuel emissions. This ion was first included in the measurement list on 3/7.

crvi_acetone

Acetone, in ppb, was measured by the Proton Transfer Mass Spectrometer operated in NO⁺ mode.

The ion at mass 88 is attributed to the NO⁺ adduct (NO⁺M) of acetone. There are no known interferences to the determination of acetone at this mass-to-charge ratio. (Koss et al., 2016) Acetone is present at persistent and sufficiently high levels in the atmosphere that it provides an excellent check for the “background zero” provided by heated catalyst system is working properly. Koss et al. note that there is a significant humidity dependence associated with the detection efficiency of acetone in which the sensitivity factor increases with increasing humidity. (Koss et al., 2016) The present measurements indicate a similar result, but no effort has been made to characterize or account for the effect of humidity.

crvi_toluene

Toluene, in ppb, was measured by the Proton Transfer Mass Spectrometer operated in NO⁺ mode.

The ion at mass 92 is attributed to the charge exchange product (M⁺) of toluene. The monoterpenes produce a fragment ion at m/z 92, but in the urban environment there is an insufficient amount of these compounds present to interfere.

crvi_MEK

Methyl ethyl ketone, in ppb, was measured by the Proton Transfer Mass Spectrometer operated in NO⁺ mode.

The ion at mass 102 is attributed to the NO⁺ adduct (NO⁺M) of methyl ethyl ketone (MEK). Koss et al. indicate that this mass is unique to MEK. (Koss et al., 2016)

Quantification of MEK is somewhat uncertain as its sensitivity factor had to be estimated and clustering reactions are more sensitive to differences in instrumental parameters such as temperature, E/N, and ion extraction potentials. This ion was first included in the measurement list on 3/7.

crvi_styrene

styrene, in ppb, was measured by the Proton Transfer Mass Spectrometer operated in NO⁺ mode.

The ion at mass 104 is attributed to the charge exchange product (M⁺) of styrene. Knighton et al. have previously measured styrene in polluted atmospheres assuming that m/z 104 is from styrene. (Knighton et al., 2012) Koss et al. with their speciated analysis indicate that there are other compounds in the ambient atmosphere that are detected at m/z 104, but do not provide any identification. (Koss et al., 2016) With the plumes that are encountered in the present work it seems highly probable that these are due to styrene. The quantification of styrene would benefit from calibrated sensitivity factors, although calibrations performed previously agree well with the current estimate. This ion was first included in the measurement list on 3/9.

crvi_C2benzene

C2-benzenes, in ppb, were measured by the Proton Transfer Mass Spectrometer operated in NO⁺ mode.

The ion at mass 106 is attributed to the charge exchange product (M⁺) of the C₈H₁₀ (C2benzene) isomers. Direct mass spectrometry doesn't provide the capability of distinguishing between structural isomers and so only the sum is reported.

crvi_C3benzene

C3-benzenes, in ppb, were measured by the Proton Transfer Mass Spectrometer operated in NO⁺ mode.

The ion at mass 120 is attributed to the charge exchange product (M^+) of the C_9H_{12} (C_3 benzene) isomers. Direct mass spectrometry doesn't provide the capability of distinguishing between structural isomers and so only the sum is reported.

Comparison with previous studies

A time series of the VOC monitored during a typical AML area survey during the SCAQMD study is depicted in Figure 3. Compounds present in gasoline vehicle exhaust (ethanol and below) all show significant enhancements with CO. The upper components: acetone, C_3 -alcohols, methyl ethyl ketone (MEK) and styrene are not significant components in exhaust and their concentrations are affected primarily by encounters with fugitive emissions. In the next sections the results from this study are examined with respect to automobile exhaust emissions measured in Caldecott Tunnel and ambient air measurements taken during the California Nexus Study.

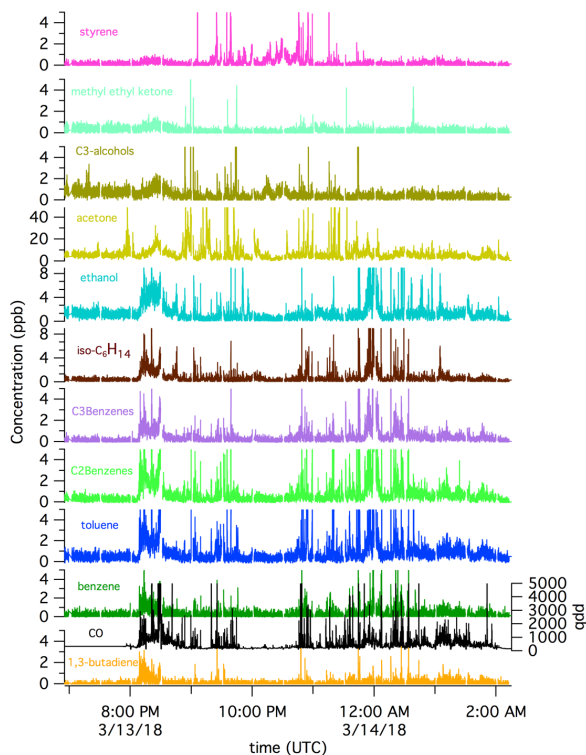


Figure 3. Representative VOC times series from an AML area survey.

PM Metals or Salts

Particulate matter mass, in micrograms per meter cubed ($\mu\text{g m}^{-3}$). Particulate matter is speciated based on its metal or salt content.

This data was collected on an Aerodyne Soot Particle Aerosol Mass Spectrometer (SP-AMS) equipped with a high-resolution time-of-flight mass spectrometer (HR-ToF). This data considers only small particles ($<1 \mu\text{m}$ initially, then $<2.5 \mu\text{m}$ after 3/18/2018). See final report for a discussion of particle sizes and coarse-mode aerosols.

The individual ions output in this file are the signal for the major isotope of that ion and do not include any minor isotopes. Additional analysis (fitting) is required to produce a total isotopes trace. Alternatively, the natural abundance of the major isotope of each ion could be used to apply a first-order correction to these traces.

Numerous metals and salts have been output from the high-resolution SP-AMS fit. Only the major isotope is included in these fits.

Some species may include small interferences due to neighboring ions at similar masses. For example, Ni may be influenced by NaCl. Ed Fortner (efortner@aerodyne.com) may be contacted directly for any questions on specific ions.

crvi_PMHCl	Hydrogen Chloride	crvi_PMP	Phosphorus
crvi_PMNaCl	Sodium Chloride	crvi_PMPb	Lead
crvi_PMKCl	Potassium Chloride	crvi_PMPd	Palladium
crvi_PMAg	Silver	crvi_PMRb	Rubidium
crvi_PMAI	Aluminum	crvi_PMRh	Rhodium
crvi_PMAIO	Aluminum Oxide	crvi_PMRu	Ruthenium
crvi_PMAAs	Arsenic	crvi_PMSb	Antimony
crvi_PMAu	Gold	crvi_PMSc	Scandium
crvi_PMCd	Cadmium	crvi_PMSn	Tin
crvi_PMCr	Chromium	crvi_PMSr	Strontium
crvi_PMCs	Cesium	crvi_PMTe	Tellurium
crvi_PMFe	Iron	crvi_PMTi	Titanium
crvi_PMI	Iodide	crvi_PMTl	Thallium
crvi_PMIn	Indium	crvi_PMV	Vanadium
crvi_PMKr	Krypton	crvi_PMW	Tungsten
crvi_PMMg	Magnesium	crvi_PMXe	Xenon
crvi_PMMn	Manganese	crvi_PMY	Yttrium
crvi_PMMo	Molybdenum	crvi_PMZn	Zinc
crvi_PMNb	Niobium	crvi_PMZr	Zirconium
crvi_PMNi	Nickel		

Hexavalent Chromium

crvi_cr6_ngm3

Hexavalent chromium (Cr6 or Cr(VI)) in nanograms per meter cubed (ng m⁻³).

This data was collected by collaborators at the Desert Research Institute (DRI), using the Steam-Jet Aerosol Collector (SJAC) system. No particle size filter was used on the SJAC inlet. Data was concatenated and put onto the common time base. SJAC-LPAS Appendix for additional experimental details.

References

- DeCarlo PF, Kimmel JR, Trimborn A, Northway MJ, Jayne JT, Aiken AC, Gonin M, Fuhrer K, Horvath T, Docherty KS, Worsnop DR, Jimenez JL. 2006. Field-deployable, high-resolution, time-of-flight aerosol mass spectrometer. *Anal Chem* **78**(24): 8281-8289. DOI:10.1021/ac061249n.
- Knighton WB, Fortner EC, Herndon SC, Wood EC, Miake-Lye RC. 2009. Adaptation of a proton transfer reaction mass spectrometer instrument to employ NO⁺ as reagent ion for the detection of 1,3-butadiene in the ambient atmosphere. *Rapid Commun Mass Spectrom* **23**(20): 3301-3308. DOI:10.1002/rcm.4249.
- Knighton WB, Herndon SC, Wood EC, Fortner EC, Onasch TB, Wormhoudt J, Kolb CE, Lee BH, Zavala M, Molina L, Jones M. 2012. Detecting fugitive emissions of 1,3-butadiene and styrene from a petrochemical facility: An application of a mobile laboratory and a modified proton transfer reaction mass spectrometer. *Ind Eng Chem Res* **51**(39): 12706-12711. DOI:10.1021/ie202794j.
- Koss AR, Warneke C, Yuan B, Coggon MM, Veres PR, de Gouw JA. 2016. Evaluation of NO⁺ reagent ion chemistry for online measurements of atmospheric volatile organic compounds. *Atmos Meas Tech* **9**(7): 2909-2925. DOI:10.5194/amt-9-2909-2016.
- McDonald BC, de Gouw JA, Gilman JB, Jathar SH, Akherati A, Cappa CD, Jimenez JL, Lee-Taylor J, Hayes PL, McKeen SA, Cui YY, Kim S-W, Gentner DR, Isaacman-VanWertz G, Goldstein AH, Harley RA, Frost GJ, Roberts JM, Ryerson TB, Trainer M. 2018. Volatile chemical products emerging as largest petrochemical source of urban organic emissions. *Science* **359**(6377): 760-764. DOI:10.1126/science.aaq0524.
- Schwarz JP, Gao RS, Fahey DW, Thomson DS, Watts LA, Wilson JC, Reeves JM, Darbeheshti M, Baumgardner DG, Kok GL, Chung SH, Schulz M, Hendricks J, Lauer A, Kärcher B, Slowik JG, Rosenlof KH, Thompson TL, Langford AO, Loewenstein M, Aikin KC. 2006. Single-particle measurements of midlatitude black carbon and light-scattering aerosols from the boundary layer to the lower stratosphere. *J Geophys Res Atmos* **111**(D16). DOI:doi:10.1029/2006JD007076.
- Spicer CW, Joseph DW, Ollison WM. 2010. A re-examination of ambient air ozone monitor interferences. *J Air Waste Manage Assoc* **60**(11): 1353-1364. DOI:10.3155/1047-3289.60.11.1353.

Appendix C: SJAC-LPAS Instrument Details

Prepared by Andrey Khlystov and David Campbell, Desert Research Institute
Edited and formatted by Tara Yacovitch, Aerodyne Research Inc.

Instrument description

The schematic of steam jet aerosol collector long pathlength absorbance spectroscopy (SJAC-LPAS) system is shown in Figure C1. Aerosol particles are collected with the Steam-Jet Aerosol Collector (SJAC) (Khlystov et al., 1995). The SJAC operates by injecting steam into the sampled air stream, which causes water vapor to condense on the sampled aerosol particles. Particles grow due to water condensation to a size of at least $1\mu\text{m}$ in diameter and are collected by a cyclone. The SJAC quantitatively collects particles down to a few nanometers in diameter (collection efficiency 99%) (Khlystov et al., 1995). The collected liquid containing dissolved aerosol species is continuously pumped out and mixed with diphenylcarbazide (DPC) reagent for colorimetric determination of Cr(VI) (Allen, 1958). To increase sensitivity, a liquid waveguide capillary cell (LWCC) is used to increase the sensitivity.

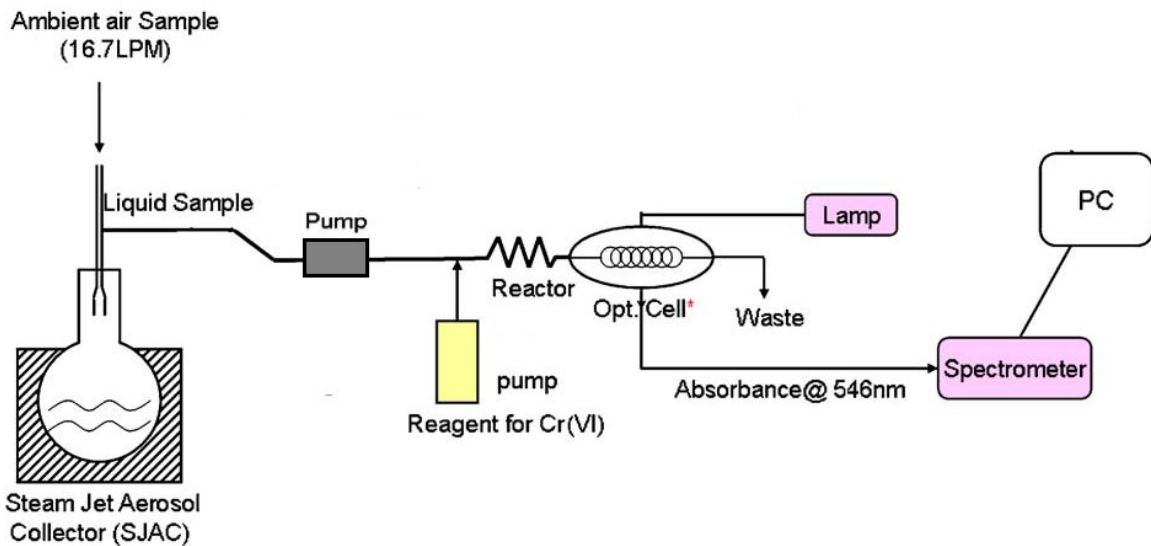


Figure C1. Instrument diagram of the SJAC-LPAS System.

Laboratory characterization

Prior to field deployment, the instrument was tested to determine its sensitivity, stability, and response time using potassium dichromate solutions of various concentrations within the range anticipated to occur during ambient monitoring. Spectra of transmitted light through the LWCC filled with water and a Cr(VI)-DPC solution are shown in Figure C2.

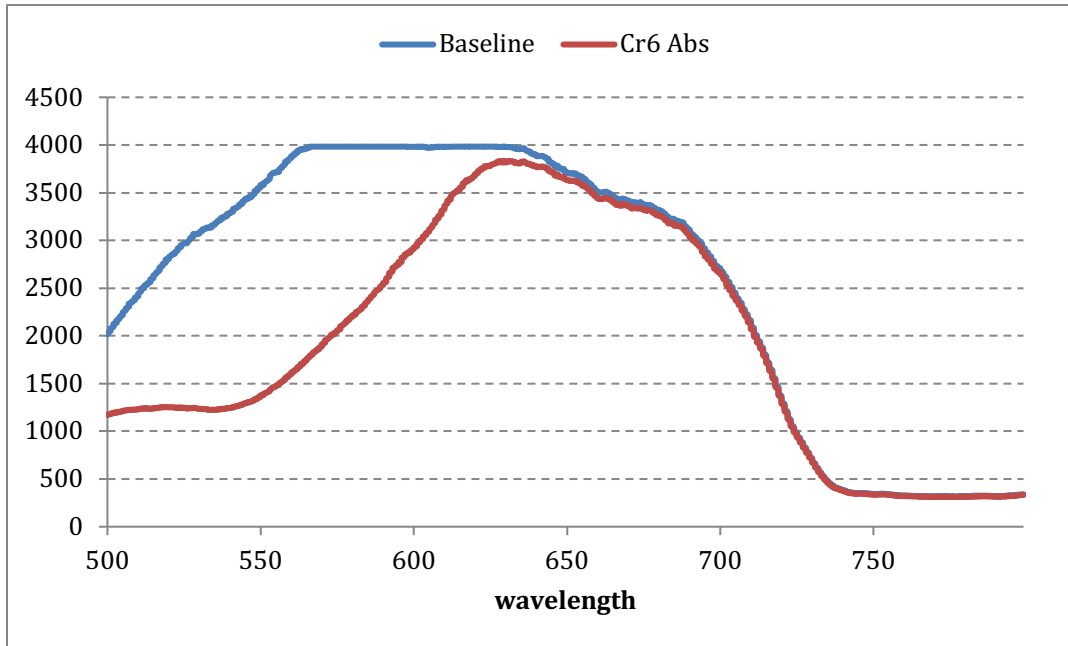


Figure C2. Spectra measured for pure water (baseline) and a Cr(VI)-DPC solution.

Step inputs of Cr(VI) solution were used to determine response characteristics of the analytical part of the instrument. The residence time distribution (RTD) was determined by differentiating the instrument response to a step input. The observed RTD was found to be stable and reproducible on several test days (Figure C3).

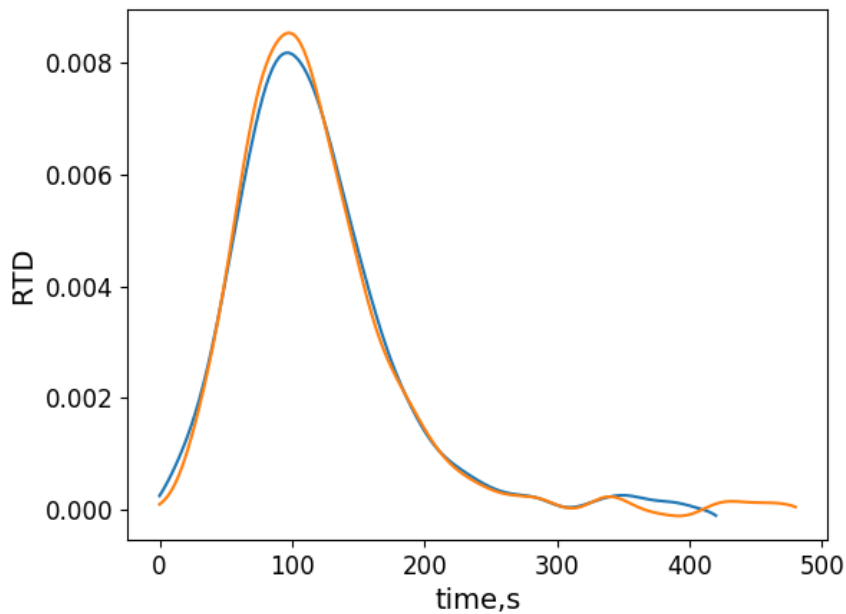


Figure C3. Residence time distribution (RTD) of the analytical part of the instrument.

Calculation of Cr(VI) concentrations

The concentration of Cr(VI) at a specific time was determined from the ratio of the measured intensity of light at 546 nm transmitted through the LWCC (I) to the intensity that would be transmitted in the absence of Cr(VI) (I_0), as per the well-known Beer-Lambert absorbance equation. Since only a single light source and detector were used, the value of I_0 could only be directly measured during periodic zero checks, when ultra-pure water was supplied to the detector in place of water from the SJAC by switching on a solenoid valve. To correct for temporal variations in the baseline intensity between these zero checks the transmitted intensity at a reference wavelength (700 nm, which is not significantly affected by the presence of Cr(VI)) was multiplied by the ratio I_{546}/I_{700} measured during zero checks and the result used as I_0 for each 1 second measurement. Measured absorbance values were converted to ambient concentrations of Cr(VI) by multiplying by a factor determined from the daily three-point calibrations (Figure C4), then dividing by the inlet air flow rate (16.7 ± 0.3 lpm) which was measured with an external flow meter during zero checks.

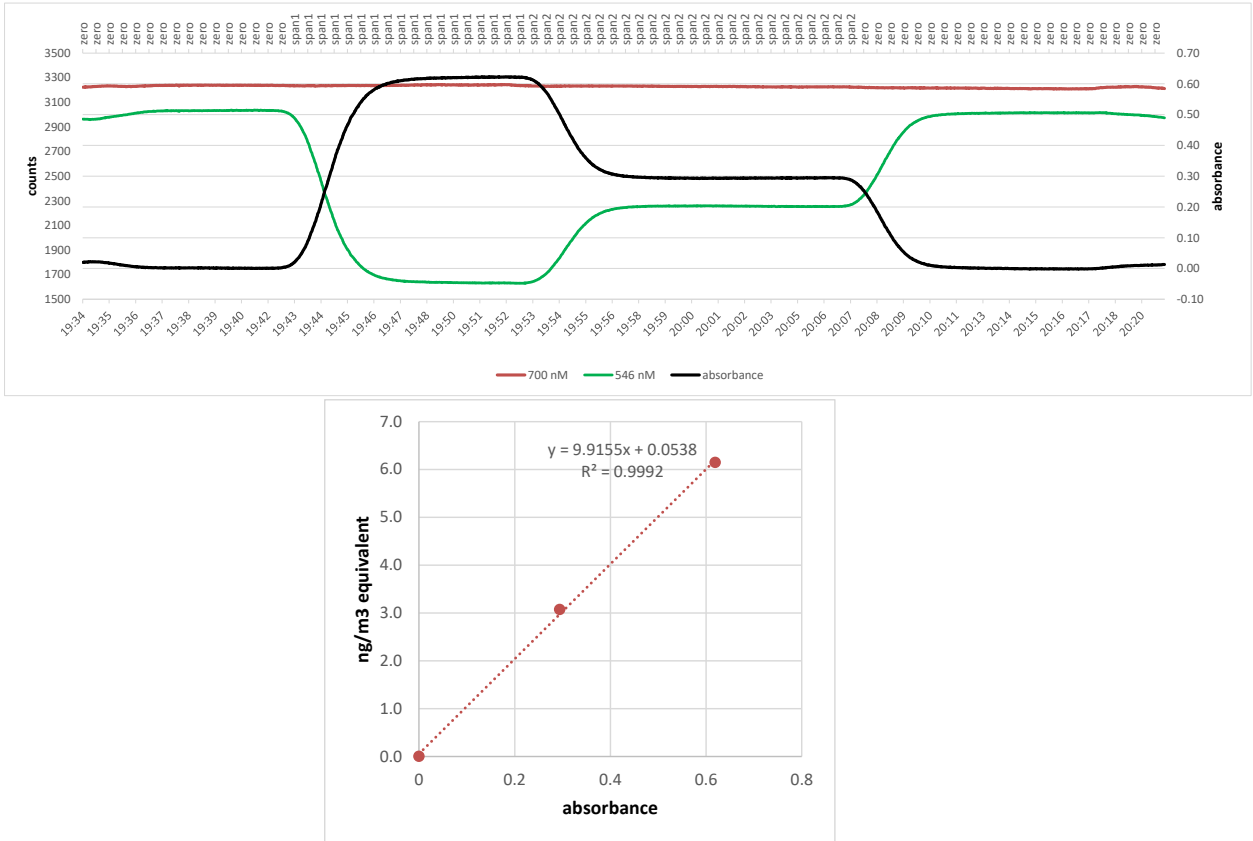


Figure C4. Example of daily 3-point calibration data and calibration curve.

Deconvolution

Due to the mixing processes in the SJAC-LPAS, the measured Cr(VI) signal appears to be smeared-out. To correct for this smearing and to restore the measurements closer to

the original signal, a deconvolution procedure was used that is briefly described here. First, the residence time distribution (RTD) of the SJAC was measured by subjecting it to a step input of a Cr(VI) solution. The RTD was calculated by differentiating the observed signal with respect to time. The measured RTD could be closely approximated as a combination of two gaussian distributions (Figure C5). The RTD was then used to restore the measured signal with Wiener deconvolution (Gonzalez et al., 2003). Using an analytical approximation of the RTD allowed for the reduction of noise amplification during the deconvolution process.

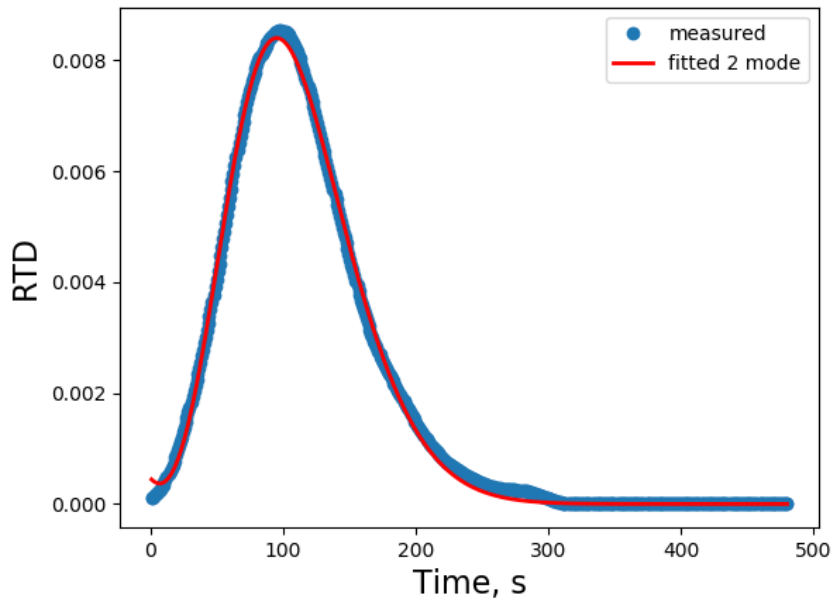


Figure C5. Measured RTD of the SJAC-LPAS and a two-mode gaussian fit.

QA/QC

The instrument was calibrated daily by direct injection of ultra-pure water and potassium dichromate solution at 2 known concentrations (initially 2.7 nM and 27.1 nM, later reduced to 4.1 and 8.2 nM to be closer to observed levels) in place of the SJAC output (Figure C4). In addition, the instrument zero was regularly checked when ultra-pure water was supplied to the detector in place of water from the SJAC by switching on a solenoid valve.

Since the AML frequently parked for periods of time during each survey we were able to gauge the effect of the considerable vibration inside the vehicle while driving on the measurement stability. As shown in Figure C6 there was a small increase in high-frequency noise when in motion, but this had little effect on the calculated Cr(VI) concentrations. Effective measurement sensitivity is $< 1 \text{ ng/m}^3$ but due to fluctuations in the baseline transmittance intensity, accuracy is estimated to be $\pm 0.2 \text{ } \mu\text{g/m}^3$ giving an effective LOQ of $0.4 \text{ } \mu\text{g/m}^3$ for the 1-second averages. Time averaging of data and peak

deconvolution can yield improved performance for time periods when persistent elevated concentrations are observed.

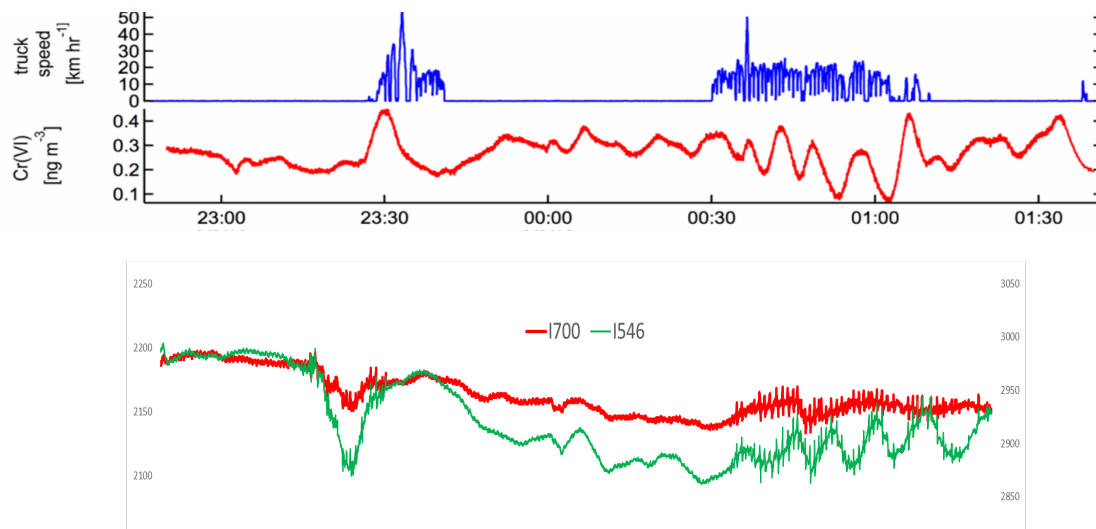


Figure C6. Time-series plots of 1-second raw (lower) and processed (upper red line) Cr(VI) data when AML was stationary and while driving.

Deconvolution was done for a subset of the data. This data has been output along with the original time trace in the final data deliverable. To request additional periods of deconvolution, please contact Andrey Khlystov.

In an attempt to confirm the accuracy of the monitor in actual use, one of the filter samplers used by the AQMD to make time-integrated Cr(VI) measurements at fixed sites (BGI PQ-100) was installed in the AML and operated with equivalent inlet and air flow rate to the continuous monitor for ~6 hr periods on 2 days. Unfortunately, the average concentrations of Cr(VI) on those days were too low ($< .02$ ng/m³) to allow meaningful inter-comparison. For similar purpose the AML also parked adjacent to the AQMD's site at the Paramount hospital for 4 to 6 hours on 2 days, however, pollutant levels were low again and no obvious correlation between the near-background Cr(VI) concentrations and hourly total Cr from the site's continuous XRF monitor was observed. Also, the stationary measurements collected by the AML at the hospital did not correspond to every-third day sample collection schedule for the AQMD's Cr(VI) filter measurements.

Since no consistently elevated ambient concentrations of Cr(VI) were encountered during the study it was not possible to determine the measurement lag time by observing the response after attaching a particle filter to the monitor inlet, as we had intended. Instead, a small amount of potassium chromate solution was injected directly into the steam jet of the aerosol collector and the lag time before a response was observed by the detector was measured. Since the transit time of aerosol particles from the external inlet to the SJAC can be calculated to be only a few seconds at the air flow rate of ~17 lpm, this approach is expected to be sufficiently accurate.

Measurement lag time was determined to be 330 seconds but could increase or decrease somewhat as the solution flow rate was adjusted to compensate for variations in liquid collection by the SJAC cyclone. In order to more accurately determine the actual time when the Cr(VI) aerosol creating an observed signal reached the monitor inlet, the internal volume of the liquid flow path in the monitor was calculated from the measured lag time and pumping rates. Second-by-second pump flow rates recorded in the datalogs were summed until the necessary volume was reached and the number of seconds required was used to adjust the timestamp of each data point.

Data recovery

Due to damage to a major component, the liquid waveguide capillary cell (LWCC), during transport from DRI to the project site the Cr(VI) monitor was not operable for the first few days of scheduled mobile monitoring. A replacement LWCC was obtained and installed on Mar. 6, allowing measurements to commence on Mar. 7. After that the monitor was operated during all mobile surveys with the exception of days when measurable Cr(VI) aerosol concentrations were unlikely due to rain or absence of activity at the source facilities (e.g. Sundays). In total, we collected mobile data on 21 days from March 7 to April 5.

References

- Allen TL. 1958. Microdetermination of chromium with 1,5-diphenylcarbohydrazide. *Anal Chem* **30**: 447-450.
- Gonzalez R, Woods R, Eddins S. 2003. *Digital image processing using Matlab*. Prentice Hall.
- Khlystov A, Wyers GP, Slanina J. 1995. The steam-jet aerosol collector. *Atmos Environ* **29**(17): 2229-234.

Appendix D: Overview Maps for PM Metals

This appendix contains overview maps for select particulate matter measurements in the study area.

All data is binned in 300 m x 300 m boxes (3000 m for the zoomed out graphs)

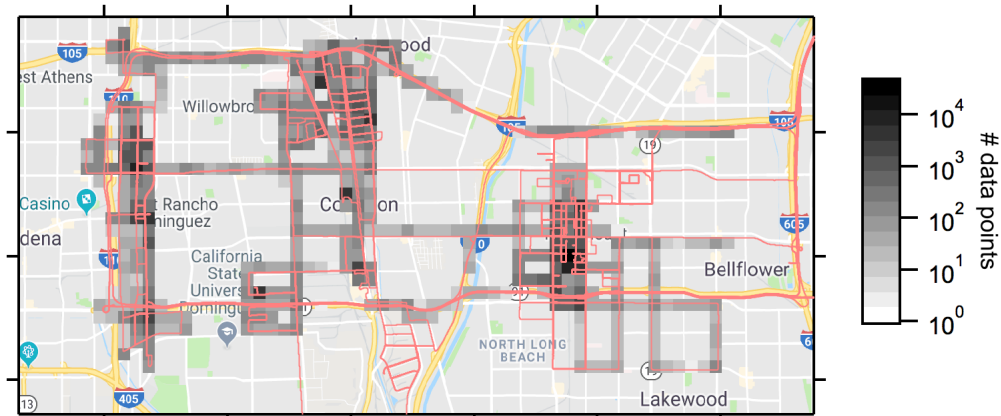
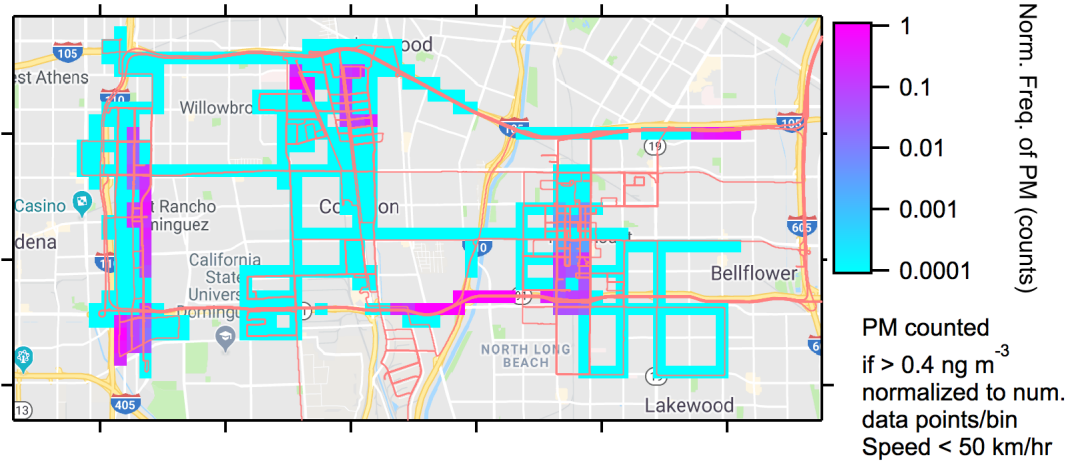
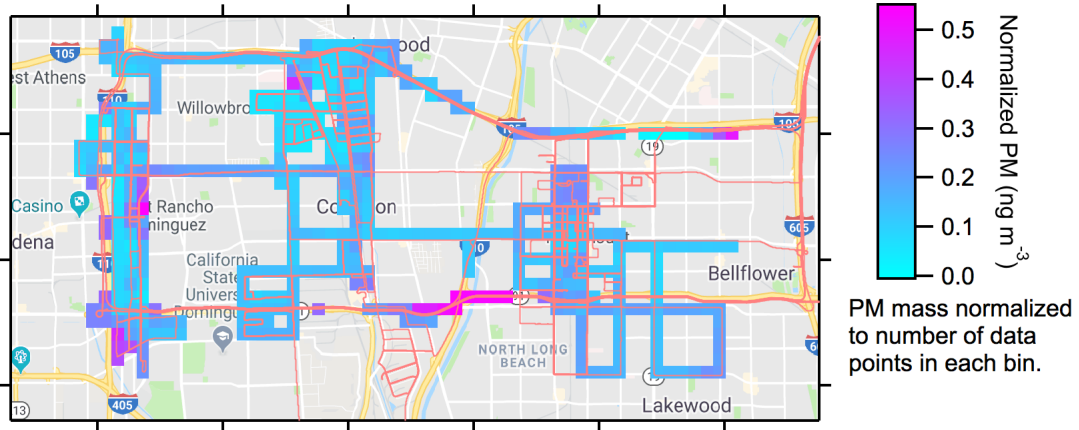
Top Panel: PM mass for the selected species is binned and normalized by the number of data points in each bin.

Middle Panel: The frequency of PM mass enhancements above a given threshold is counted, and normalized by the number of data points in each bin. Note log OR linear scale.

Bottom Panel: number of data points (log scale) in each bin.

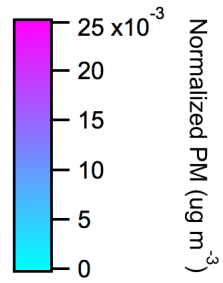
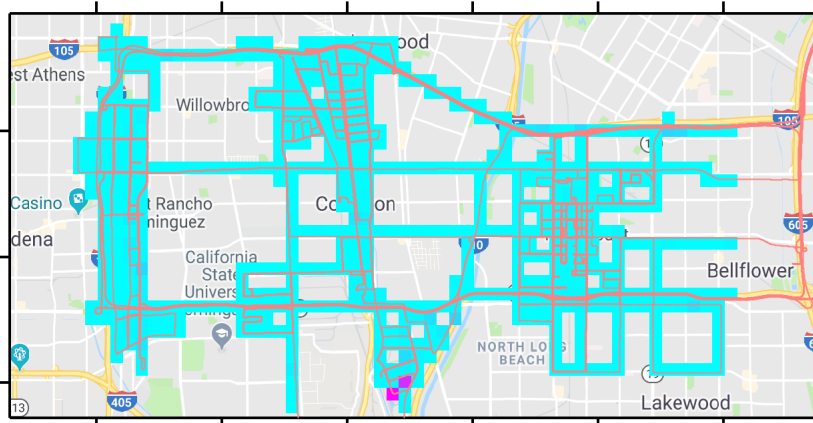
PM (Cr(VI), size and metals) for Paramount, Compton and surrounding areas:

SJAC Cr6

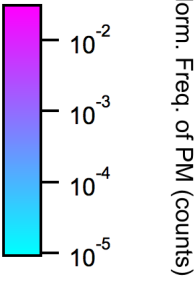
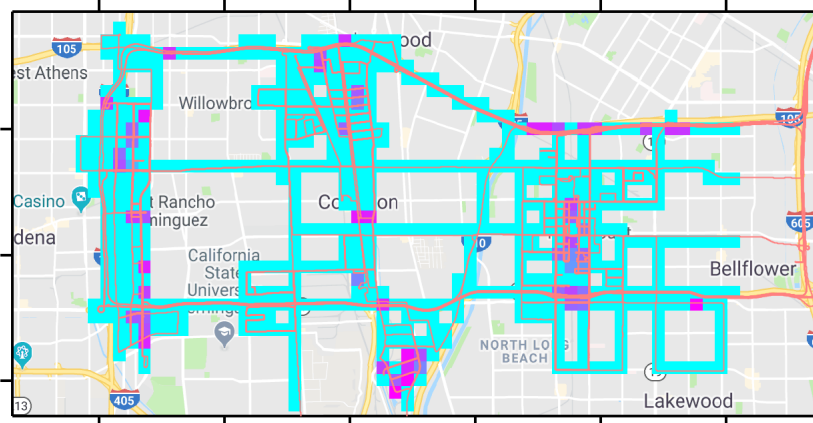


Note that some of the enhancements observed on highways may be “smeared” out due to vehicle speed.

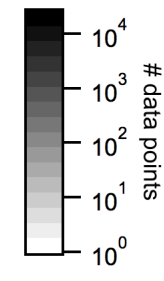
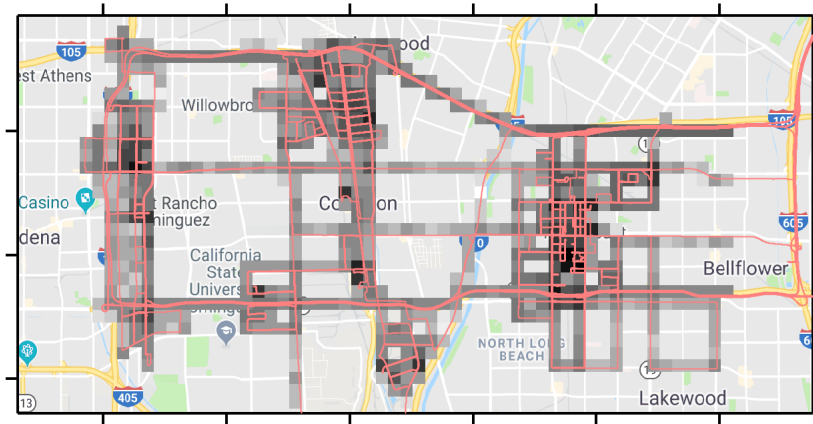
PM Cr



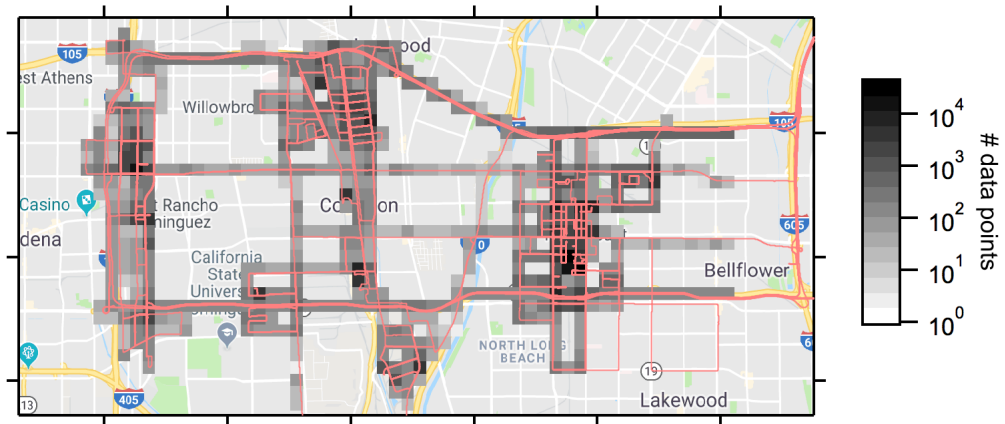
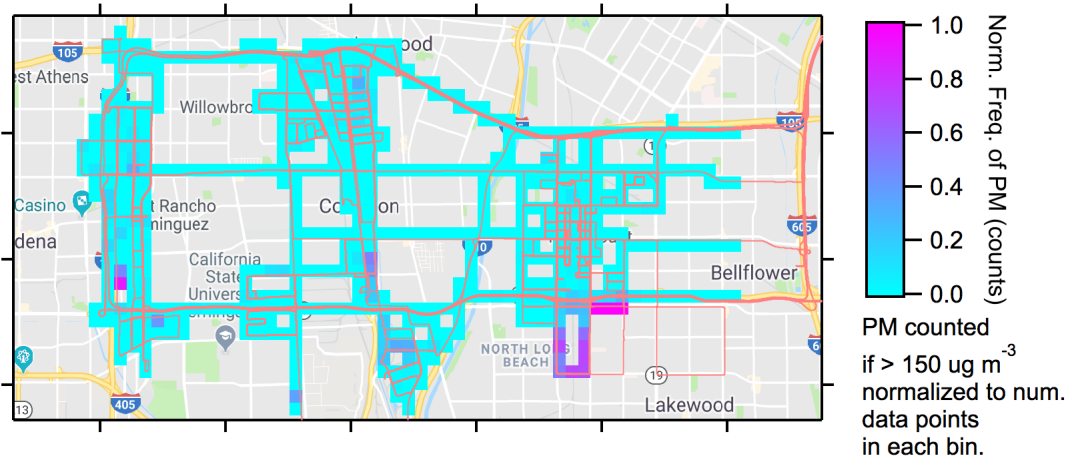
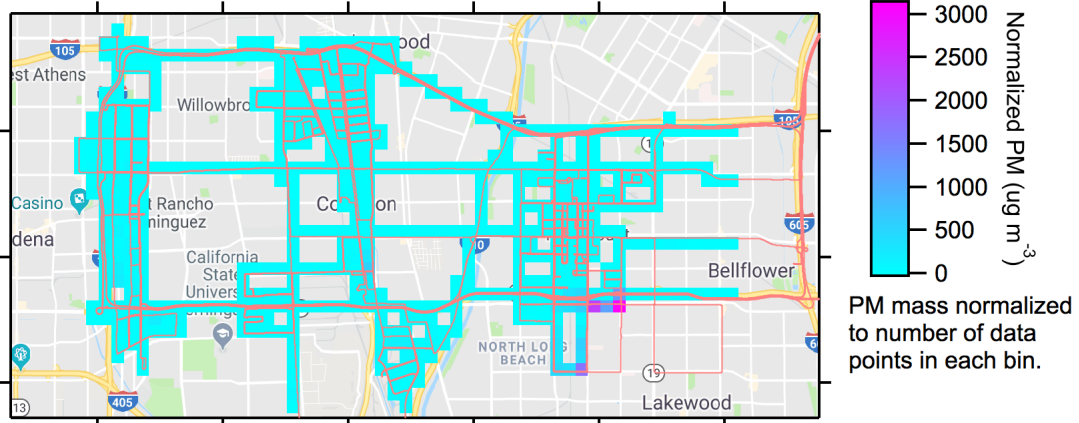
PM mass normalized to number of data points in each bin.



PM counted if $> 0.05 \mu\text{g m}^{-3}$ normalized to num. data points in each bin.

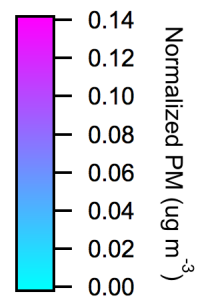
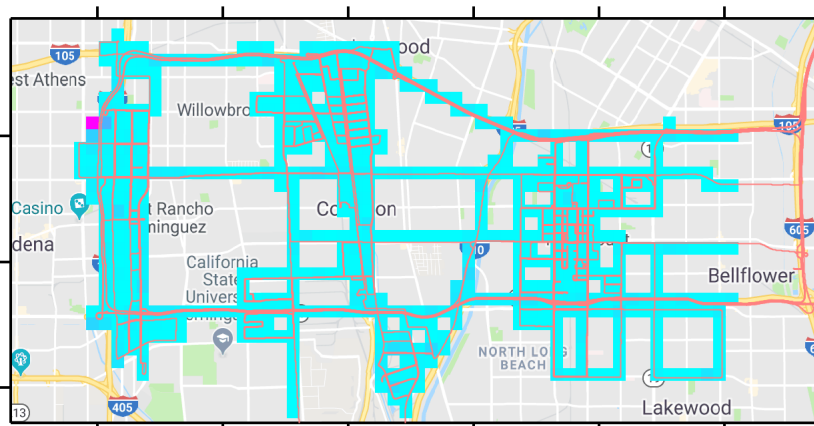


PM_{large}

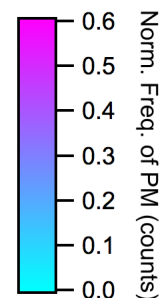
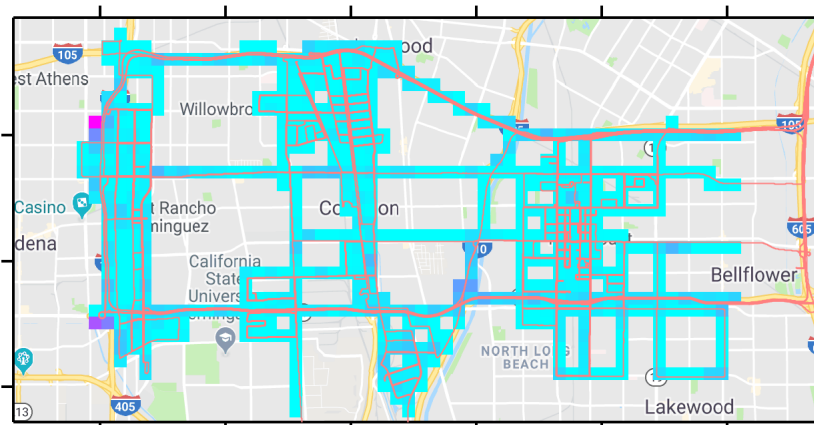


Note that PM_{large} refers to particulate matter between 2 and 10 μm . The enhancements noted in North Long Beach are at least partially due to foggy conditions (see data quality assurance document for PM_{large})

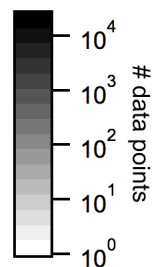
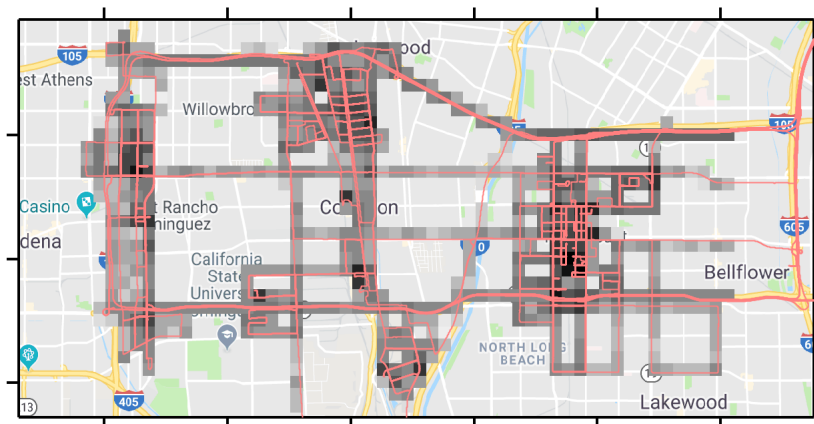
PMFe



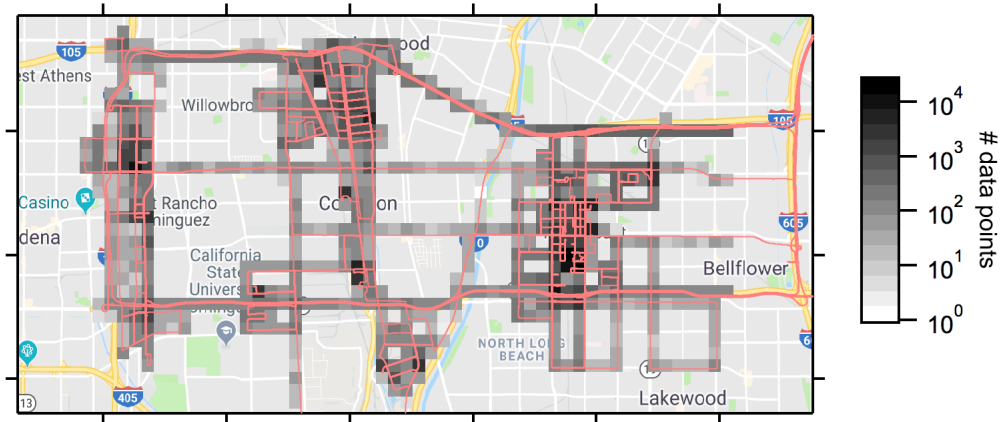
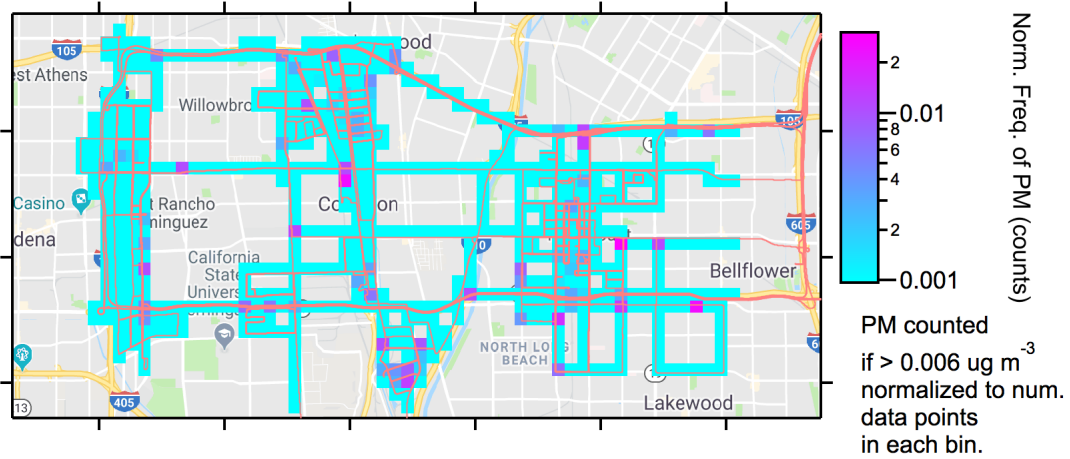
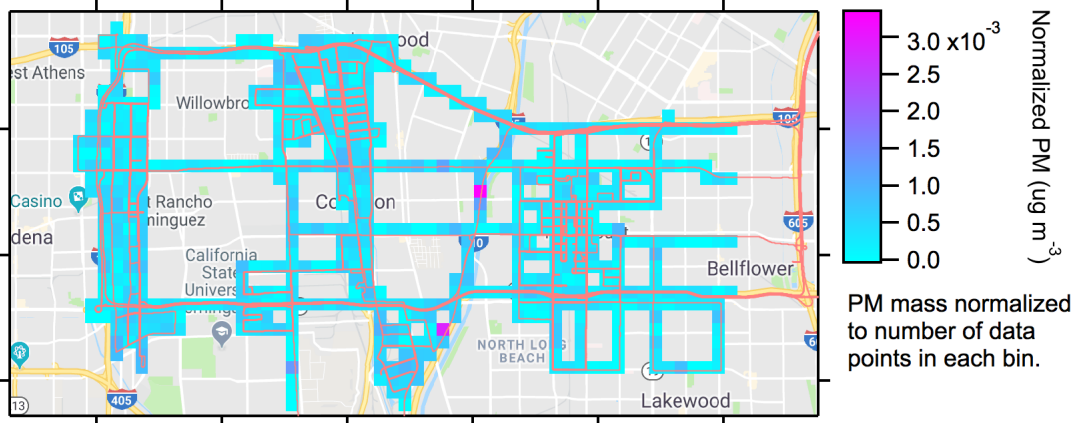
PM mass normalized to number of data points in each bin.



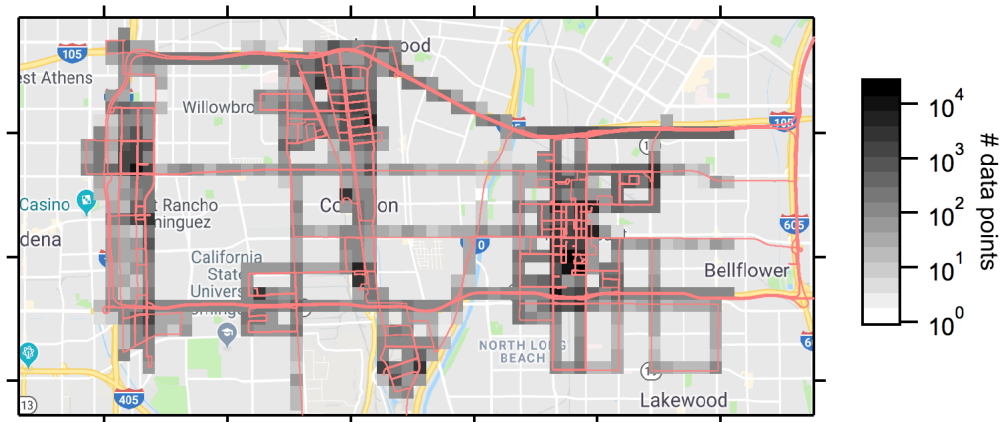
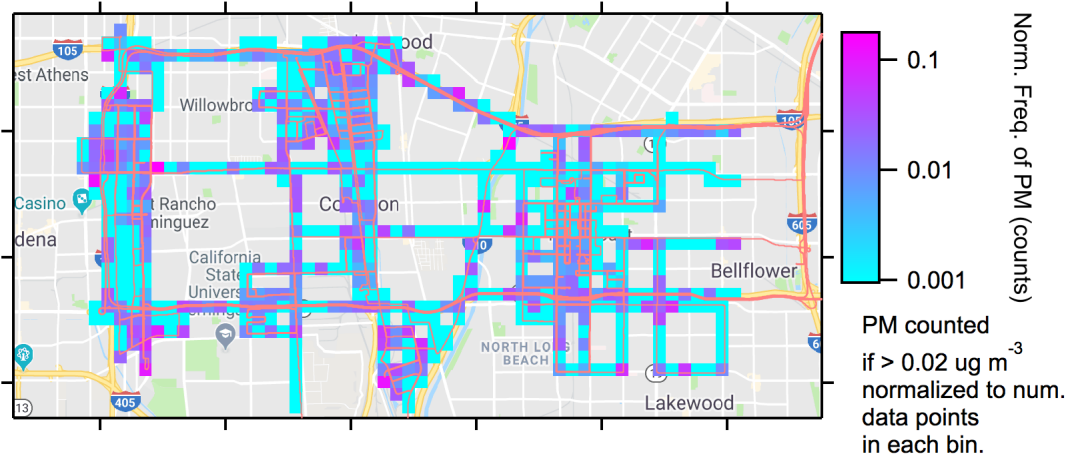
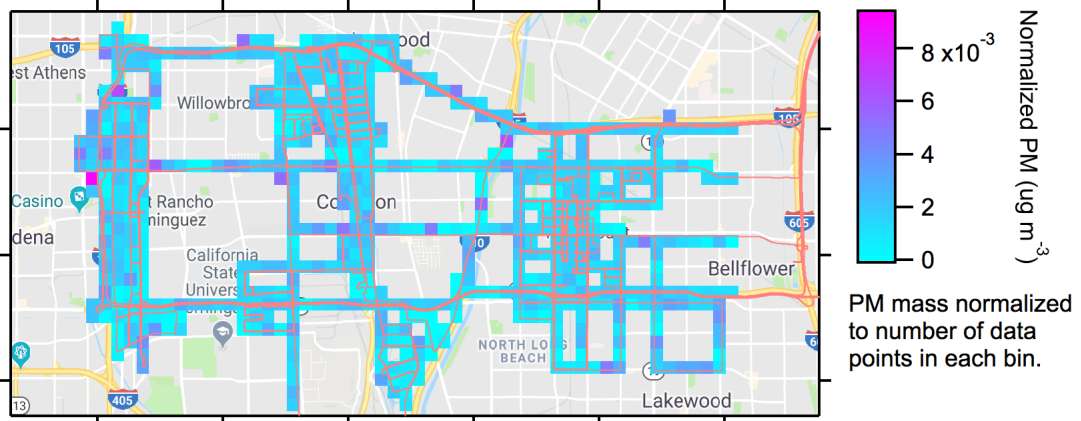
PM counted if $> 0.02 \mu\text{g m}^{-3}$ normalized to num. data points in each bin.



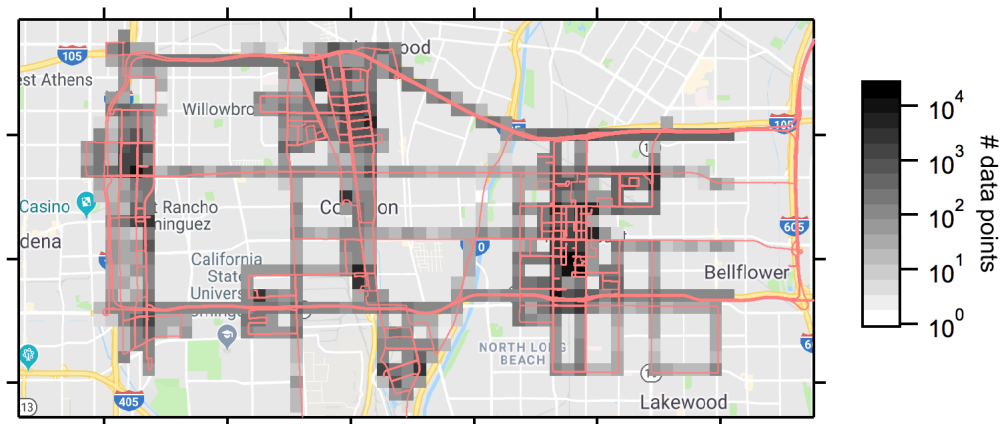
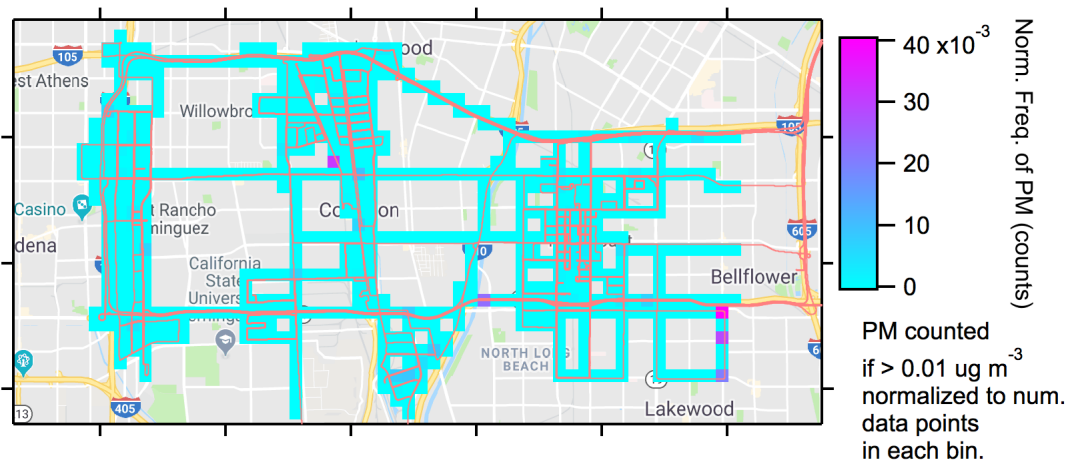
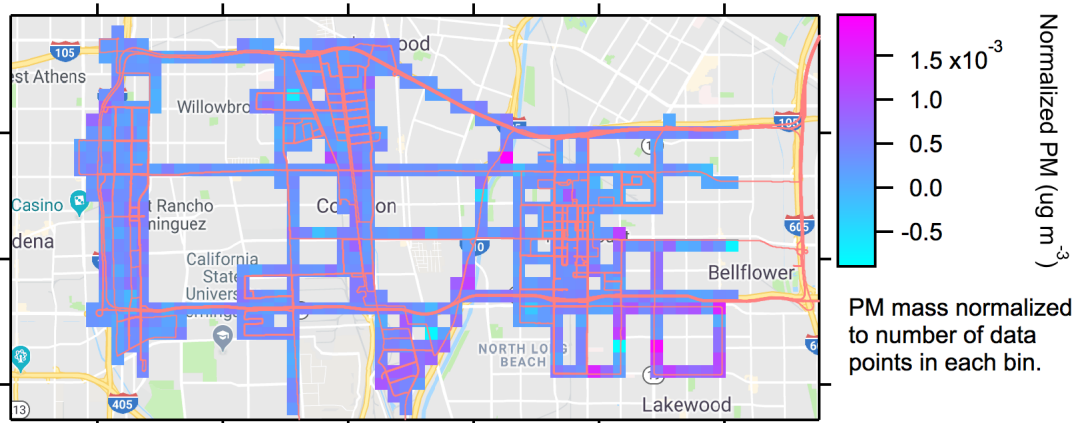
PMV



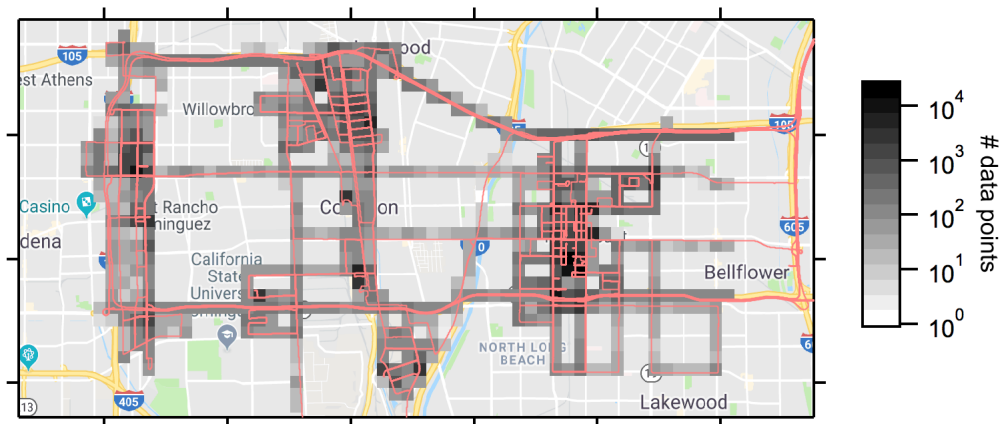
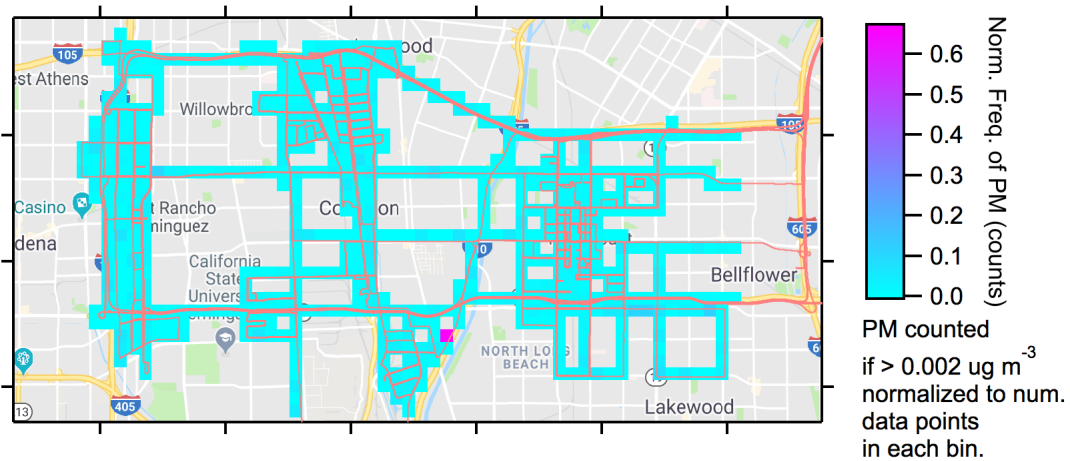
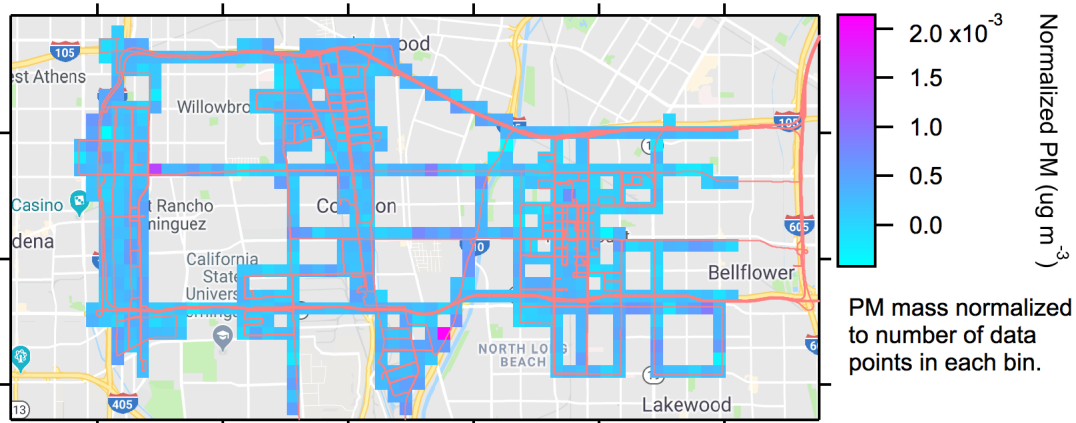
PMTi



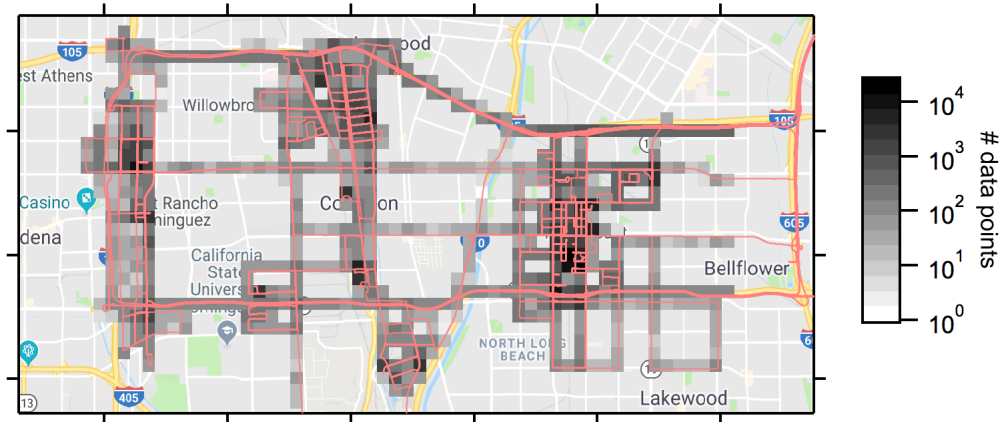
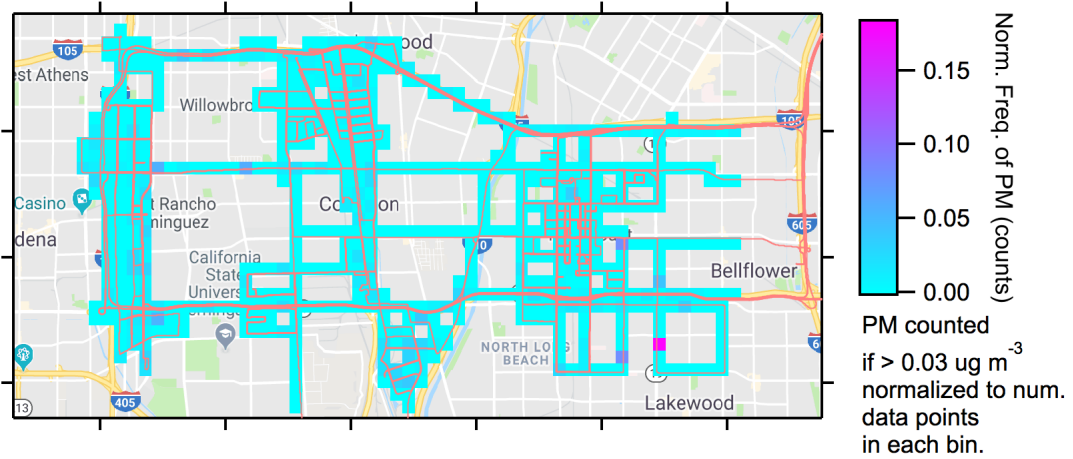
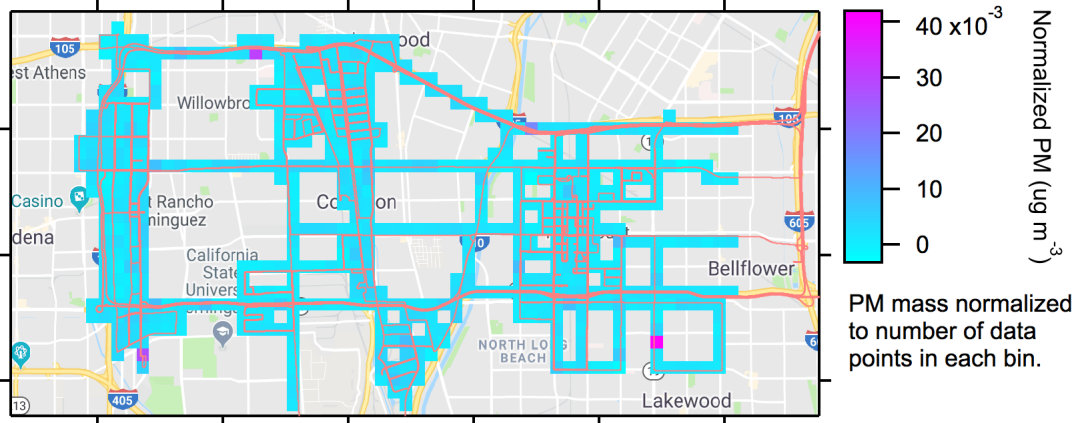
PMNi



PMSn

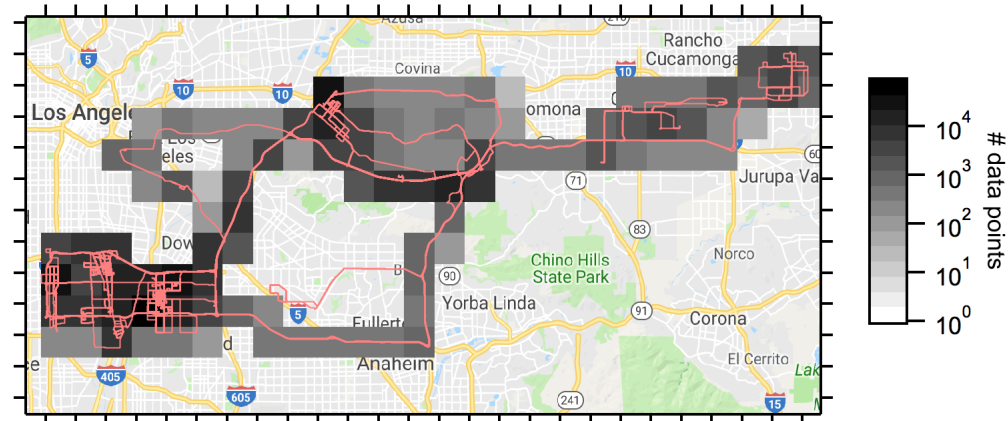
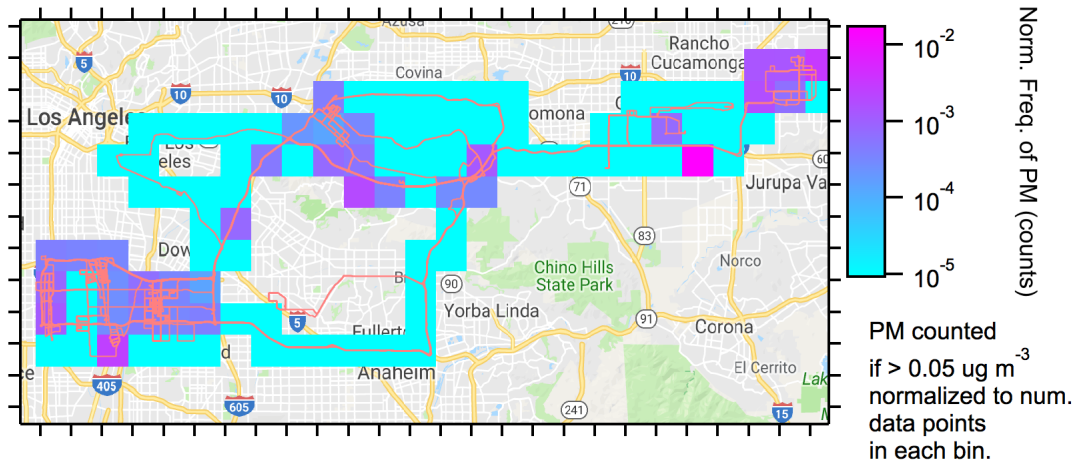
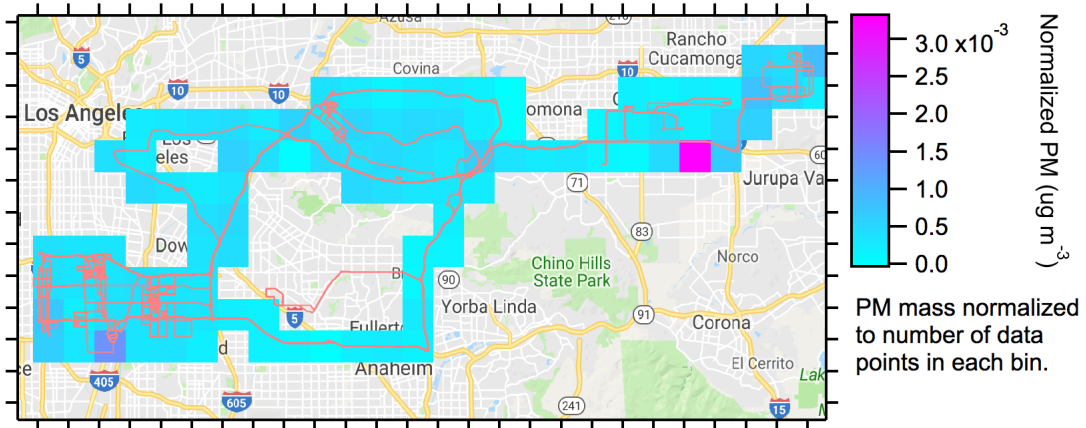


PMAI



Zoomed-out view of PM Cr and Cr(VI) for the entire campaign

PM Cr



SJAC Cr6

